**Metallacycle–Based Nickel–Catalyzed Reductive Couplings
and Reductive Cross–Electrophile Couplings**

by

Amie Renee Frank

A dissertation submitted in partial fulfillment
of the requirements for the degree of
Doctor of Philosophy
(Chemistry)
in the University of Michigan
2020

Doctoral Committee:

        Professor John Montgomery, Chair
        Associate Professor Amanda L. Garner
        Associate Professor Corinna S. Schindler
        Professor John P. Wolfe

Amie Renee Frank

amiebf@umich.edu

ORCID iD: 0000-0002-6155-3632

Dedication

To my husband, Caleb Frank. Your love, patience, support and encouragement throughout this adventure makes me want to grow old with you even more. On to the next adventure.

Acknowledgements

I would like to thank my advisor, Professor John Montgomery, for allowing me the opportunity to work in his lab the past five years. His guidance and mentorship provided me with the tools necessary to grow as a scientist and develop as a person. Thank you for your support and the freedom to explore my own interests.

I would also like to thank Professor John Wolfe for allowing me the opportunity to rotate in his lab as a first–year graduate student. His support, advice and feedback throughout my graduate career were always greatly appreciated. To the other members on my committee, Professor Corinna Schindler and Amanda Garner, thank you for being inspiring female role models in science. Their support, advice and feedback were also extremely helpful throughout my graduate career. Additionally, I would like to thank Professor Anne McNeil for her support as my original research proposal mentor. Lastly, I would like to thank Professor Brian Coppola and Professor Adam Matzger for their support and advice during times of adversity.

I am also tremendously grateful to all of the Montgomery lab members including postdoctoral researchers, undergraduate students and visiting students that I had the pleasure overlapping with during my graduate career. A special thanks goes to Dr. Alex Nett, Dr. Wanxiang Zhao, and Dr. Michael Gilbert for their mentorship early on. Additionally, a special thanks goes to Dr. Jessica Stachowski and Dr. Hilary Kerchner for their support and being great female role models. I would also like to thank the lab members in my cohort, Annabel Ansel and Dr. Alexander Rand, for their support while navigating through graduate school together. Furthermore, I would

iii

like to thank Wes for his support and taking the time to edit chapters of my dissertation. Lastly, I would like to thank Dr. Cole Cruz for not only taking the time to edit chapters of my dissertation, but also his support, feedback, advice and encouragement during the last few years of my graduate career.

I am also incredibly grateful for the wonderful friendships that transpired from graduate school. A special thanks for the love and support goes to Dr. Janelle Kirsch, Dr. Annabel Ansel and Dr. Becky Watson.

Lastly, I need to thank my family and my husband, Caleb. I would not have made it this far without each and every single one of you. Thank you so much for all the love, support and encouragement.

Table of Contents

List of Figures

List of Schemes

List of Tables

List of Abbreviations

α: alpha

approx: approximately

Ac: acetate

Ar: aryl

β: beta

BAC: bis(amino)cyclopropenylidenes

BiOX: bioxazoline

bipy: 2,2'–bypyridine

BOX: bis(oxazoline)

Bu: butyl

c: cyclo

C: Celsius

Cy: cyclohexyl

COD: 1,5–cyclooctadiene

COSY: ^1H–^1H correlation spectroscopy

d: doublet

DFT: density function theory

dme: dimethoxyethane

DMF: *N, N'*–dimethylformamide

DMFU: dimethyl fumarate

DMPU: *N, N*–dimethylpropyleneurea

DMSO: dimethyl sulfoxide

ee: enantiomeric excess

EH: Extended Hückel

EI:* electron impact ionization

ESI: electrospray ionization

Et: ethyl

EtOAc: ethyl acetate

Eq: equivalent

g: gram

GCMS: gas chromatography mass spectroscopy

h: hour

Hept: heptyl

Hex: hexyl

HOMO: highest occupied molecular orbital

HRMS: high resolution mass spectroscopy

i: iso

IMes: 1,3–dimesityl–1*H*–imidazol–3–ium-2-ide

IPr: 1,3–bis(2,6–diisopropylphenyl)–2,3–dihydro–1*H*–imidazole

IPr*OMe: 1,3–bis(2,6–dibenzhydryl–4–methoxyphenyl)–2,3–dihydro–2*H*–imidazole

***i*-Pr-BAC:** bis(diisopropylamino)cyclopropenylidene

ITol: 1,3–di–*p*–tolyl–1*H*–imidazole–3–ium–2–ide

J: coupling constant

L: ligand; liter

μ: micro

μL: micromolar

μm: micromolar

m: multiplet

M: molarity

Me: methyl

Mes: mesityl

mg: milligram

MHz: mega hertz

mL: milliliter

MA: methyl acrylate

MMA: methyl methacrylate

mmol: millimole

mol: mole

n: normal

NOESY: nuclear overhauser enhancement spectroscopy

NHC: *N*–heterocyclic carbene

NMR: nuclear magnetic resonance

π: pi

PA: phenyl acrylate

Ph: phenyl

ppm: parts per million

Pr: propyl

PyBOX: pyridine–bis(oxazoline)

R: generic group

rt: room temperature

σ: sigma

s: singlet

SET: single electron transfer

SFC: supercritical fluid chromatography

SIPr: 1,3–bis(2,6–diisopropylphenyl)imidazolidine

*t***:** tertiary

t: triplet

TBAF: tetrabutylammonium fluoride

TBDMS/TBS: *tert*-butyldimethylsilane

TBDPSCl: *tert*-butyl(chloro)diphenylsilane

TES: triethylsilane

TESCl: triethylchlorosilane

TIPS: triisopropylsilane

TIPSCL: triisopropylsilyl chloride

Tf: trifluoromethansulfonate, triflate group

THF: tetrahydrofuran

Tol: 4–methylbenzyl

TM: transition metal

TS: transition state

V: volume

wt: weight

X: halogen; leaving group; generic group

Abstract

The development of nickel catalysis has become more prominent over the years for organic transformations due to its low cost and widespread availability. This thesis discusses the impact of nickel catalysis in organic transformations such as metallacycle–based nickel-catalyzed reductive couplings and reductive cross–electrophile couplings.

Chapter 1 provides background literature to the various strategies developed by the Montgomery lab to control regioselectivity and enantioselectivity of stereodefined silyl–protected allylic alcohol products in the reductive couplings of aldehydes and alkynes. Chapter 2 discusses the challenges associated with synthesizing small, chiral BAC ligands along with the challenges faced with developing a strategy using small, chiral ligands to control regioselectivity and enantioselectivity in the reductive couplings of aldehydes and alkynes. During the strategy development process, an endo product in the ynal cyclizations was serendipitously discovered. However, the formation of endo product was only observed for one privileged substrate. With obtaining moderate regioselectivity and low enantioselectivity using small, chiral ligands, future work will need to investigate the synthesis of other novel BAC ligands to simultaneously obtain great regioselectivity and high enantioselectivity.

Chapter 3 provides background literature to the design, synthesis and reactivity of novel, well–defined NHC–Ni(0) complexes to avoid the use of unstable Ni(0) precursors and *in–situ* protocols to generate the Ni(0) catalyst. Chapter 4 discusses the synthesis of novel BAC–Ni(0) complexes with fumarate ligands, which were the first of this class to be synthesized. Although

these novel BAC–Ni(0) complexes showed to be inactive in the reductive coupling of aldehydes and alkynes compared to the IMes–Ni(0) complexes, it was shown computationally that the BAC–Ni(0) complexes prefer to undergo the ketene first pathway for catalyst activation. This pathway leads to a nickel hydride species that is too endergonic and not capable of forming an active catalyst. Future work will need to consist of determining what pi–acidic additives can allow for BAC–Ni(0) to be stable, yet active in the reductive coupling of aldehydes and alkynes.

Chapter 5 provides background literature to the recent metallacycle–based reductive cross-electrophile coupling method developed by the Montgomery to synthesize tetrasubstituted olefins. Chapter 6 discusses the challenges in preventing oligomerization and / or polymerization from occurring in the metallacycle–based reductive cross-electrophile coupling method when utilizing electron–deficient substrates such as alkynyl enamides, alkynyl enals, alkynyl enones and alkynyl enoates. Moderate yields were obtained after optimization with an alkynyl enamide. Future work would consist of looking at various primary alkyl halides to generate a potential substrate scope with alkynyl enamides. Additionally, there is the potential to synthesize bipyridine–Ni(0) complexes using pi–acidic additives, such as fumarates and acrylates. This would limit the reduction step needed to reduce the Ni(II) complex to the active Ni(0) complex and potentially increase the yield of product formation.

Chapter 1 Introduction to Nickel–Catalyzed Reductive Couplings: Small Ligand Protocol Versus Large Ligand Protocol

1.1 General Overview of Precious Versus Base Metal Catalysis

For many years, the development of precious metal catalysis has been more prominent compared to the development of catalysis employing base metals for organic transformations. Precious metals are not as readily available and are often mined in countries with unstable political infrastructures, leading to concerns about cost and availability. This brings attention to the ever–growing demand for the development of methods that utilize first–row transition metals (TMs) as an alternative to precious metals for catalyzing organic transformations (Figure 1-1).[1] Developing novel base metal catalysis for organic transformations would not only be cost–effective due to the natural abundance of base metals compared to precious metals but would also limit the use and exposure of toxic metals as base metals are less toxic than precious metals. The effects of transitioning toward base metal catalysis have and will continue to be felt in large, industrial–scale processes from pharmaceuticals to agrochemicals. The content throughout this thesis will show the impact of nickel catalysis in organic transformations such as metallacycle base reductive couplings and reductive cross–electrophile couplings.
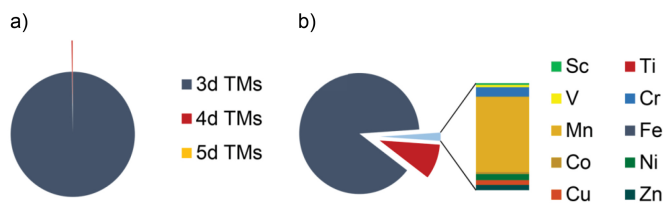
Figure 1-1: a) Natural abundance of 3d, 4d and 5d transition metals (TMs)[1]; b) Natural abundance of 3d transition metals (TMs)[1]

1.2 Mechanistic Outcome for Aldehyde–Alkyne Reductive Couplings

The Montgomery lab has a long–standing focus in the development of novel nickel–catalyzed processes.[2] Specifically, the Montgomery lab was able to generate various strategies to control not only the regioselectivity but also the enantioselectivity of stereodefined silyl–protected allylic alcohol products in the reductive coupling of aldehydes and alkynes.[2-8]

To understand these various strategies to control regioselectivity and enantioselectivity, the proposed mechanism needs to be understood (Scheme 1-1).[2-8] Initially, an aldehyde and an alkyne in the presence of a Ni(0) catalyst will form complex **1-1**. Complex **1-1** undergoes an oxidative cyclization to form the five-membered metallacycle **1-2**. A silane enters the catalytic cycle and performs a σ–bond metathesis with the Ni–O bond of the five-membered metallacycle **1-2** to form the vinylnickel(II) complex **1-3**. Finally, complex **1-3** undergoes reductive elimination to afford the desired silyl–protected allylic alcohol product **1-4**.
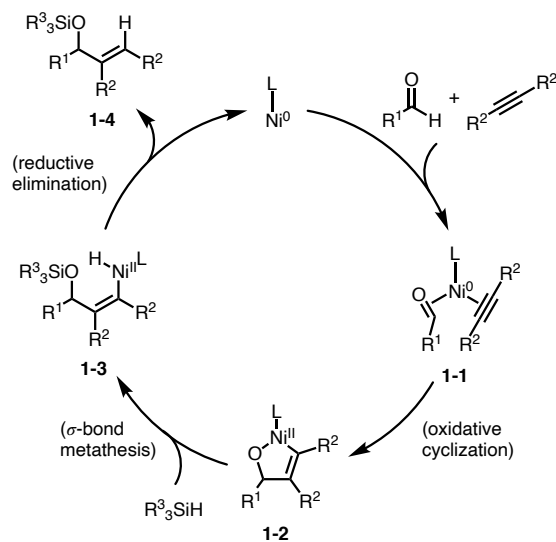
Scheme 1-1: Proposed mechanism for aldehyde–alkyne reductive couplings

With an unsymmetrical alkyne, the substituents on the alkyne can differ based on sterics and electronics. For simplicity, R^S will represent the smaller substituent on the alkyne where R^L will represent the larger substituent on the alkyne. An unsymmetrical alkyne in the presence of an

aldehyde, silane and Ni catalyst will result in two regiochemical products (Scheme 1-2). Product **1-5** acquires R^S at the terminal position of the alkene. Product **1-6** acquires R^L at the terminal position of the alkene.
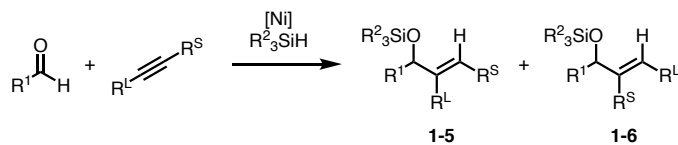
Scheme 1-2: Regiochemical outcome in aldehyde–alkyne reductive couplings

1.3 Regiocontrol in Aldehyde–Alkyne Reductive Couplings

Early work from the Montgomery lab demonstrated that the ligand structure could provide moderate regiocontrol in the reductive coupling of aldehydes and alkynes.[3,9-11] Collaborations between the Jamison and Houk labs determined that phosphine ligands could only provide minimal regiocontrol in the reductive coupling of aldehydes and alkynes.[12,13] Later work from the Montgomery lab exhibited good to excellent regiocontrol in the reductive coupling of aldehydes and alkynes after synthesizing and screening various carbene ligands.[4] The two main classes of carbene ligands utilized for this work were *N*–heterocyclic carbenes (NHCs) and bis(amino)cyclopropenylidenes (BACs) (Figure 1-2).
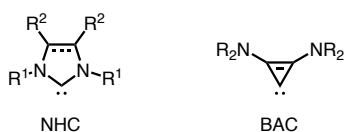
Figure 1-2: Skeletal framework of NHC and BAC ligands

The NHC and BAC ligands not only provided good to excellent regiocontrol, but also provided regiochemical reversal depending on the size of carbene ligand (Table 1-1).[4] The use of a large ligand was found to favor product **1-5** as the major product and the use of a small ligand was found to favor product **1-6** as the major product. Additionally, regiochemical reversal worked for a variety of substrate classes, such as unbiased internal alkynes (Entry 1, Table 1-1), aryl

alkynes (Entry 2, Table 1-1), conjugated enynes (Entry 3, Table 1-1) and strongly biased terminal alkynes (Entries 4 and 5, Table 1-1), making this strategy extremely useful and efficient as it overrides substrate biases and requires no directing functional group installation.
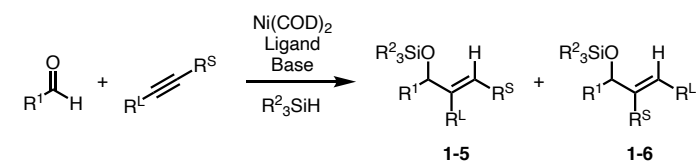
Entry	R^1	R^L	R^S	1-5:1-6 (Yield (%))[a]	1-5:1-6 (Yield (%))[a]
1	n-Hex	n-Pr	Me	**A**, 93:7 (85)	**C**, 12:88 (78)
2	Ph	Ph	Me	**A**, 81:19 (99)	**D**, >2:98 (84)
3	n-Hex	c-Hexenyl	Me	**A**, 91:9 (77)	**D**, 3:97 (99)
4	Ph	CH$_2$OTBS	H	**B**, 85:15 (86)	**D**, 7:93 (88)
5	Ph	n-Hex	H	**B**, 88:12 (71)	**D**, 3:97 (82)

[a]Conditions: **A**: Ligand = **1-8**, Base = KO-t-Bu, (i-Pr)$_3$SiH; **B**: Ligand = **1-7**, Base = BuLi, Et$_3$SiH; **C**: Ligand = **1-10**, Base = BuLi, (t-Bu)$_2$SiH$_2$; D: Ligand = **1-9**, Base = KO-t-Bu, (i-Pr)$_3$SiH or Et$_3$SiH
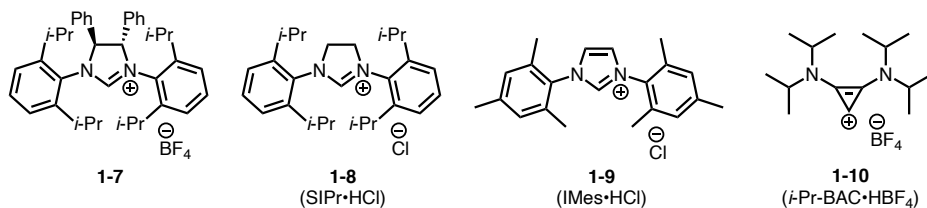
Table 1-1: Regiochemical reversal in aldehyde–alkyne reductive couplings

1.3.1 NHC Ligands

Over the years, the Montgomery lab has been able to isolate and characterize diverse NHCs of varying steric profiles to implement and use for screening purposes in the reductive coupling of aldehydes and alkynes (Figure 1-3).[2-8] Ligands **1-8** (SIPr•HCl) and **1-9** (IMes•HCl) are commercially available, while ligand **1-7** is not commercially available. When assessing the steric profiles of each ligand, it is best to imagine the ligand bound to a metal center, such as nickel. The isopropyl groups at the 2 and 6 positions of the aryl groups on ligands **1-7** and **1-8** are positioned to generate significant steric crowding around the metal center where the reactivity is taking place, thus creating a larger steric profile. The methyl groups at the 2 and 6 positions of the aryl groups

on ligand **1-9** generate less steric crowding around the metal center where the reactivity is taking place in comparison to ligands **1-7** and **1-8**, thus creating a small steric profile. Additionally, the percent buried volumes ($\%V_{Bur}$) can be calculated using Density Functional Theory (DFT) to compare the steric profiles of each ligand.[8,14] The $\%V_{Bur}$ measures the space occupied by the ligand within the first coordination sphere by a percentage. Therefore, the higher the $\%V_{Bur}$, the larger the ligand.[8,14] For ease in understanding regiocontrol in the reductive couplings of aldehydes and alkynes, ligands **1-7** and **1-8** will be referred to as large ligands where ligand **1-9** will be referred to as a small ligand.[4]

1-7	**1-8** (SIPr•HCl)	**1-9** (IMes•HCl)
37.5 $\%V_{Bur}$	36.1 $\%V_{Bur}$	28.7 $\%V_{Bur}$[a]

[a]$\%V_{Bur}$ was calculated with a NHC-Metal distance of 2.28 Å instead of 3.5 Å
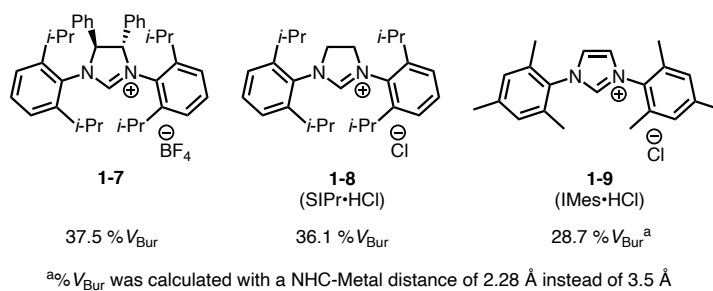
Figure 1-3: NHCs of varying steric profiles

1.3.2 BAC Ligands

Inspired by the development of using carbenes, such as NHCs, as ligands in the reductive coupling of aldehydes and alkynes, the Montgomery lab branched into implementing and studying a new class of carbenes called bis(amino)cyclopropenylidenes (BACs).[4] This new class of carbenes was recently developed by the Bertrand lab, therefore, the diversity and evaluation of this ligand scaffold are lacking.[15] As such, investigation in the scope of BAC ligands pose opportunities in broadening the synthetic utility for a variety of nickel–catalyzed processes. Ligand **1-10** (*i*-Pr-BAC•HBF₄), initially developed by the Bertrand lab, is the most easily synthesized and commonly used BAC ligand (Figure 1-4). When assessing the steric profile of **1-10**, the diisopropylamino groups are positioned to generate less steric crowding around the metal center where the reactivity

is taking place, thus creating a small steric profile. For ease in understanding regiocontrol in the reductive couplings of aldehydes and alkynes, ligand **1-10** will be referred to as a small ligand with ligand **1-9** (IMes•HCl).[4]

1-10
(*i*-Pr-BAC•HBF$_4$)
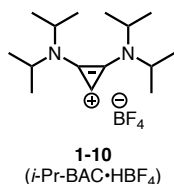
Figure 1-4: i-Pr-BAC

1.3.3 NHC Ligands Versus BAC Ligands

There are distinct steric and electronic differences between NHCs and BACs, which has piqued interest into further development of these specific carbenes.[15-18] Bertrand reports that these Hückel aromatic compounds exhibit reasonable singlet–triplet energy separation by means of density functional calculations.[19] Using Extended Hückel (EH) calculations on cyclopropenylidene **1-11**, Bertrand was able to describe the HOMO in a simple cyclopropenylidene as the σ orbital, centered on the carbon with singlet-carbene character. Unoccupied higher energy orbitals were defined as π_2 and π_3 (Figure 1-5). Based off of this model, multiple triplet states could be described. Further calculations showed that the excitation of one electron from the σ orbital to the π_3 orbital provided the lowest-energy triplet. This is due to the bonding character seen in the π_3 orbital whereas the π_2 orbital contains only antibonding character and a node at the carbene carbon. The addition of amino groups to the olefinic carbons resulted in an approximate 20 kcal mol^{-1} increase of the singlet-triplet energy. An increase in the singlet-triplet energy separation imparted by the amino-groups for BACs is observed, however, it is still smaller than the singlet-triplet energy separation seen with its NHC counterparts. Although NHCs are calculated to have a larger singlet-triplet energy separation, the energy of the HOMO for cyclopropenylidenes is higher than the energy of the HOMO for NHCs. As a result,

cyclopropenylidenes are more nucleophilic. Taking careful consideration of sterics and electronics for the substituents attached to the olefinic carbons will determine the singlet-triplet energy separation and thus, the stability of the carbene.
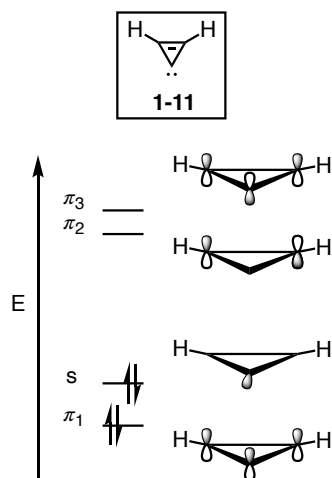
*Figure 1-5: Energy diagram of **1-11** using EH calculations*

The engineering and design opportunities available for BAC ligands could evolve into unique influences for a variety of catalytic processes due to the exceptional σ-donating character and small effective size exemplified by parameters such as percent buried volume ($\%V_{buried}$). This stands in contrast to most NHC ligands, which exert considerable steric demand directed towards the metal center.

Taking advantage of the steric and electronic differences between NHCs and BACs, the Montgomery lab was able to look at these ligands and classify them into two groups for the reductive coupling of aldehydes and alkynes.[4] As previously discussed, ligands **1-7** and **1-8** were classified as large ligands (L^L) and ligands **1-9** and **1-10** were classified as small ligands (L^S). The large ligands (L^L) provided a different regiochemical outcome compared to the small ligands (L^S), which led to the development of the large ligand protocol and the small ligand protocol for the reductive coupling of aldehydes and alkynes (Scheme 1-4).
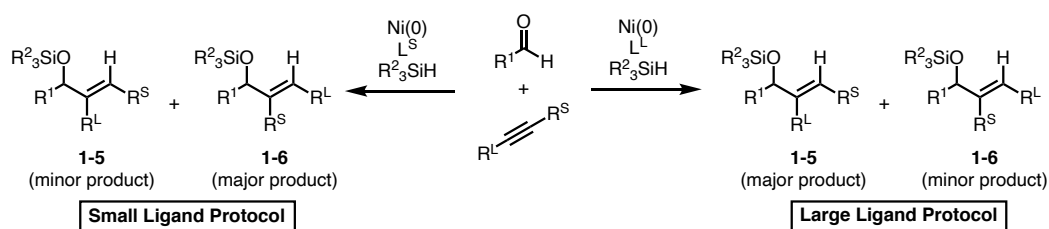
Scheme 1-3: Regiochemical outcome in the small ligand protocol versus the large ligand protocol

1.3.4 Large Ligand Protocol

To understand the regiochemical outcome of favoring product **1-5** over **1-6**, it is best to look at the first step in the catalytic cycle where the aldehyde and the alkyne are bound to Ni(0) catalyst (Scheme 1-5).[4-7] The alkyne can be positioned in two different ways. The smaller substituent can lie closer in proximity to the ligand providing complex **1-12**. Alternatively, the larger substituent can lie closer in proximity to the ligand providing complex **1-13**. When looking at complex **1-13**, there is a large amount of steric crowding between the large ligand and the large substituent of the alkyne. Therefore, the formation of complex **1-12** is favored over the formation of complex **1-13**, thus making the major product **1-5**.
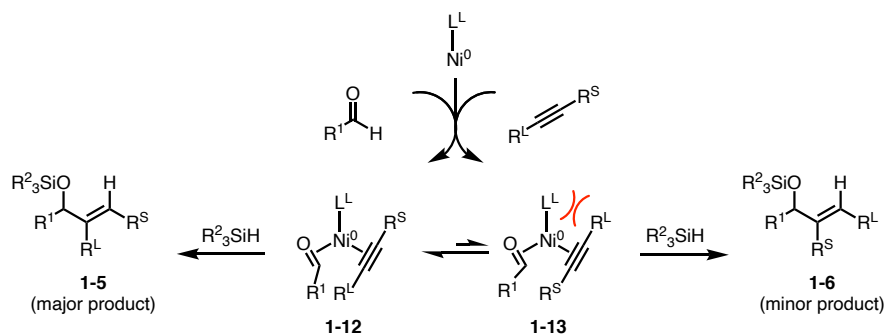
*Scheme 1-4: Comparison of complexes **1-12** and **1-13** in the large ligand protocol*

The Montgomery lab compared the regioselectivities of large ligands, **1-7** and **1-8** (Table 1-2).[4] Both ligands, **1-7** and **1-8**, provided excellent regioselectivity favoring the desired product **1-14** over **1-15**. With ligand **1-8** being commercially available, this makes for a great ligand to use, however, ligand **1-7** was found to provide higher selectivity, particularly with terminal alkynes.

*Table 1-2: Regioselectivity in aldehyde–alkyne reductive couplings with ligands **1-7** and **1-8***
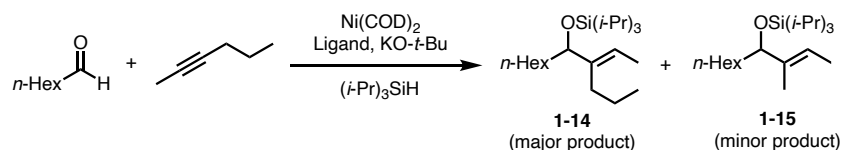
Entry	Ligand	Regioselectivity (**1-14:1-15**)	Yield (%)
1	**1-7**	94:6	69
2	**1-8**	93:7	85

1.3.5 Small Ligand Protocol

To understand the regiochemical outcome of favoring product **1-5** over **1-6**, it is best to look at the first step in the catalytic cycle where the aldehyde and the alkyne are bound to Ni(0) catalyst (Scheme 1-6).[4-7] The alkyne can be positioned in two different ways. The smaller substituent can lie closer in proximity to the ligand providing complex **1-16**. Alternatively, the larger substituent can lie closer in proximity to the ligand providing complex **1-17**. When looking at complex **1-16**, there is a large amount of steric crowding between the substituent on the aldehyde and the large substituent of the alkyne. Therefore, the formation of complex **1-17** is favored over the formation of complex **1-16**, thus making the major product **1-6**.
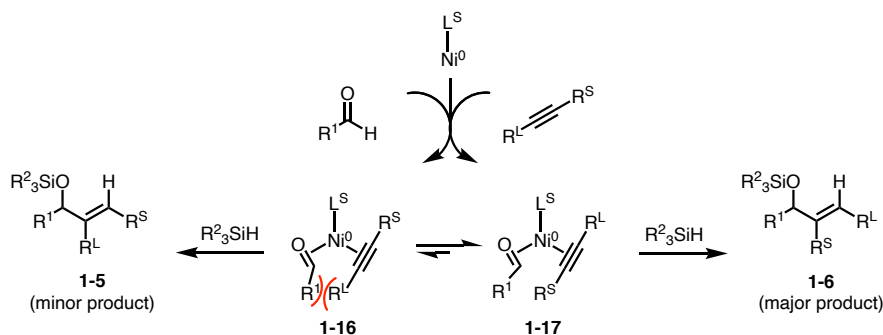
*Scheme 1-5: Comparison of complexes **1-16** and **1-17** in the small ligand protocol*

9

The Montgomery lab compared the regioselectivities of large ligands, **1-9** and **1-10** (Table 1-3).[4] Both ligands, **1-9** and **1-10**, provided moderate to excellent regioselectivity favoring the desired product **1-15** over **1-14**. With ligand **1-9** being commercially available, this makes for a great ligand to use, however, ligand **1-10** was found to provide higher selectivity, particularly with internal bis–aliphatic substituted alkynes.
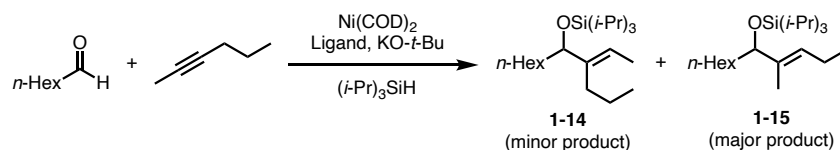
Entry	Ligand	Regioselectivity (**1-14:1-15**)	Yield (%)
1	**1-9**	33:67	83
2	**1-10**	14:86	29
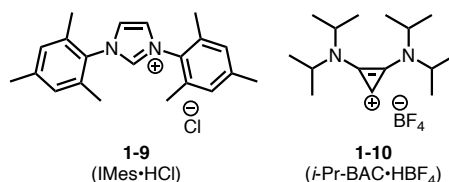
Table 1-3: Regioselectivity in aldehyde–alkyne reductive couplings with ligands **1-9** and **1-10**

1.4 Complementary Regiocontrol and Enantiocontrol in Aldehyde–Alkyne Reductive Couplings

With a strategy to control regioselectivity in the reductive coupling of aldehydes and alkynes via careful consideration of ligand size, the Montgomery lab became interested in developing a strategy to simultaneously control regioselectivity along with enantioselectivity.[8] When developing a strategy to control only regioselectivity, one of the two products needs to be favored. When developing a strategy to simultaneously control regioselectivity and enantioselectivity, one of the four products needs to be favored leading to a fundamental redesign of the ligand to render it chiral (Scheme 1-7).
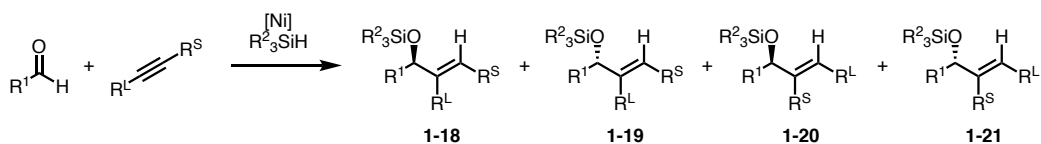
Scheme 1-6: Regiochemical and enantiochemical outcome in aldehyde–alkyne reductive couplings

To specifically favor the formation of products **1-18** and **1-19** over products **1-20** and **1-21**, the Montgomery lab focused on using the large ligand protocol.[8] From there, further development in the synthesis of large, chiral NHCs was employed to see if high enantioselectivity of either product **1-18** or **1-19** could be achieved. Results from these studies showed that large, chiral ligand **1-22** was capable of simultaneously providing high regioselectivity and high enantioselectivity favoring product **1-23** (Entry 1, Table 1-4). Additionally, high regioselectivity and high enantioselectivity was obtained at lower catalyst loadings (Entries 2 and 3, Table 1-4), however, yields were compromised (Entries 2 and 3, Table 1-4).
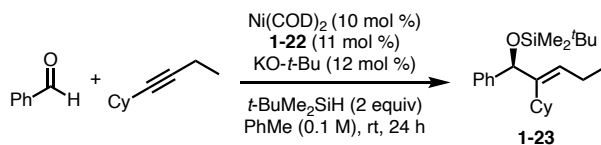
Entry	Regioselectivity	Yield (%)	Enantioselectivity (%)[c]
1	>95:5	80	92
2[a]	>95:5	47	91
3[b]	>95:5	46	87

[a]5 mol % catalyst loading; 72 h. [b]2 mol % catalyst loading; 72 h. [c]all enantioselectivity data was determined by supercritical fluid chromatography (SFC) analysis of the corresponding alcohols generated by n-Bu$_4$NF deprotextion.
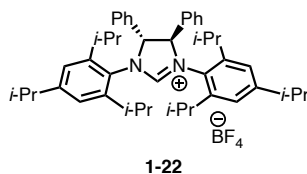
Table 1-4: Simultaneous regiocontrol and enantiocontrol in aldehyde–alkyne reductive couplings

Further studies showed that as the small substituent of the alkyne becomes larger, for example a hydrogen (Entry 1, Table 1-5) to a methyl group (Entry 2, Table 1-5) and then to an

ethyl group (Entry 3, Table 1-5), the enantioselectivity increases from 13% to 28% and then to 92%, respectively.[8] The explanation behind the enantioselectivity was determined through computations in collaboration with the Liu lab.
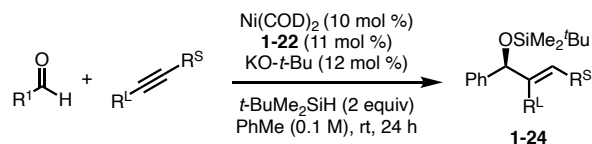
Entry	R^1	R^L	R^S	Regioselectivity	Yield (%)	Enantioselectivity (%)[a]
1	Ph	Cy	H	>95:5	72	13
2	Ph	Cy	Me	>95:5	79	28
3	Ph	Cy	Et	>95:5	80	92

[a]all enantioselectivity data was determined by supercritical fluid chromatography (SFC) analysis of the corresponding alcohols generated by n-Bu$_4$NF deprotextion.

1-22
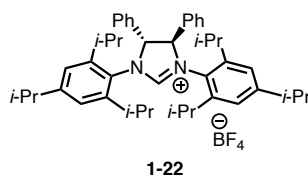
Table 1-5: Differences in enantioselectivity with changes in size of R^S

Specifically, the Liu lab used Density Functional Theory (DFT) calculations to study the oxidative cyclization transition states (Figure 1-6).[8] The major enantiomeric product (*S*) is observed due to steric interactions between the phenyl substituent on the NHC backbone and from the ethyl substituent on the alkyne, which allows the aryl group on the NHC to lay horizontal and diminish the clashing between the NHC ligand and the aldehyde. The minor enantiomeric product (*R*) is also observed due to the steric interactions between the phenyl substituent on the NHC backbone and from the ethyl substituent on the alkyne, however, the aryl group of the NHC tilts causing disfavored clashing between the NHC ligand and the aldehyde.
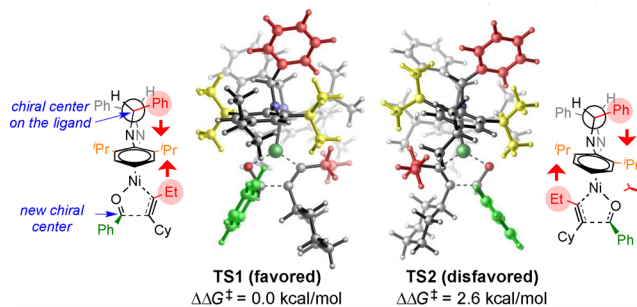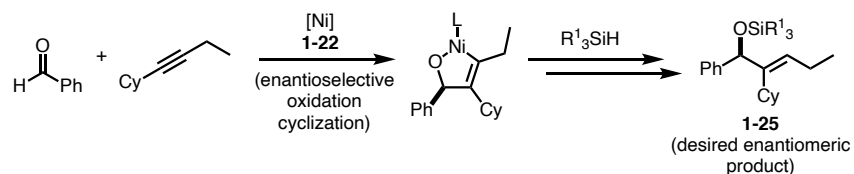
Figure 1-6: Oxidative cyclization transition states using DFT calculations[8]

1.5 Conclusion

As discussed in this chapter, the Montgomery lab developed a strategy to control regioselectivity in reductive coupling of aldehydes and alkynes without having steric and electronic biases or directing groups.[4] This strategy consisted of either utilizing the large ligand protocol or the small ligand protocol depending on the desired regioisomer product of interest. Additionally, the Montgomery lab developed a strategy to simultaneously control regioselectivity along with enantioselectivity for the large ligand protocol.[8] However, future work would need to be completed in order to develop a strategy to simultaneously control regioselectivity along with enantioselectivity for the small ligand protocol (Scheme 1-8).
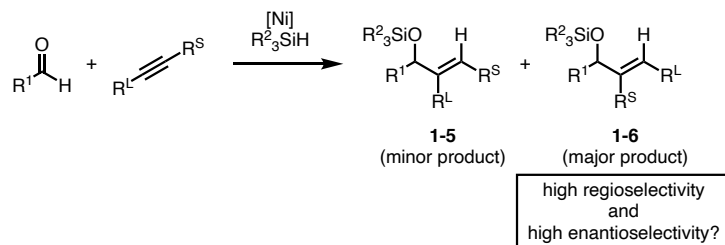
Scheme 1-7: Simultaneous regiocontrol and enantiocontrol in aldehyde–alkyne reductive couplings?

1.6 References

1. Gandeepan, P.; Muller, T.; Zell, D.; Cera, G.; Warratz, S.; Ackermann, L. *Chem. Rev.* **2019**, *119*, 2192–2452.

2. Montgomery, J. Organonickel Chemistry. In *Organometallics in Synthesis: Fourth Manual*; Lipshutz, B. H., Ed.; Wiley: Hoboken, NJ, 2013; pp 319–428.

3. Chaulagain, M. R.; Sormunen, G. J.; Montgomery, J. *J. Am. Chem. Soc.* **2007**, *129*, 9568–9569.

4. Malik, H. A.; Sormunen, G. J.; Montgomery, J. *J. Am. Chem. Soc.* **2010**, *132*, 6304–6305.

5. Liu, P.; Montgomery, J.; Houk, K. N. *J. Am. Chem. Soc.* **2011**, *133*, 6956–6959.

6. Jackson, E. P.; Montgomery, J. *J. Am. Chem. Soc.* **2015**, *137*, 958–963.

7. Jackson, E. P.; Malik, H. A.; Sormunen, G. J.; Baxter, R. D.; Liu, P.; Wang, H.; Shareef, A.; Montgomery, J. *Acc. Chem. Res.* **2015**, *48*, 1736–1745.

8. Wang, H.; Lu, G.; Sormunen, G. J.; Malik, H. A.; Liu, P.; Montgomery, J. *J. Am. Chem. Soc.* **2017**, *139*, 9317–9324.

9. Malik, H. A.; Chaulagain, M. R.; Montgomery, J. *Org. Lett.* **2009**, *11*, 5734–5737.

10. Knapp–Reed, B.; Mahandru, G. M.; Montgomery, J. *J. Am. Chem. Soc.* **2005**, *127*, 13156–13157.

11. Oblinger, E.; Montgomery J.; *J. Am. Chem. Soc.* **1997**, *119*, 9065–9066.

12. Liu, P.; McCarren, P.; Cheong, P. H. Y.; Jamison, T. F.; Houk, K. N. *J. Am. Chem. Soc.* **2010**, *132*, 2050–2057.

13. Huang, W. S.; Chan, J.; Jamison, T. F. *Org. Lett.* **2000**, 2, 4221–4223.

14. Clavier, H.; Nolan, S. P. *Chem. Commun.* **2010**, *46*, 841–861.

15. Lavallo, V.; Canac, Y.; Donnadieu, B.; Schoeller, W. W.; Bertrand, G. *Science* **2006**, *312*, 722–724.

16. Kuchenbeiser, G.; Soleilhavoup, M.; Donnadieu, B.; Bertrand, G. *Chem. Asian J.* **2009**, *4*, 1745–1750.

17. Holschumache, D.; Hrib, C. G.; Jones, P. G.; Tamm, M. *Chem. Commun.* **2007**, 3661–3663.

18. Wilde, M. M. D.; Gravel, M. *Angew. Chem. Int. Ed.* **2013**, *52*, 12651–12654.

19. Schoeller, W. W.; Frey, G. D.; Bertrand, G. *Chem. Eur. J.* **2008**, *14*, 4711–4718.

Chapter 2 Investigation of Nickel–Catalyzed Reductive Couplings: Regioselectivity and Enantioselectivity in Small Ligand Protocol and Ynal Cyclizations

2.1 Small Ligand Protocol Reproducibility

The Montgomery lab developed a small ligand protocol in the reductive coupling of aldehydes and alkynes utilizing ligand **2-1** to obtain excellent regioselectivity favoring the desired product **2-3** over **2-2** as discussed in the previous chapter (Table 2-1).[1] Reproducing these results was found to be very challenging as low yields and moderate regioselectivity were observed.
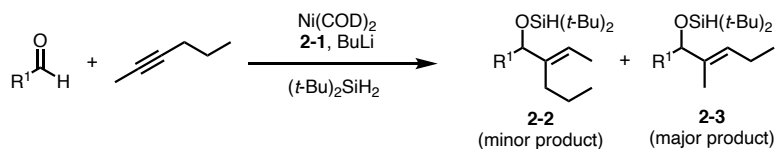
Entry	R^1	Regioselectivity (**2-2:2-3**)	Yield (%)
1	*n*-Hex	12:88	78
2	*c*-Hex	18:82	75
3	Ph	16:84	72
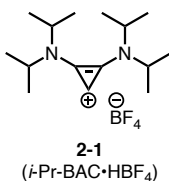
Table 2-1: Regioselectivity in aldehyde–alkyne reductive couplings with ligand 2-1

The low yields were believed to be due to the inconsistency in the deprotonation step of the *i*-Pr-BAC•HBF$_4$ salt **2-1**. To mitigate the reproducibility issue, the *i*-Pr-BAC free carbene **2-4** was made from the *i*-Pr-BAC•HBF$_4$ salt **2-1**. By using the *i*-Pr-BAC free carbene **2-4**, base was no longer needed in the reaction mixture and the deprotonation step of the ligand was removed.

Therefore, the formation of the active nickel catalyst could proceed more efficiently. Using the *i*-Pr-BAC free carbene **2-4** in combination with (*i*-Pr)$_3$SiH as the reducing agent instead of *t*-Bu$_2$SiH$_2$, higher yields and better reproducibility was observed in the reductive coupling of aldehydes and alkynes (Table 2-2). However, the yields were still only moderate. To improve yields while still obtaining high regioselectivity, engineering and design opportunities for BAC ligands were explored.
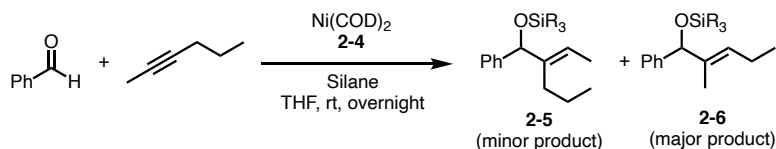
Entry	Silane	Regioselectivity (**2-5:2-6**)	Yield (%)
1	(*t*-Bu)$_2$SiH$_2$	28:72	29
2	(*i*-Pr)$_3$SiH	19:81	40
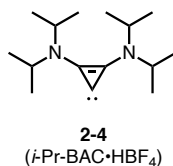
Table 2-2: Regioselectivity in aldehyde–alkyne reductive couplings with ligand **2-4**

2.1.1 Synthesis of Small Ligands

Initial studies began by synthesizing BAC ligands with appending heterocyclic amines, specifically imidazolidinones, to the cyclopropenium scaffold. By synthesizing these types of BAC ligands, the inherent chirality of the imidazolidinones would provide not only regioselectivity, but also enantioselectivity. Additionally, imidazolidinones are attractive due to their modular design and synthetic availability. With previous literature procedures, imidazolidinone **2-7** was synthesized for ease of generating preliminary studies (Scheme 2-1). The synthesis of imidazolidinone **2-7** was straight forward and relatively easy to separate from imidazolidinone **2-8**. The synthesis began with an esterification of reagent grade material L-phenylalanine, followed

by an acyl substitution to generate the corresponding amide product. The amide product underwent a Lewis acid–catalyzed cyclization with pivaldehyde to generate imidazolidinones **2-7** and **2-8**. The Lewis acid–catalyzed cyclization step to provide imidazolidinones **2-7** and **2-8** was attempted via two different pathways, pathway A and pathway B. Pathway B, developed by the Tomkinson lab, was attempted first and no product was obtained.[2] Pathway A, developed by the MacMillan lab, was attempted after Pathway B failed and resulted in low yields of imidazolidinones **2-7** and **2-8**.[3]
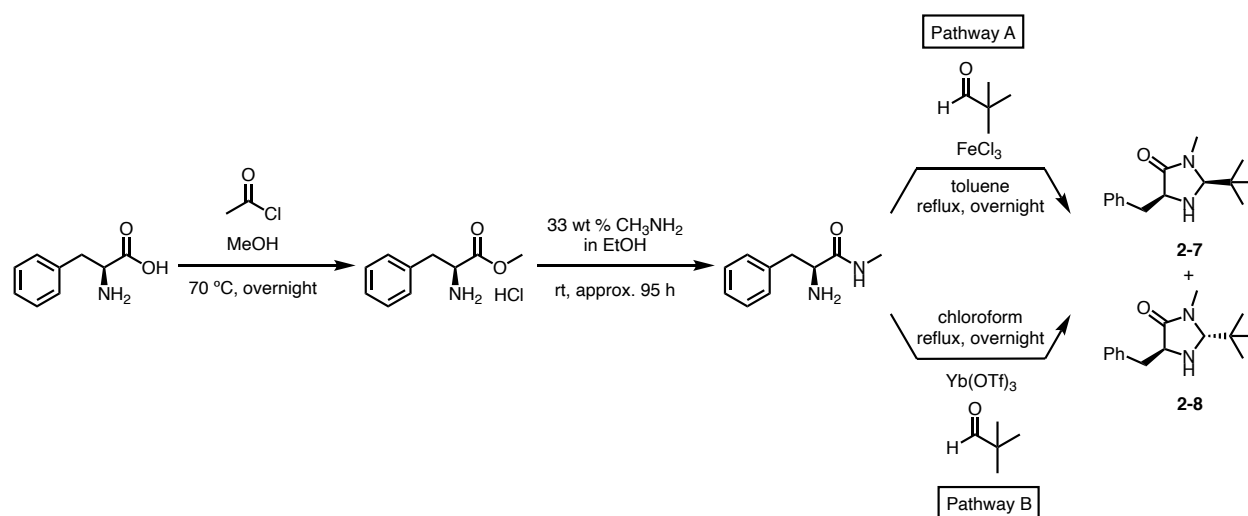
*Scheme 2-1: Synthesis of imidazolidinone **2-7***

Although imidazolidinone **2-7** was successfully separated from imidazolidinone **2-8**, there was still unknown impurities present. To remove the impurities, imidazolidinone **2-7** was converted to the HCl salt and then free based (Scheme 2-2).
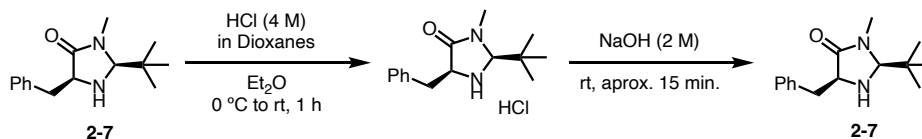
*Scheme 2-2: Purification steps for imidazolidinone **2-7***

Using a modified procedure of the *i*-Pr-BAC•HBF₄ salt **2-1** developed from the Bertrand lab, imidazolidinone **2-7** was subjected as the amine of choice to tether to the cyclopropenium

scaffold to generate a novel BAC ligand (Scheme 2-3).[4] Under those conditions, the characterization data confirmed that the tri-substituted product **2-9** was observed over the desired di-substituted product **2-10**.
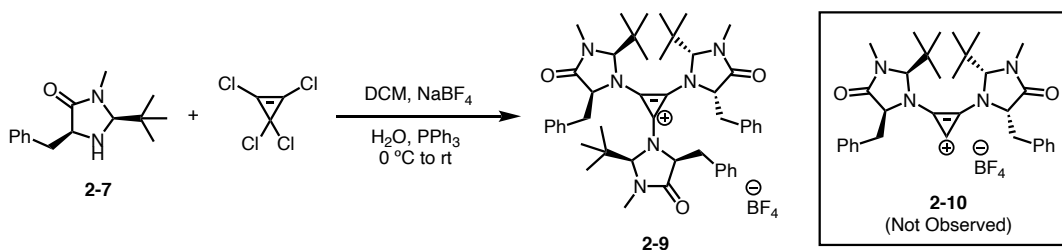
*Scheme 2-3: Attempted synthesis of BAC ligand **2-10** using Bertrand's conditions*

In an attempt to overcome tri-substitution and favor di-substitution, the amount of imidazolidinone **2-5** was reduced from 5 equivalents to 2.2 equivalents. To make up for the loss of base needed for the reaction to occur, 3 equivalents of Hünig's base was added to the reaction mixture. However, no isolation of the desired di-substituted product was acquired. Additionally, a modified BAC procedure developed by Tamm was attempted to produce the desired di-substituted product **2-10** (Scheme 2-4).[5] Again, only the tri-substituted product **2-9** was observed.
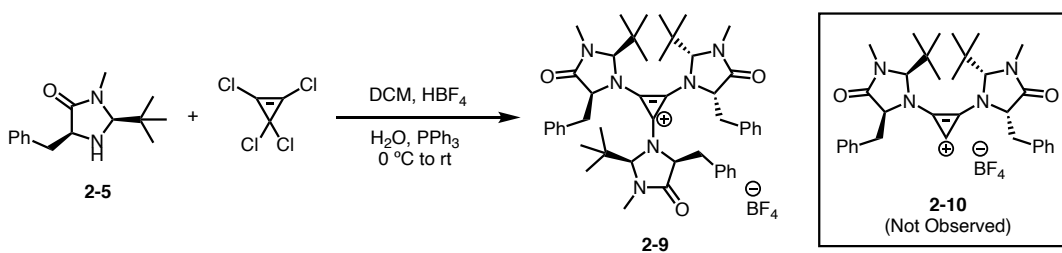
*Scheme 2-4: Attempted synthesis of BAC ligand **2-10** using Tamm's conditions*

With little success in synthesizing novel BAC ligands containing heterocyclic amines, specifically imidazolidinone **2-7**, efforts were focused on synthesizing known chiral BAC ligands **2-11** and **2-12** (Figure 2-1). Ligand **2-11** was developed by the Tamm lab and ligand **2-12** was developed by the Gravel lab.[5-6] Additionally, small, chiral NHC ligands **2-13** through **2-16** were also synthesized (Figure 2-1). These chiral ligands were then subjected to the small ligand protocol

in the reductive coupling of aldehydes and alkynes to compare yield, regioselectivity and enantioselectivity data.
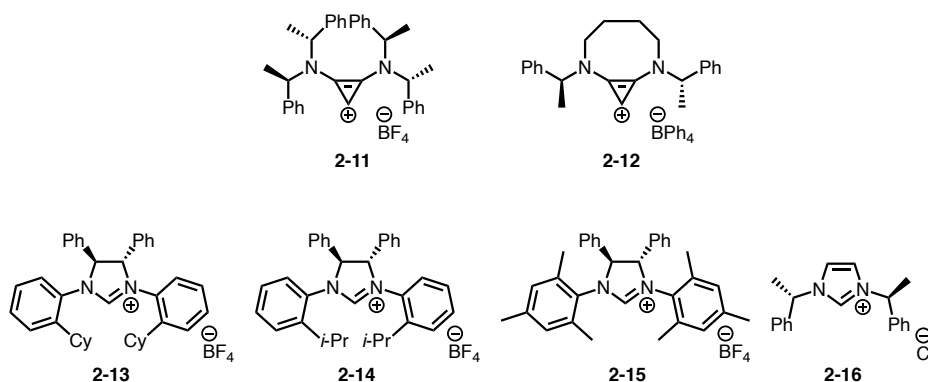
Figure 2-1: Small, chiral BAC and NHC ligands

2.2 Enantiocontrol in Small Ligand Protocol

As previously discussed, ligands **2-11** through **2-16** were subjected to the small ligand protocol in the reductive coupling of aldehydes and alkynes to compare yield, regioselectivity and enantioselectivity data (Scheme 2-5). Ligand **2-11** provided moderate yield with good regioselectivity, but poor enantioselectivity. Even though ligand **2-12** was predicted to outperform ligand **2-11** due to its more rigid structure, the ligand unfortunately provided no product formation. Ligands **2-13** through **2-15** all had the chirality located on the backbone of the NHC. Ligands **2-13** and **2-14** provided low yields with moderate regioselectivity, while ligand **2-15** provide a moderate yield with poor regioselectivity. Ligand **2-16**, with the chirality appended off the imidazolium, provided low yields with great regioselectivity, but poor enantioselectivity.
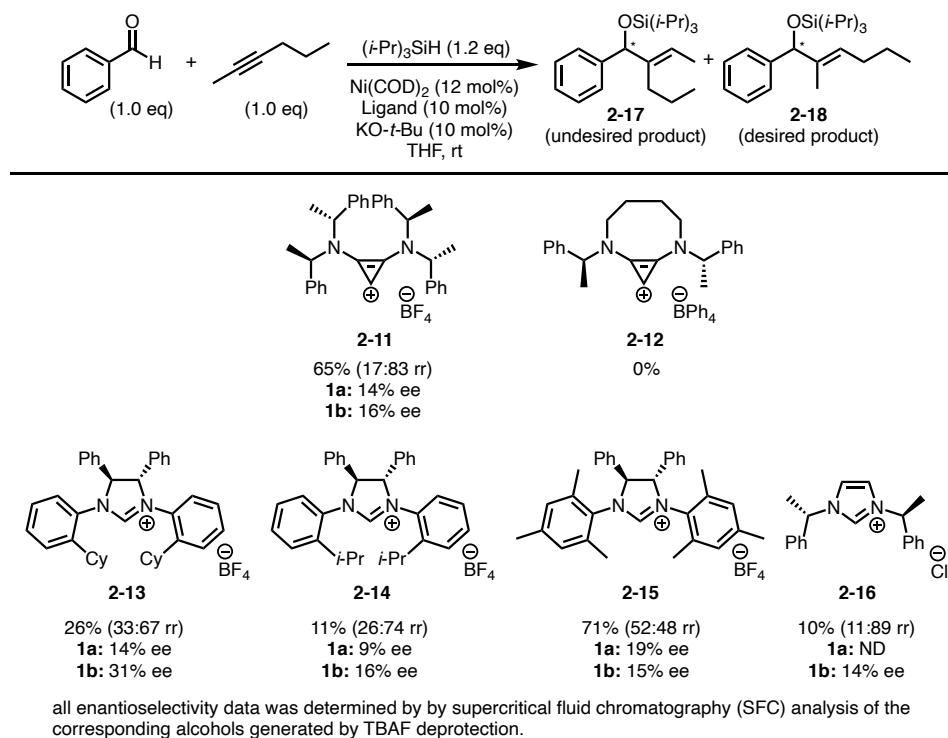
Scheme 2-5: Regioselectivity and enantioselectivity in aldehyde–alkyne reductive couplings with small, chiral ligands

Overall, ligands **2-11** through **2-16** provided poor enantioselectivity in the reductive coupling of aldehydes and alkynes. Additionally, the yields and regioselectivity were uncomplimentary as high yields did not result in good regioselectivity. To further understand the complexity of simultaneously obtaining great regioselectivity and high enantioselectivity, the reaction components would need to be reduced in order to simplify the system.

2.3 System Simplification with Intramolecular Cyclizations

The reaction components were simplified to looking at ynals where the aldehyde and alkyne are tethered. In doing so, the regiochemical outcome is determined with a bias substrate to provide product **2-19** selectively (Scheme 2-6). Therefore, chiral ligands of various sizes, both small and large, can be explored thus allowing for enantioselectivity to be the main priority of focus.
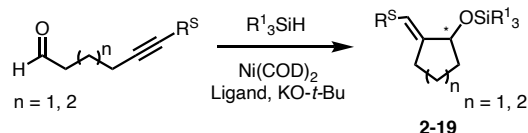
Scheme 2-6: Ynal cyclizations

2.3.1 Serendipitous Endo Product Formation

Initial studies utilized chiral ligand **2-20** in the ynal cyclizations. Surprisingly, the desired exo product **2-21** was not observed as the major product (Scheme 2-7). Instead, endo product **2-22** was observed as the major product. The formation of endo product **2-22** represents an unprecedented reaction pathway in ynal cyclizations. Ligands **2-23** through **2-25** were also subjected to the reaction conditions, however, none provided the endo product **2-22** as the major product. To understand how the formation of endo product **2-22** was favored over the exo product **2-21** in the presence of using ligand **2-20**, mechanistic studies would need to be conducted.
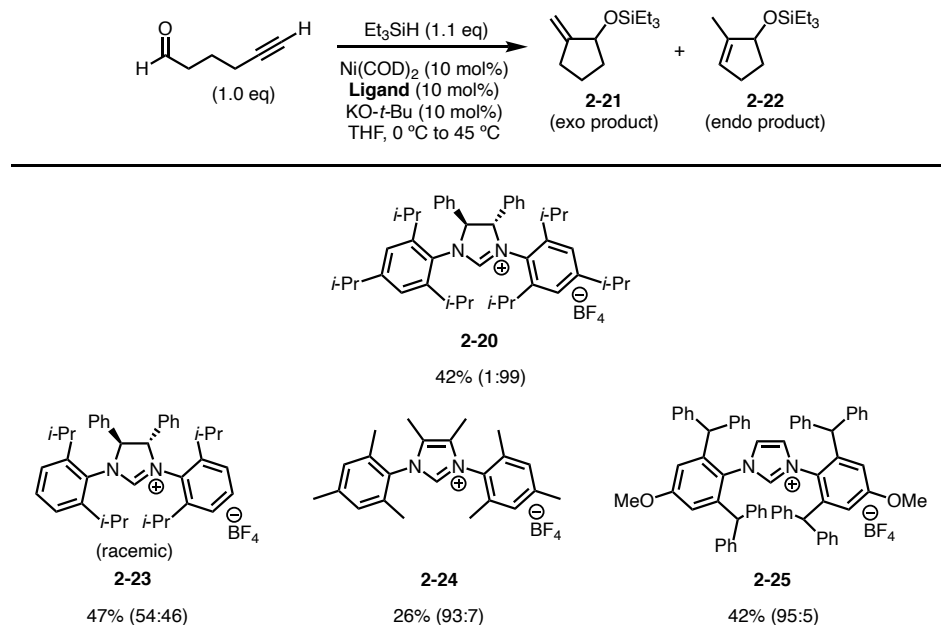
Scheme 2-7: Regioselectivity in ynal cyclizations with various ligands

2.4 Mechanistic Studies for Formation of Endo Product Formation

The formation of endo product **2-22** was hypothesized to be kinetically controlled or the result of a post–reductive coupling isomerization of product **2-21**. Various control reactions were

assessed to determine what reaction components and factors controlled the formation of endo product **2-22** (Table 2-3). A 95:5 mixture of exo product **2-21** to endo product **2-22** was subjected to the reaction conditions to evaluate a change, if any, to the ratio. When only the silane and base were present in the reaction mixture, there was no change to the ratio of exo to endo product (Entry 1, Table 2-3). When only the Ni(COD)$_2$, ligand **2-20** and base were present in the reaction mixture, there was also no change to the ratio of exo to endo product (Entry 2, Table 2-3). Additionally, when only the silane, **2-20** and base were present in the reaction mixture, there was no change to the ratio of exo to endo product (Entry 3, Table 2-3). A change in the ratio of exo to endo product was only observed when the silane and Ni(COD)$_2$ were present in the reaction mixture (Entry 4, Table 2-3). Finally, when the when the mixture was subjected to the standard reaction conditions, there was an enrichment of endo product **2-22** (Entry 5, Table 2-3).

Entry	Deviations	Regioselectivity **2-21:2-22**
1	Et$_3$SiH + KO-*t*-Bu	94:6
2	Ni(COD)$_2$ + **2-20** + KO-*t*-Bu	92:8
3	Et$_3$SiH + **2-20** + KO-*t*-Bu	95:5
4	Et$_3$SiH + Ni(COD)$_2$	70:30
5	no deviation	16:84

*Table 2-3: Control reaction studies in ynal cyclizations with ligand **2-20***

Additionally, the ratio of exo product **2-21** to endo product **2-22** was observed as a function of reaction time during the ynal cyclization to determine if the endo product **2-22** was initially formed or if gradually formed after the exo product **2-21** was formed (Table 2-4). When the

reaction was quenched after 2 minutes, the ratio of exo product **2-21** to endo product **2-22** was 96:4 (Entry 1; Table 2-4). When the reaction was quenched after 16 hours, the ratio of exo product **2-21** to endo product **2-22** was 50:50 (Entry 2, Table 2-4).
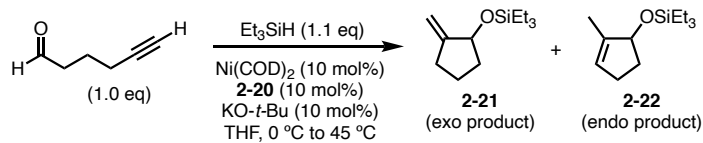
Entry	Time	Regioselectivity (**2-21:2-22**)	Yield (%)
1	2 min	96:6	58
2	16 h	50:50	40
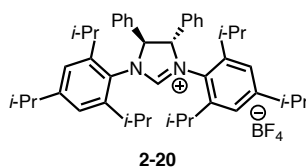
*Table 2-4: Timed reaction studies in ynal cyclizations with ligand **2-20***

In combination of the control and timed reactions, these studies showed that the Ni(COD)$_2$, **2-20**, base and silane were all needed to be present in the reaction mixture. Additionally, the endo product **2-22** gradually formed as the reaction time increased suggesting that the formation of the endo product **2-22** was occurring via an isomerization pathway (Scheme 2-8). After forming the exo product **2-21**, it is proposed that a nickel-hydride species can conduct a 1,2 migratory insertion followed by a β-hydride elimination to acquire endo product **2-22**.
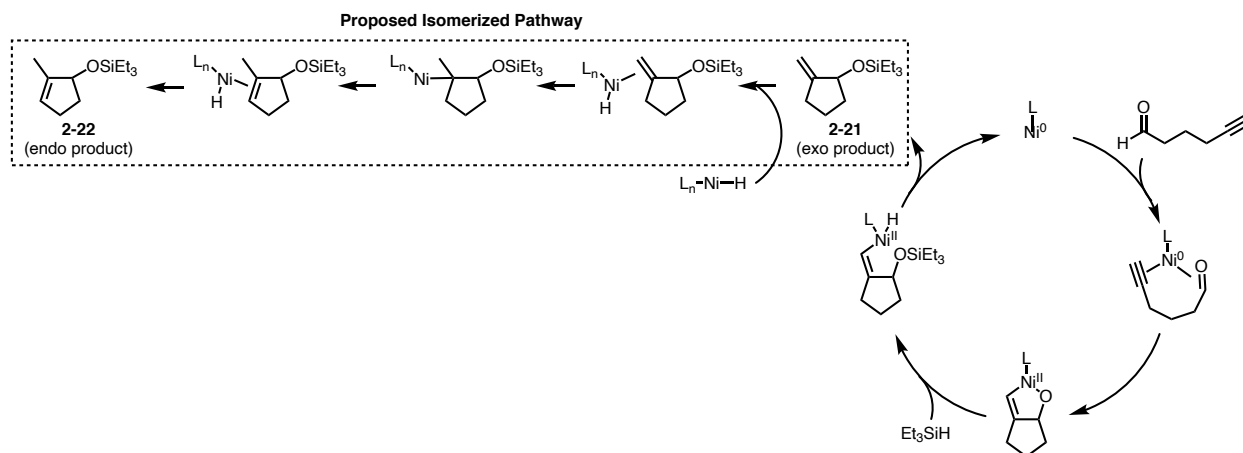
*Scheme 2-8: Proposed mechanism for endo product formation **2-22***

2.5 Enantiocontrol in Intramolecular Ynal Cyclizations

With a better understanding of the mechanism for the endo product **2-27**, various ynals were subjected to the reaction conditions with ligand **2-20** to compare yield, regioselectivity and enantioselectivity data (Table 2-5). Unfortunately, the ynal with R^S=H and n=5 was the only substrate to provide formation of the endo product **2-27** (Entries 1 and 2, Table 2-5). Furthermore, the enantioselectivity was low. If the small substituent (R^S) on the alkyne increased in sterics from a hydrogen to a methyl group or ethyl group, the enantioselectivity drastically decreased (Entries 3 through 6, Table 2-5). Lastly, the ynal with R^S=H and n=5 not only provided no formation of the endo product **2-27**, but also provided poor enantioselectivity (Entries 7 and 8, Table 2-5).

Et₃SiH (1.1 eq)

Ni(COD)₂ (10 mol%)
2-20 (10 mol%)
KO-*t*-Bu (10 mol%)
THF, 0 °C to 45 °C

(1.0 eq)

2-26
(exo product)

+

2-27
(endo product)
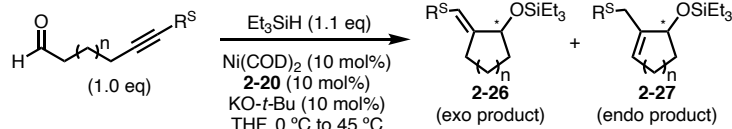
Entry	RS	n	Time	% Yield	2-26:2-27	2-26 (% ee)[a]	2-27 (% ee)[a]
1	H	1	2 min	58	94:6	32	29
2	H	1	16 h	40	50:50	33	7
3	Me	1	2 min	27	100:0	5	–
4	Me	1	16 h	50	100:0	1	–
5	Et	1	2 min	27	100:0	5	–
6	Et	1	16 h	35	100:0	5	–
7	H	2	2 min	56	100:0	6	–
8	H	2	16 h	50	100:0	2	–

[a]all enantioselectivity data was determined by Mosher Ester Analysis of the corresponding alcohols generated by TBAF deprotection.

2-20
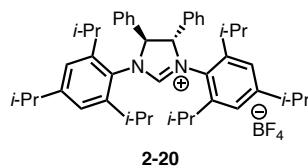
*Table 2-5: Regioselectivity and enantioselectivity in ynal cyclizations with ligand **2-20***

Although it was unfortunate that the ynal with R^S=H and n=5 was the only substrate to provide formation of the endo product **2-27**, this suggests that the Ni-H species only allows for isomerization to occur for very specific substrate classes, diminishing the value of this new reactivity. Additionally, it is interesting that the formation of the more stable endo product **2-28** was never observed under the standard reaction reactions (Figure 2-2). However, it is proposed that the silyl ether group is sterically encumbering to allow for the isomerization to take place providing the more stable endo product **2-28**.

2-22
(endo product)

2-28
(endo product)
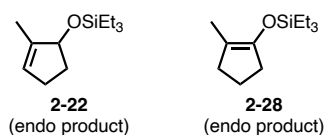
*Figure 2-2: Endo product **2-22** versus endo product **2-28***

26

2.6 Conclusion and Future Directions

As discussed in this chapter, the synthesis of novel BAC ligands was more challenging than expected. Also, obtaining great regioselectivity and high enantioselectivity simultaneously in the small ligand protocol proved to be extremely challenging. Even though an endo product in the ynal cyclizations was serendipitously discovered, it was only observed for one privileged substrate. To further explore and understand how to simultaneously obtain great regioselectivity and high enantioselectivity, future work will need to investigate the synthesis of other novel BAC ligands. However, efforts were shifted to synthesizing discrete Ni(0) complexes in order to further improve reproducibility in yields, while also obtaining mechanistic data to gain further insights on how to improve regioselectivity and enantioselectivity in the small ligand protocol (Figure 2-3).
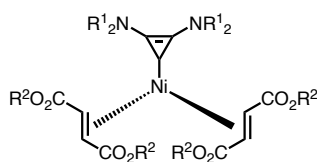
Figure 2-3: Discrete Ni(0) complexes

2.7 References

1. Malik, H. A.; Sormunen, G. J.; Montgomery, J. *J. Am. Chem. Soc.* **2010**, *132*, 6304–6305.

2. Samulis, L.; Tomkinson, N. C. O. *Tetrahedron* **2011**, *67*, 11413–11424.

3. Lee, S.; MacMillan, D. W. C. *Tetrahedron* **2006**, *62*, 11413–11424.

4. Kuchenbeiser, G.; Soleilhavoup, M.; Donnadieu, B.; Bertrand, G. *Chem. Asian J.* **2009**, *4*, 1745–1750.

5. Holschumache, D.; Hrib, C. G.; Jones, P. G.; Tamm, M. *Chem. Commun.* **2007**, 3661–3663.

6. Wilde, M. M. D.; Gravel, M. *Angew. Chem. Int. Ed.* **2013**, *52*, 12651–12654.

Chapter 3 Introduction to Nickel–Catalyzed Reductive Couplings: Utility of Well–Defined Ni(0) Complexes

3.1 General Overview of Ni(0) Complexes

As discussed in the previous chapters, the development of catalysis employing base metals, such as nickel, for organic transformations has become a vested interest for the synthetic community over the past couple decades.[1-4] The Montgomery lab has a long–standing focus in the development of novel nickel–catalyzed processes, particularly with NHC ligands.[1,5-15] Generally speaking, the active Ni(0) catalyst is generated *in situ*, which can be undesirable and create many limitations for various processes (Scheme 3-1). First, Ni(COD)$_2$ is used as the Ni(0) source, which is not air-tolerant and requires the use of a glovebox for storage. Second, the NHC used can be in the salt form or the free carbene form. The salt form **3-1**, although stable, requires base for deprotonation in order to generate the active NHC–Ni(0) catalyst. The free carbene **3-2**, although does not require base for deprotonation, is not stable and needs to be stored in the glovebox. Third, the quantity of NHC–Ni(0) catalyst **3-3** generated via the *in situ* protocols is not well defined.

3-1
(IMes·HCl)

3-3

3-2
(IMes)
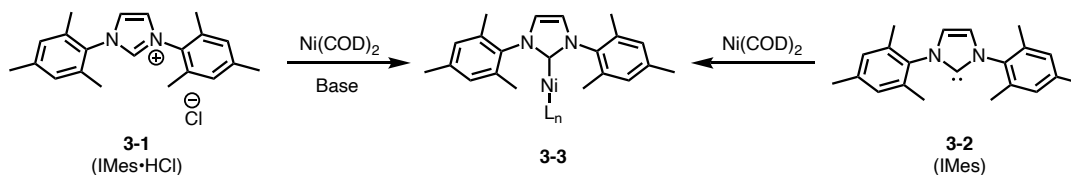
Scheme 3-1: NHC–Ni(0) catalyst formation

To overcome these undesirable limitations, various types of NHC–Ni(0) complexes have been synthesized over the years.[16-28] However, many of these NHC–Ni(0) complexes were not able to overcome all of the limitations, specifically stability and sensitivity. Therefore, the

widespread use of these catalysts has been limited. In addition to these various types of NHC–Ni(0) complexes synthesized, there were two complexes that did bring awareness to the Montgomery lab, which were complexes **3-4** and **3-5** (Figure 3-1).[16,17] The Cavell lab developed the well–defined IMes–Ni(0) complex **3-4** and the Navarro lab developed the well–defined IPr–Ni(0) complex **3-5**.[16,17] Both complexes showed ability to be air–tolerant, however, this came at the expense of reduced reactivity, specifically in the reductive coupling of aldehydes and alkynes. The stability of these complexes was attributed to the ancillary ligands bound to the nickel center. For both complexes, the ancillary ligand of choice was dimethyl fumarate (DMFU). The design of these particular complexes sparked interest in the Montgomery lab to use various π–acidic additives as ancillary ligands to generate a variety of NHC–Ni(0) complexes. Acquiring well–defined and easy to synthesize NHC–Ni(0) complexes that maintain air–stability, but are still reactive was desired and had the potential to be achieved by changing the steric and electronic profile of π–acidic additives such as fumarate and acrylates.

3-4   **3-5**
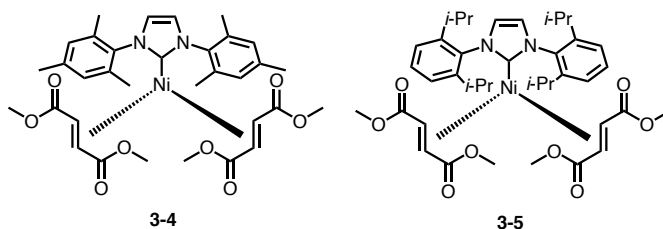
Figure 3-1: Ni(IMes)(dimethyl fumarate)₂ 3-4 and Ni(IPr)(dimethyl fumarate)₂ 3-5

3.2 NHC–Ni(0) Complexes in Skipped Diene Formation

As discussed previously, the Montgomery lab was interested in utilizing various π–acidic additives as ancillary ligands to generate active, but air-tolerant NHC–Ni(0) complexes that are well–defined and easy to make. In a quest to develop a nickel–catalyzed net four–electron reductive coupling of enones / enals with alkynes to provide skipped diene product **3-6**, ITol•HBF$_4$ salt **3-7** provided a moderate yield of 37% (Scheme 3-2).[29]
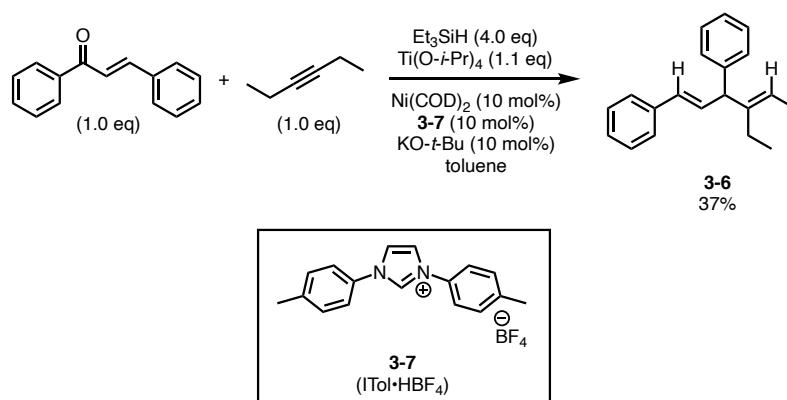
*Scheme 3-2: Skipped diene formation with ligand **3-7***

Preceding studies with BAC and small NHC ligands, as discussed in chapter 2, indicated that it was common to observe low to moderate yields along with inconsistency in reproducing results.[29] With ITol being considered a small NHC ligand, this created limitations in developing a method to generate the skipped diene products in high yields. To obtain high and consistent yields of the skipped diene products, well–defined complex **3-8** was synthesized. For this particular complex, methyl methacrylate (MMA) was utilized as the ancillary ligands. This easy to synthesize complex not only provided high yields increasing the reactivity from 37% to 90%, but also offered moderate stability upon air exposure (Scheme 3-3). Additionally, it demonstrated the utility of using these well–defined Ni(0) complexes.
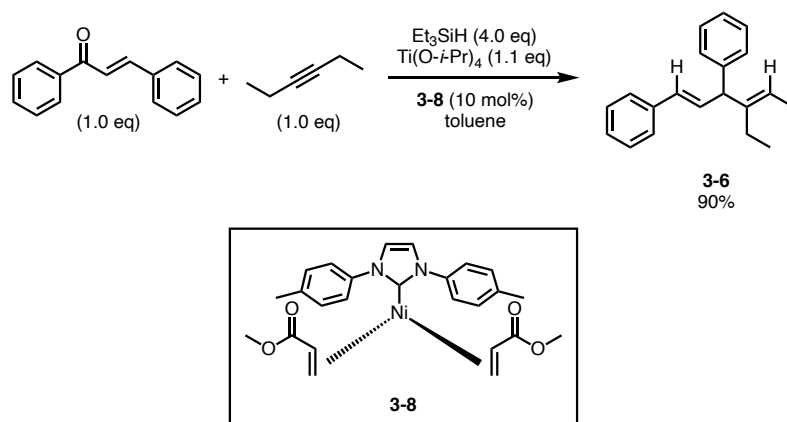
*Scheme 3-3: Skipped diene formation with complex **3-8***

3.3 NHC–Ni(0) Complexes in Aldehyde–Alkyne Reductive Couplings

The well–defined IMes–Ni(0) complex **3-4** developed by the Cavell lab was subjected to the reaction conditions for the reductive coupling of aldehydes and alkynes (Scheme 3-4).[5,16] Unfortunately, only a trace amount of the reductive coupling product **3-9** was observed. To further investigate the utility of these well–defined Ni(0) complexes, the Montgomery lab synthesized a series of NHC–Ni(0) complexes by varying the π–acidic additives using fumarates and acrylates. The fumarates and acrylates varied by properties such as sterics and electronics. The Ni(0) complexes were then subjected to the reaction conditions for the reductive coupling of aldehydes and alkynes to evaluate and compare their stability and activity profiles.
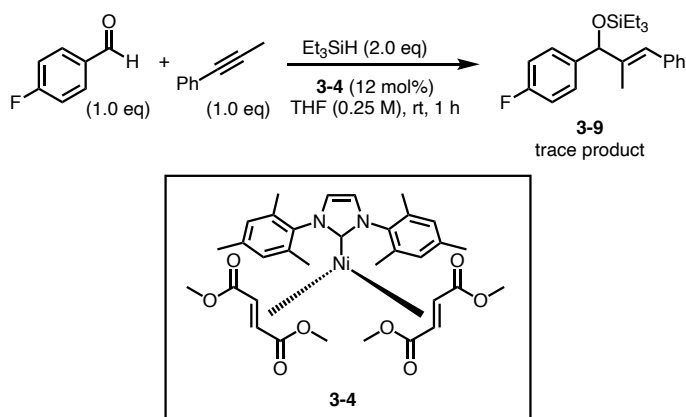
*Scheme 3-4: Aldehyde–alkyne reductive couplings with complex **3-4***

3.3.1 Synthesis of IMes–Ni(0) Complexes

Looking back at the well–defined IMes–Ni(0) complex **3-4** developed by the Cavell lab, it was thought to have performed poorly in the reductive coupling of aldehydes and alkynes due to the ineffective dissociation of the fumarate ligands.[5,16] To improve dissociation of the fumarate ligands, the Montgomery lab hypothesized that the ester moiety on the fumarate would need to increase in size. By increasing the steric bulk of the ester moiety on the fumarate, this would create disfavoring steric interactions with the IMes ligand (Figure 3-2). Therefore, the binding energies of the fumarates to the nickel species would be weaker and easier to dissociate.
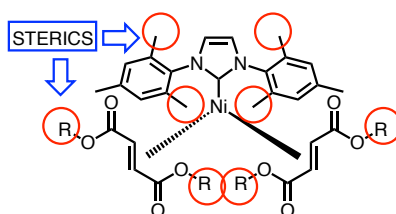
Figure 3-2: Steric interactions between IMes and the fumarate ligands

Using IMes free carbene **3-2** in the presence of Ni(COD)$_2$, various fumarates and acrylates were subjected to the reaction mixture to generate a series of IMes–Ni(0) complexes, **3-10** through **3-15** (Scheme 3-5).[5] Steric bulk of the ester moiety on the fumarate increased in size ranging from a methyl group to a tert-butyl group to generate well–defined Ni(0) complexes. Methyl acrylate and methyl methacrylate also generated well–defined Ni(0) complexes. In terms of the ease of synthesis, dimethyl fumarate is the only commercially available fumarate. The other fumarates all had to be synthesized.[5] Methyl acrylate (MA) and methyl methacrylate (MMA) are commercially available; however, they need to be distilled prior to use to remove the stabilizer. It is also important to note that the acrylates should be used immediately following distillation to avoid polymerization.
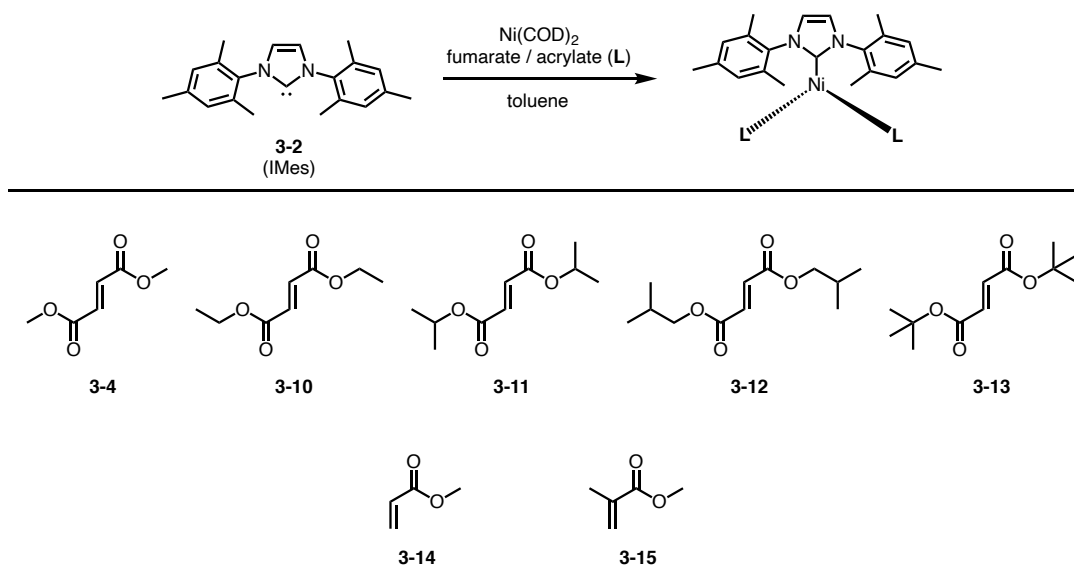
*Scheme 3-5: Synthesis of Ni(IMes)(fumarate / acrylate)₂ complexes **3-4** and **3-10** through **3-15***

3.3.2 Analysis of IMes–Ni(0) Complexes in Aldehyde–Alkyne Reductive Couplings

The Ni(0) complexes were subjected to the reaction conditions for the reductive coupling of aldehydes and alkynes to evaluate and compare their stability and activity profiles (Figure 3-3).[5] Analyzing the reaction progress data, all of the Ni(0) complexes except for complex **3-4** provided product formation. Complexes **3-10** through **3-12** with small amounts of steric bulk on the ester moiety of the fumarate provided slower rates of product formation. Complex **3-13** with large amounts of steric bulk on the ester moiety of the fumarate provided a faster rate of product formation. Complex **3-13** not only provided the fastest rate of product formation, but also had the best overall performance. This supports the hypothesis that increasing the steric bulk of the ester moiety on the fumarate creates disfavoring steric interactions with the IMes ligand, thus allowing for dissociation to occur easier. Additionally, complex **3-15** performed better than complex **3-14**.
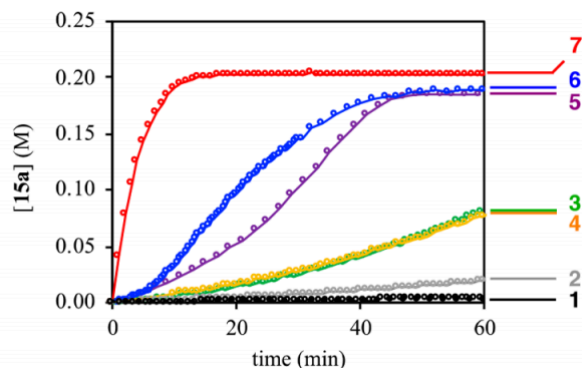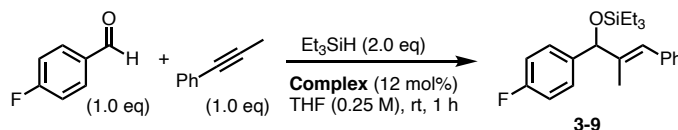
Figure 3-3: Reaction progress data for IMes–Ni(0) complexes in aldehyde–alkyne reductive couplings[5]

Reaction progress data was also analyzed with the same complexes after they had been exposed to air for 24 hours (Figure 3-4).[5] Complexes **3-10**, **3-12** and **3-13** with fumarate ligands maintained their catalytic activity as seen previously when not exposed to air. However, the catalytic activity of complexes **3-14** and **3-15** with acrylate ligands was compromised. This

suggests that complexes with acrylate ligands are more susceptible to decomposition when exposed to air as compared to complexes with fumarate ligands.
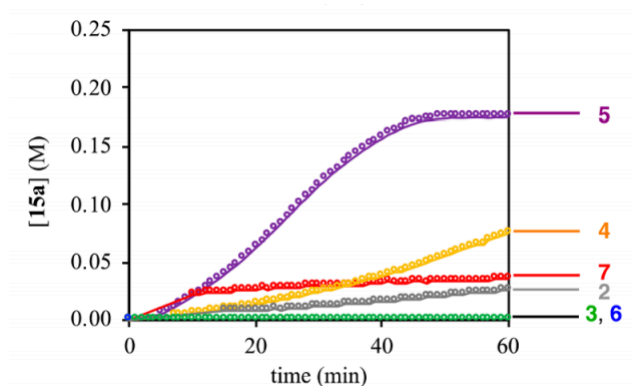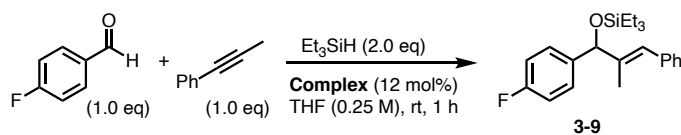
Figure 3-4: Reaction progress data for IMes–Ni(0) complexes after 24 h air exposure in aldehyde–alkyne reductive couplings[5]

Of the various complexes that were synthesized and subjected to the reaction conditions for the reductive coupling of aldehydes and alkynes, complex **3-13** was found to provide the best reactivity without being compromised after being exposed to air.[5]

3.4 Synthesis of Other NHC–Ni(0) Complexes

As discussed previously, increasing the steric bulk of the ester moiety on the fumarate creates disfavoring steric interactions with the IMes ligand.[5] When IMes is replaced with a much larger NHC such as IPr or SIPr, the sterics between the NHC ligand and the steric bulk of the ester moiety on the fumarate can be further enhanced making it difficult to form the NHC–Ni(0) complex of interest (Figure 3-5).
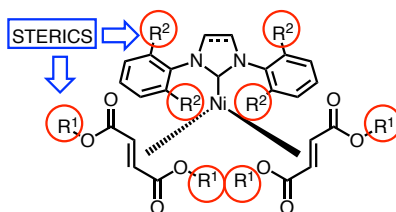
Figure 3-5: Steric interactions between a large NHC and the fumarate ligands

In addition to the IMes–Ni(0) complexes, other NHC–Ni(0) complexes were synthesized specifically with large NHCs (Scheme 3-6).[5] With inherently large steric crowding from the NHCs, the complexes were easily synthesized and well-defined using acrylate ligands.
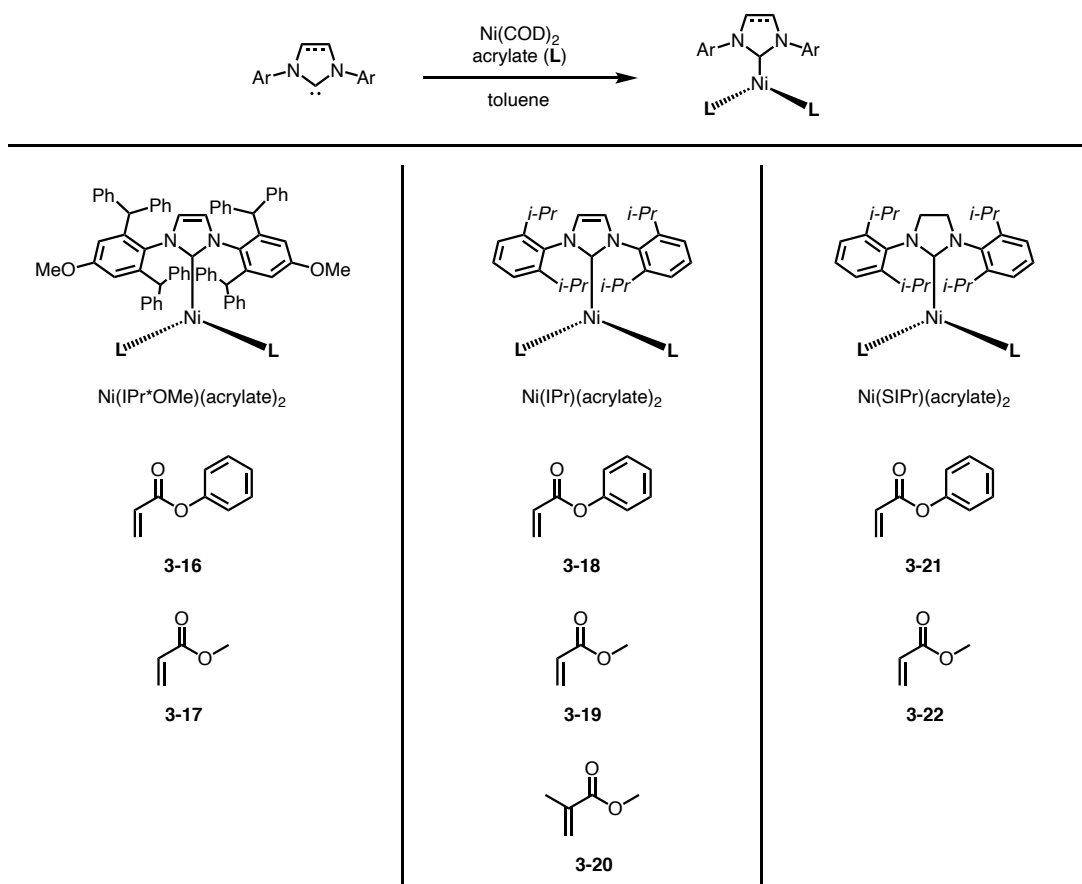
*Scheme 3-6: Synthesis of Ni(NHC)(acrylate)₂ complexes **3-16** through **3-22***

3.5 Synthesis of BAC–Ni(0) Complexes

Up until this point in time, there has been very little investigation into the synthesis of BAC–Ni(0) complexes. The only known nickel complex with a BAC ligand synthesized is

complex **3-22** (Figure 3-5).[30] This particular complex of interest acquires two BAC ligands bound to the nickel center with the chelation of COD. It is hypothesized that two BAC ligands can be bound to the nickel center simultaneously due to its small steric profile.

3-23

Figure 3-6: Ni(BAC)₂(COD) **3-23**

With BAC–Ni(0) scaffolds lacking, the Montgomery lab became interested in synthesizing these novel complexes as it poses opportunities to broaden the synthetic utility for a variety of nickel–catalyzed processes. Since the BAC ligands proved to be successful ligand in the reductive coupling of aldehydes and alkynes, the BAC–Ni(0) scaffolds could be evaluated for reactivity, reproducibility and stability. Furthermore, the Montgomery lab was also interested to see if the mono BAC–Ni(0) complex **3-25** could be favored over the bis BAC–Ni(0) complex **3-24** (Scheme 3-7).

3-24   **3-25**

Scheme 3-7: Favoring mono BAC–Ni(0) complex **3-25** *over bis BAC–Ni(0) complex* **3-24**

3.6 Conclusion

As discussed in this chapter, the Montgomery lab was successful at synthesizing various NHC–Ni(0) complexes that provided a range of reactivity and stability profiles in various nickel-catalyzed processes.[5,21,22,29] However, it was still unclear how the dissociation of the ancillary ligands was occurring to form the active catalyst, particularly in the reductive coupling of

aldehydes and alkynes (Scheme 3-8). Was it just a simple ligand dissociation in exchange for the

reactive substrates or was it something more complex?
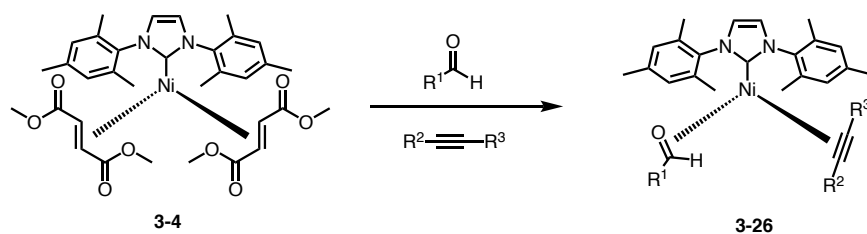
Scheme 3-8: Ni(0) catalyst activation

3.7 References

1. Montgomery, J. Organonickel Chemistry. In *Organometallics in Synthesis: Fourth Manual*; Lipshutz, B. H., Ed.; Wiley: Hoboken, NJ, 2013; pp 319–428.

2. Tasker, S. Z.; Standley, E. A.; Jamison, T. F. Recent Advances in Homogenous Nickel Catalysis. *Nature* **2014**, *509*, 299–309.

3. Prakasham, A. P.; Ghosh, P. Nickel N-Heterocyclic Carbene Complexes and Their Utility in Homogenous Catalysis. *Inorganica Chim. Acta* **2015**, *431*, 61–100.

4. Arévalo, A.; García, J. J. Bond Activation with Low–Valent Nickel in Homogenous Systems. *Eur. J. Inorg. Chem.* **2010**, *2010*, 4063–4074.

5. Nett, A. J.; Cañellas, S.; Higuchi, Y.; Robo, M. T.; Kochkodan, J. M.; Haynes, M. T.; Kampf, J. W.; Montgomery, J. *ACS Catal.* **2018**, *8*, 6606–6611.

6. Malik, H. A.; Sormunen, G. J.; Montgomery, J. *J. Am. Chem. Soc.* **2010**, *132*, 6304–6305.

7. Liu, P.; Montgomery, J.; Houk, K. N. *J. Am. Chem. Soc.* **2011**, *133*, 6956–6959.

8. Jackson, E. P.; Montgomery, J. *J. Am. Chem. Soc.* **2015**, *137*, 958–963.

9. Jackson, E. P.; Malik, H. A.; Sormunen, G. J.; Baxter, R. D.; Liu, P.; Wang, H.; Shareef, A.; Montgomery, J. *Acc. Chem. Res.* **2015**, *48*, 1736–1745.

10. Wang, H.; Lu, G.; Sormunen, G. J.; Malik, H. A.; Liu, P.; Montgomery, J. *J. Am. Chem. Soc.* **2017**, *139*, 9317–9324.

11. Malik, H. A.; Chaulagain, M. R.; Montgomery, J. *Org. Lett.* **2009**, *11*, 5734–5737.

12. Montgomery, J.; Sormunen, G. J. *Topp. Curr. Chem.* **2007**, *279*, 1–23.

13. Chaulagain, M. R.; Sormunen, G.; Montgomery, J. *J. Am. Chem. Soc.* **2007**, *129*, 9568–9569.

14. Knapp–Reed, B.; Mahandru, G. M.; Montgomery, J. *J. Am. Chem. Soc.* **2005**, *127*, 13156–13157.

15. Oblinger, E.; Montgomery J.; *J. Am. Chem. Soc.* **1997**, *119*, 9065–9066.

16. Clement, N. D.; Cavell, K. J.; Ooi, L.–1. *Organometallics* **2006**, *25*, 4155–4165.

17. Berini, C.; Winkelmann, O. H.; Otten, J.; Vicic, D. A.; Navarro, O. *Chem. Eur. J.* **2010**, *16*, 6857–6860.

18. Wu, J.; Faller, J. W.; Hazari, N.; Schmeier, T. J. *Organometallics* **2012**, *31*, 806–809.

19. Wu, J.; Hazari, N.; Incarvito, C. D. *Orgnaometallics* **2011**, *30*, 3142–3150.

20. Rodrigo, S. K.; Guan, H. *J. Org. Chem.* **2017**, *82*, 5230–5235.

21. Nett, A. J.; Zhau, W.; Zimmerman, P. M.; Montgomery, J. *J. Am. Chem. Soc.* **2015**, *137*, 7636–7639.

22. Nett, A. J.; Montgomery, J.; Zimmerman, P. M. *ACS Catal.* **2017**, *7*, 7352–7362.

23. Elsby, M. R.; Johnson, S. A. *J. Am. Chem. Soc.* **2017**, *139*, 9401–9407.

24. Iglesias, M. J.; Blandez, J. F.; Fructos, M. R.; Prieto, A.; Álvarez, E.; Belderrain, T. R.; Nicasio, M. C. *Organometallics* **2012**, *31*, 6312–6316.

25. Blair, J. S.; Schramm, Y.; Sergeev, A. G.; Clot, E.; Eisenstein, O.; Hartwig, J. F. *J. Am. Chem. Soc.* **2014**, *136*, 13098–13101.

26. Hoshimoto, Y.; Hayashi, Y.; Suzuki, H.; Ohashi, M.; Ogoshi, S. *Organometallics* **2014**, *33*, 1276–1282.

27. Schramm, Y.; Takeuchi, M.; Semba, K.; Nakao, Y.; Hartwig, J. F. *J. Am. Chem. Soc.* **2015**, *137*, 12215–12218.

28. Laskowski, C. A.; Miller, A. J. M.; Hillhouse, G. L.; Cundari, T. R. *J. Am. Chem. Soc.* **2011**, *133*, 771–773.

29. Todd, D. P.; Thompson, B. B.; Nett, A. J.; Montgomery, J. *J. Am. Chem. Soc.* **2015**, *137*, 12788–12791.

30. Kuchenbeiser, G.; Donnadieu, B.; Bertrand, G. *J. Organomet. Chem.* **2008**, *693*, 899–904.

Chapter 4 Investigation of Nickel–Catalyzed Reductive Couplings: Catalyst Activation of Ni(0) Complexes

4.1 Synthesis of IMes–Ni(0) Complexes Extension

The Montgomery lab synthesized various novel NHC–Ni(0) complexes that provided a range of reactivity and stability profiles as discussed in the previous chapter.[1-4] Specifically focusing on the IMes–Ni(0) complexes with fumarate ligands, this particular class of complexes was expanded including additional fumarates of varying steric and electronic properties (Scheme 4-1).[1] This sizable class of IMes–Ni(0) complexes with fumarate ligands allowed for a large pool of data to be obtained in order to better compare their activity and stability profiles in the reductive coupling of aldehydes and alkynes.
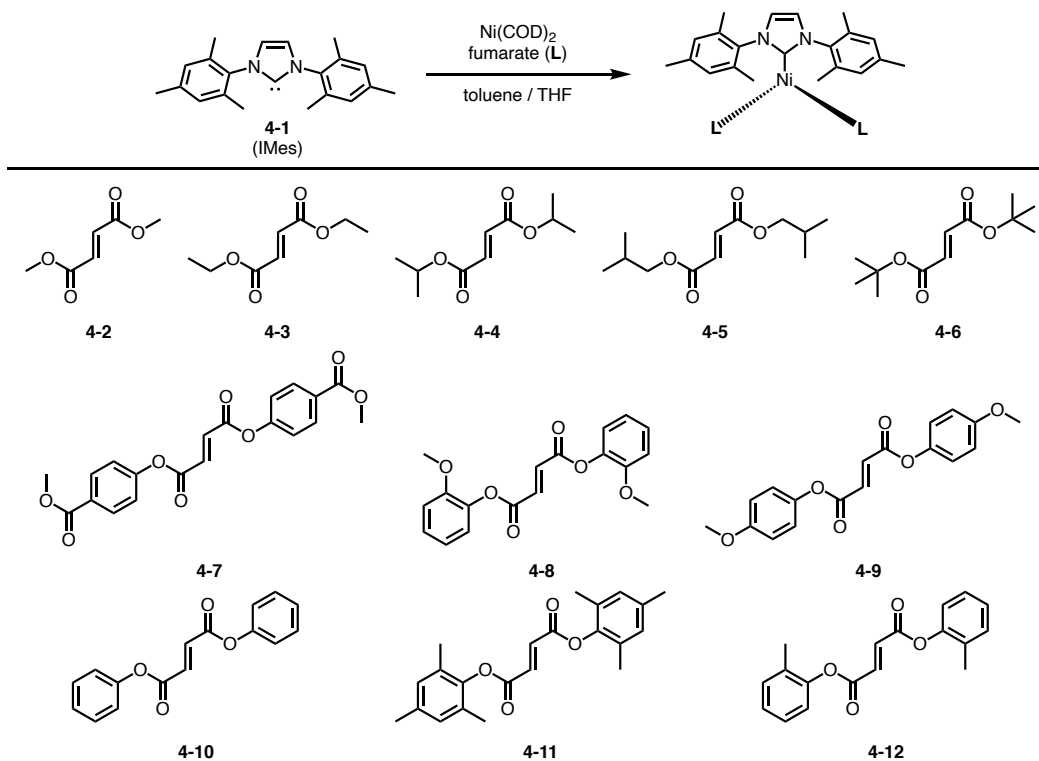
Scheme 4-1: Expansion on the synthesis of IMes–Ni(0) complexes

4.2 IMes–Ni(0) Complexes in Aldehyde–Alkyne Reductive Couplings Extension

The IMes–Ni(0) complexes were subjected to the reaction conditions for the reductive coupling of aldehydes and alkynes to evaluate and compare their stability and activity profiles. The IMes–Ni(0) complexes with alkyl fumarates provided high yields of product **4-13** with the exception of complex **4-2** (Figure 3-3). As seen in previous studies, it was expected to see little to no formation of product **4-13** due to the ineffective dissociation of the fumarate ligands.[1]
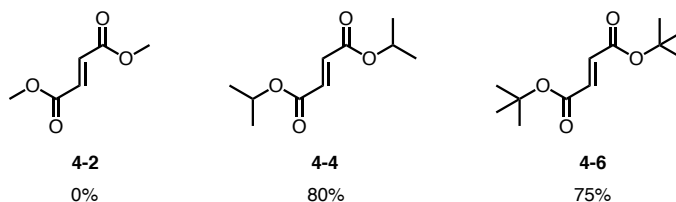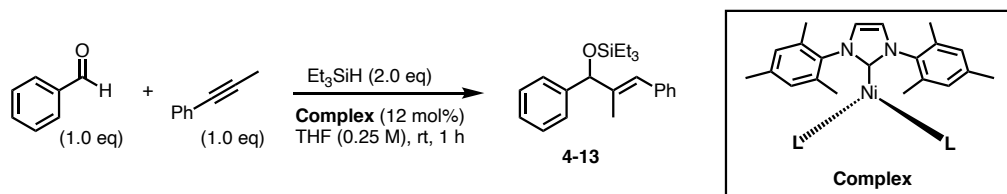
*Scheme 4-2: Aldehyde–alkyne reductive couplings with IMes–Ni(0) complexes **4-2, 4-4** and **4-6***

The IMes–Ni(0) complexes with aryl fumarates all provided product formation of **4-13**. However, the yields varied between the different IMes–Ni(0) complexes. Complexes **4-10**, **4-7** and **4-8** gave the lowest yields of 17%, 20% and 27%, respectively, for product **4-13**. Complex **4-9** gave a modest yield of 55% for product **4-13**. Lastly, complexes **4-11** and **4-12** gave high yields of 76% and 80%, respectively, for product **4-13**. Between the data shown here and the data discussed in the previous chapter, complex **4-6** of the IMes–Ni(0) complexes with alkyl fumarates and complex **4-12** of the IMes–Ni(0) complexes with aryl fumarates provided the best reactivity in the reductive coupling of aldehydes and alkynes.[1]
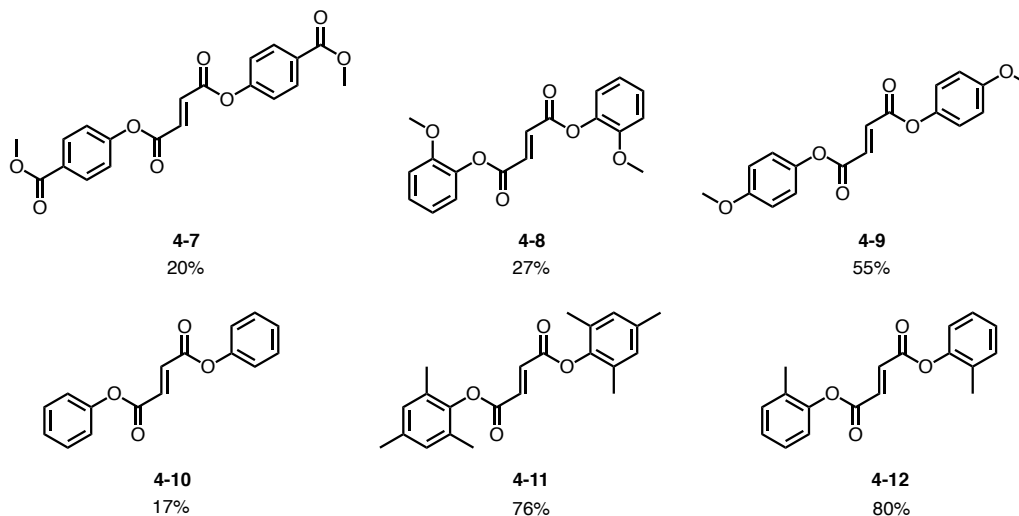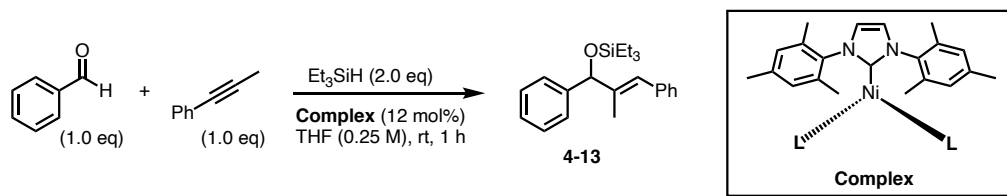
*Scheme 4-3: Aldehyde–alkyne reductive couplings with IMes–Ni(0) complexes **4-7** through **4-12***

Additionally, reaction progress data was analyzed for some selected IMes–Ni(0) complexes with aryl fumarates and compared to reaction progress data for IMes–Ni(0) complexes with alkyl fumarates discussed in the previous chapter (Figure 4-1).[1] As previously discussed, complex **4-6** was found to provide the best reactivity of the IMes–Ni(0) complexes with alkyl fumarates. Using complex **4-6** as a reference, complex **4-12** provided great reactivity. However, complex **4-7** provided no reactivity. This is thought to be due to the electron–withdrawing groups on the aryl groups of the fumarates. These electron–withdrawing groups on the fumarate allow for significant π back–bonding of the Ni to the fumarate. Therefore, the dissociation of the fumarate ligands is difficult resulting in a stable complex.
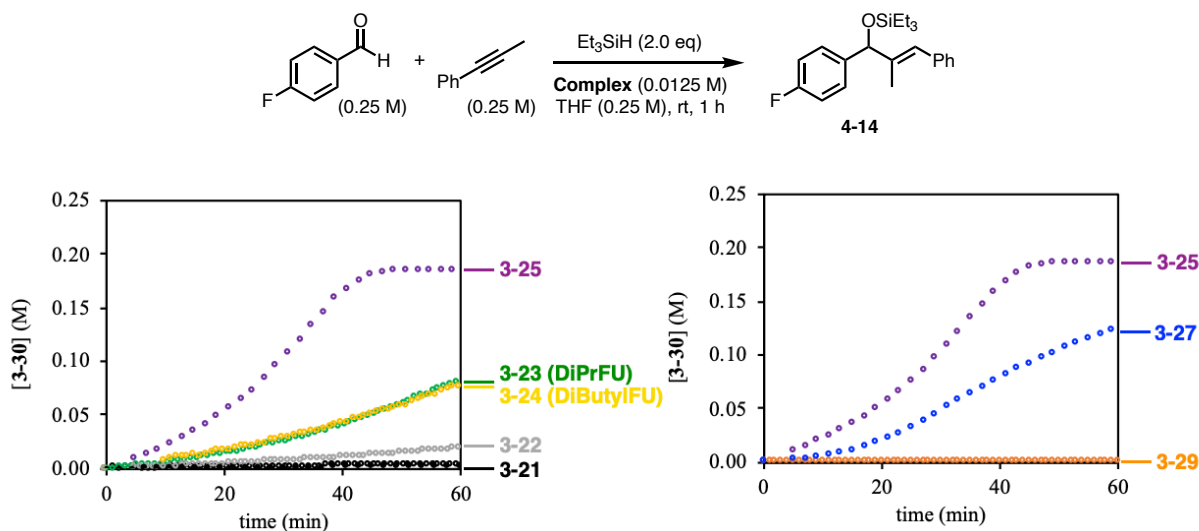
Figure 4-1: Reaction progress data for IMes–Ni(0) complexes in aldehyde–alkyne reductive couplings extension[5]

4.3 Synthesis of BAC–Ni(0) Complexes Extension

Since the only known nickel complex with a BAC ligand synthesized is complex **4-15**, the Montgomery lab was interested in synthesizing novel BAC–Ni(0) complexes (Figure 4-2).[6] This posed new opportunities in broadening the synthetic utility for a variety of nickel–catalyzed processes such as the reductive coupling of aldehydes and alkynes. The successful design and synthesis of NHC–Ni(0) complexes using π–acidic additives, such as fumarates and acrylates, became the inspiration to synthesizing BAC–Ni(0) complex **4-16** (Scheme 4-5).
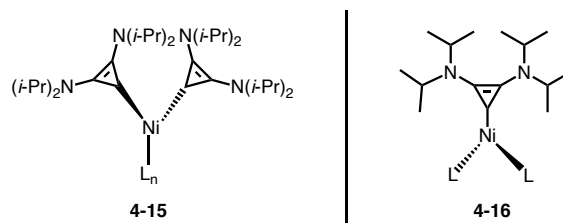
*Figure 4-2: BAC–Ni(0) complexes **4-15** and **4-16***

Using *i*-Pr-BAC free carbene **4-17** in the presence of Ni(COD)$_2$, various fumarates and acrylates were subjected to the reaction mixture to generate a series of BAC–Ni(0) complexes, **4-18** through **4-20** (Scheme 4-4). Of the various fumarates and acrylates subjected to the reaction mixture, only a few fumarates were successful at generating well-defined BAC–Ni(0) complexes.

The synthesis of these were complexes were relatively straight forward. The solvent of choice for the reaction was THF and the *i*-Pr-BAC free carbene **4-17**: Ni(COD)$_2$:fumarate ratio was 1:1:2, respectfully. During the purification of complexes **4-18** and **4-20**, a brown-black sludge would precipitate out. It was assumed that this black-brown sludge consisted of metal decomposition products. Once the sludge was filtered away via a cotton plug, the complexes could then be crystallized using Et$_2$O and pentane. Complex **4-19** was crystallized using THF and pentane. All three complexes provided an orange crystalline powder. Although complex **4-18** was obtained in low yields, complexes **4-19** and **4-20** were obtained in moderately high yields.
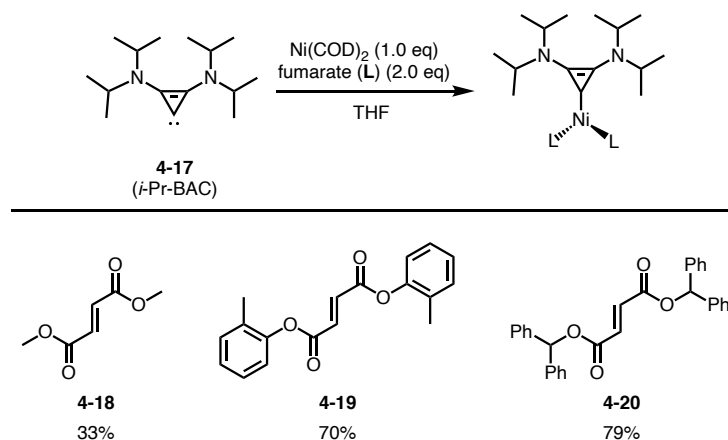
*Scheme 4-4: Synthesis of Ni(BAC)(fumarate)2 complexes **4-18** through **4-20***

4.4 BAC–Ni(0) Complexes in Aldehyde–Alkyne Reductive Couplings

The BAC–Ni(0) complexes, specifically **4-18** and **4-19**, were subjected to the reaction conditions for the reductive coupling of aldehydes and alkynes to evaluate and compare their stability and activity profiles (Table 4-1). Unfortunately, neither complex allowed for product formation to occur. This was very surprising because previous studies discussed in previous chapters have shown that *i*-Pr-BAC was capable of being a great ligand in these types of reductive coupling reactions. Additionally, previous studies discussed earlier in this chapter have shown that Ni(0) complexes with fumarates were capable of undergoing dissociation to allow for active

catalyst formation. This data suggested that the active catalyst may not form through a simple ligand dissociation.

*Table 4-1: Aldehyde–alkyne reductive couplings with BAC–Ni(0) complexes **4-18** and **4-19***
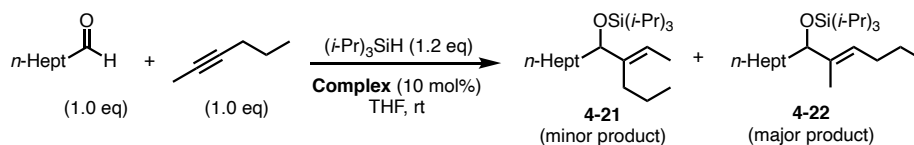
Entry	Complex	Regioselectivity (**4-21:4-22**)	Yield (%)
1	**4-18**	–	–
2	**4-19**	–	–

4.5 Catalyst Activation Pathways Via Computational Investigations

Thus far, this chapter has shown that most of the NHC–Ni(0) complexes were capable of forming product **4-23** in the reductive coupling of aldehydes and alkynes (Scheme 4-5). However, the BAC–Ni(0) complexes were uncapable of forming product **4-23** in the reductive coupling of aldehydes and alkynes (Scheme 4-5). To gain more insight into why the NHC–Ni(0) complexes were more active than the BAC–Ni(0) complexes, the pathways to catalyst activation were studied computationally.
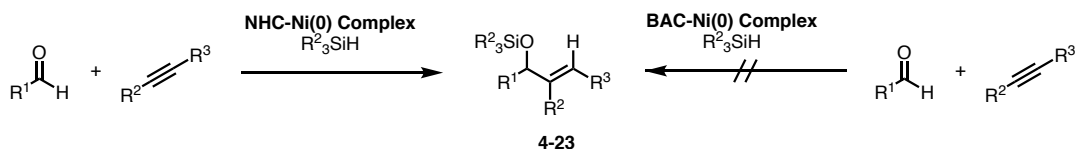
Scheme 4-5: Ni(0) complexes in aldehyde–alkyne reductive couplings

Previous computational studies for the three–component cycloaddition of aldehydes, alkynes and enoates proposed two potential pathways to product formation (Scheme 4-6).[7] Between the aldol first pathway and the ketene first pathway, the relative rates generally favored the ketene first pathway. However, the aldol first pathway was favored in the presence of α-substituted enoates.
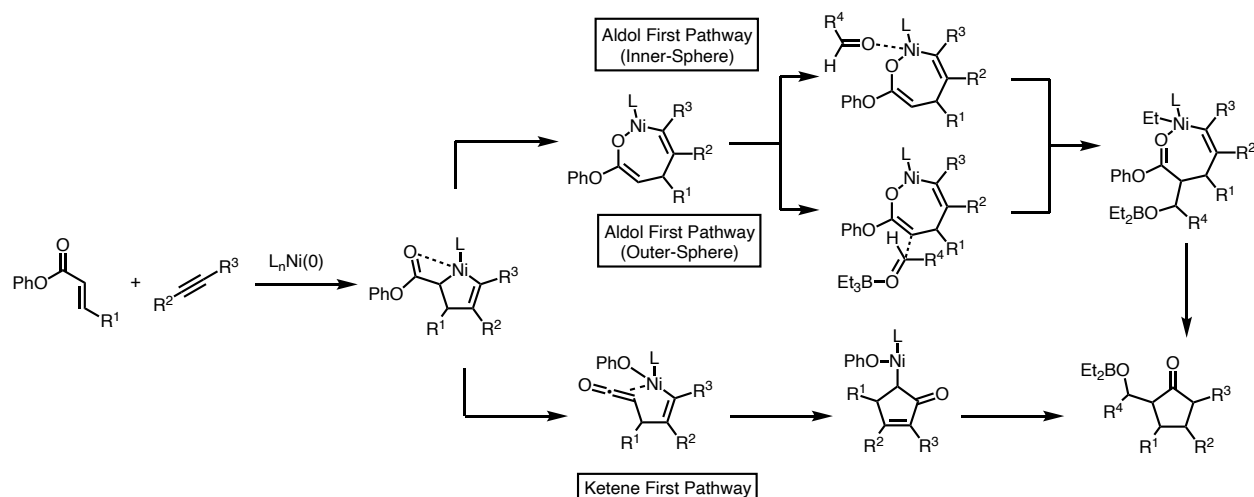
Scheme 4-6: Potential pathways for three–component cycloaddition of aldehydes, alkynes and enoates

These computational studies provided insight to the potential pathways for the Ni(0) catalyst activation in the reductive coupling of aldehydes and alkynes.[7] With the ability to map intermediate structures for the Ni(0) catalyst activation based off of the previous computational data from the three–component cycloaddition, it was also proposed that the Ni(0) catalyst activation could undergo a ketene first pathway or an aldol first pathway (Scheme 4-7). Initial computational studies began by investigating IMes–Ni(0) complex **4-12** and BAC–Ni(0) complex **4-19**.
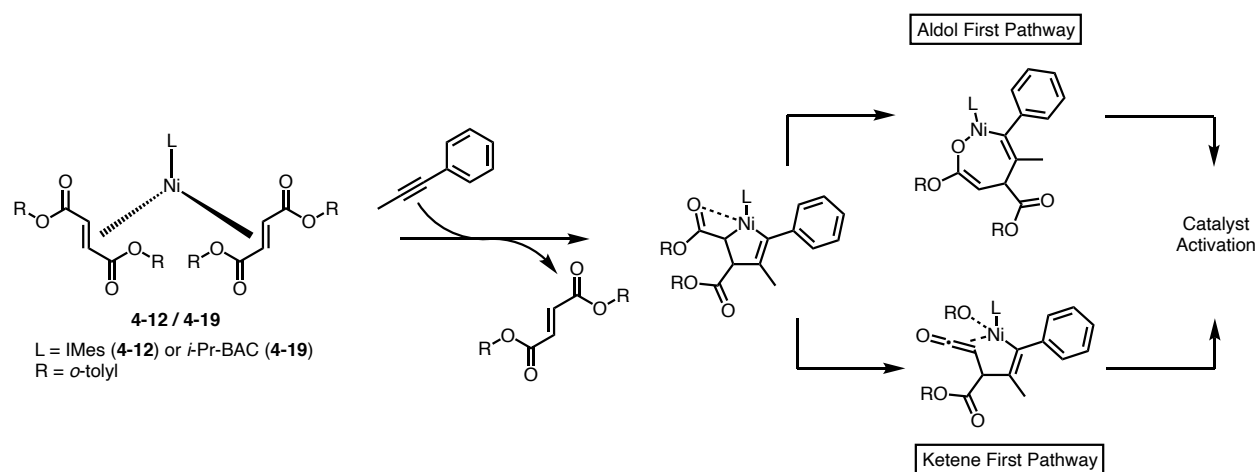
Scheme 4-7: Potential pathways for catalyst activation

For both complexes **4-12** and **4-19**, the potential energy surfaces were mapped out for the aldol first pathway and the ketene first pathway (Figure 4-3). IMes–Ni(0) complex **4-12** is represented in blue and BAC–Ni(0) complex **4-19** is represented in red. When comparing the aldol first pathway (dark blue) to the ketene first pathway (light blue) for IMes–Ni(0) complex **4-12**, the ketene elimination of IMes-II to IMes-III-B is slower (IMes-TS-II-B, 22.0 kcal/mol) than the isomerization of IMes-II to IMes-III-A (IMes-TS-II-A, 15.1 kcal/mol). Therefore, IMes–Ni(0) complex **4-12** is proposed to go through the aldol first pathway. When comparing the aldol first pathway (dark red) to the ketene first pathway (light red) for BAC–Ni(0) complex **4-19**, the ketene elimination of BAC-II to BAC-III-B is faster (BAC-TS-II-B, 13.4 kcal.mol) than the isomerization of BAC-III-A to BAC-IV-A (BAC-TS-III-A, 19.5 kcal/mol). Therefore, BAC–Ni(0) complex **4-19** is proposed to go through the ketene first pathway.
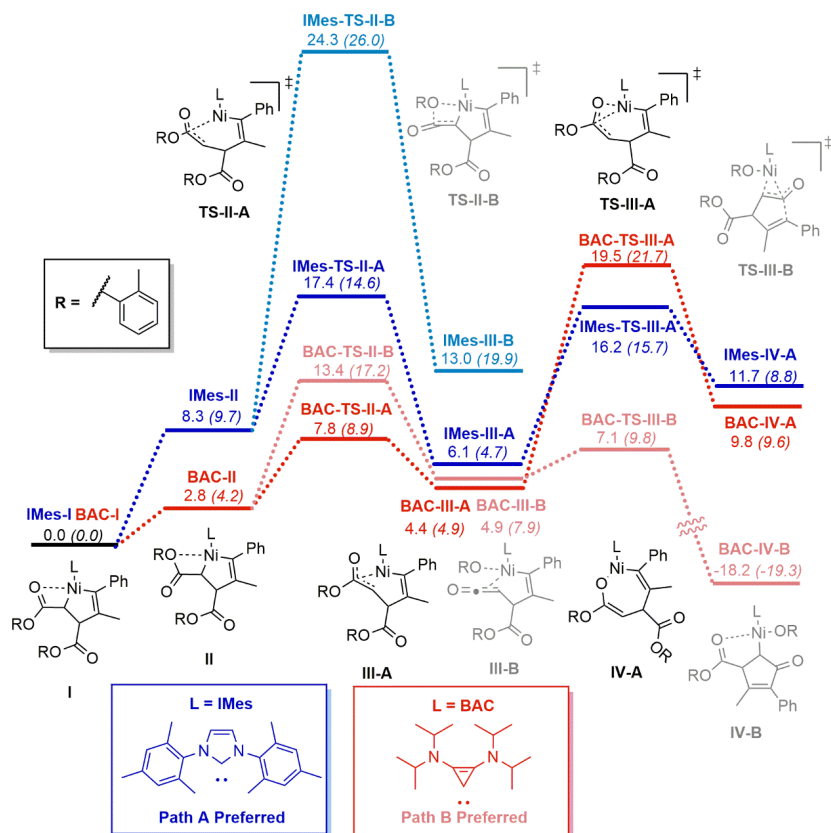
Figure 4-3: Potential energy surfaces for Ni(0) catalyst activation pathways of complexes **4-12** *and* **4-19**[8]

Since IMes–Ni(0) complex **4-12** is proposed to go through the aldol first pathway and BAC–Ni(0) complex **4-19** is proposed to go through the ketene first pathway, additional computational studies were conducted for each Ni(0) complex pathway to see why IMes–Ni(0) complex **4-12** is active and BAC–Ni(0) complex **4-19** is inactive. For IMes–Ni(0) complex **4-12**, the mechanism allows for active catalyst formation (Figure 4-4 and Figure 4-5).
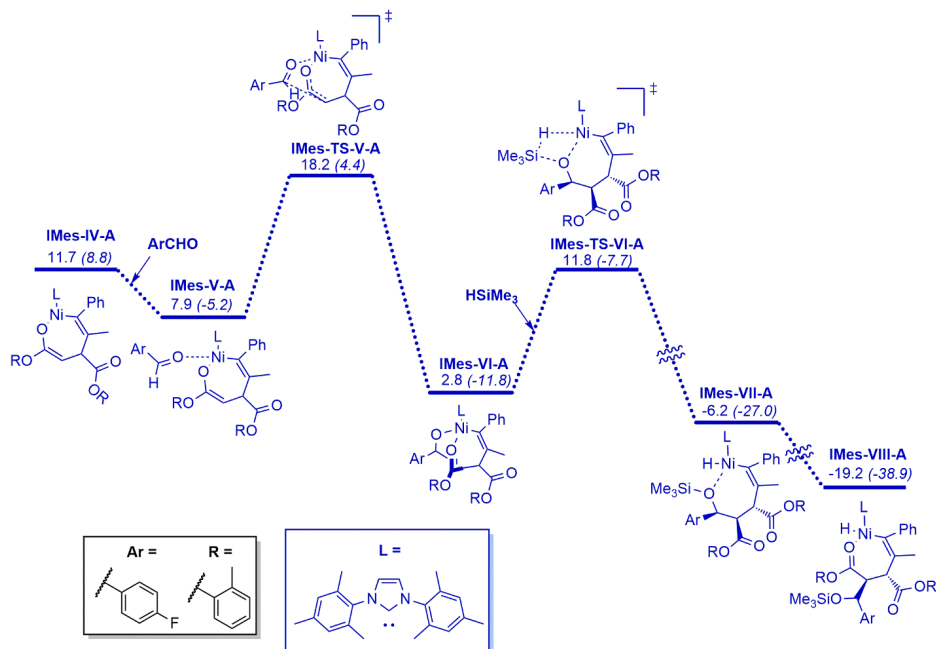
*Figure 4-4: Potential energy surfaces for complex **4-12** in the aldol first pathway part 1[8]*
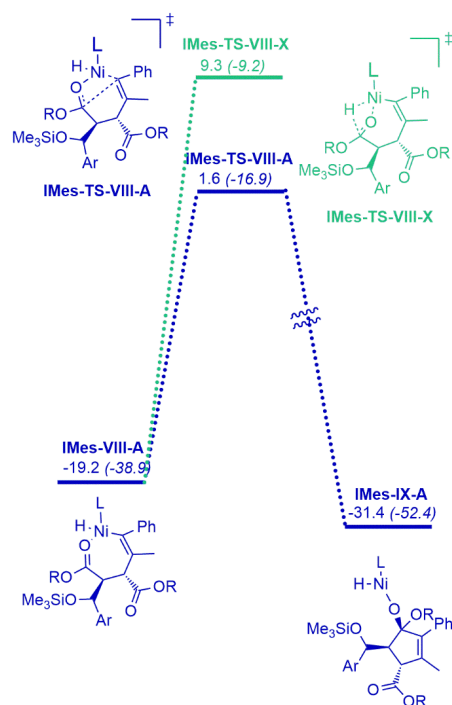
*Figure 4-5: Potential energy surfaces for complex **4-12** in the aldol first pathway part 2[8]*

Experimentally, a reaction was conducted to see if any intermediates could be isolated. From the reaction mixture, a small amount of **4-23** was cleanly isolated and **4-24** was detected by GCMS (Scheme 4-8). The ability to isolate and detect products **4-23** and **4-24** confirmed that the computations were accurate with IMes–Ni(0) complex **4-12** proceeding through an aldol first pathway through fumarate decomposition.
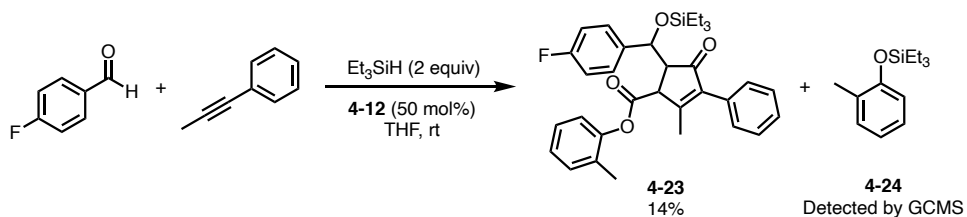
*Scheme 4-8: Fumarate decomposition provides products **4-23** and **4-24***

As for BAC–Ni(0) complex **4-19**, the mechanism allows for nickel hydride species BAC-V-B to form (Figure 4-6). Unfortunately, the reductive elimination of this nickel hydride species is too endergonic and not capable of forming an active catalyst. Therefore, the favored ketene

pathway for BAC–Ni(0) complex **4-19** does not yield product formation in the reductive coupling of aldehydes and alkynes.
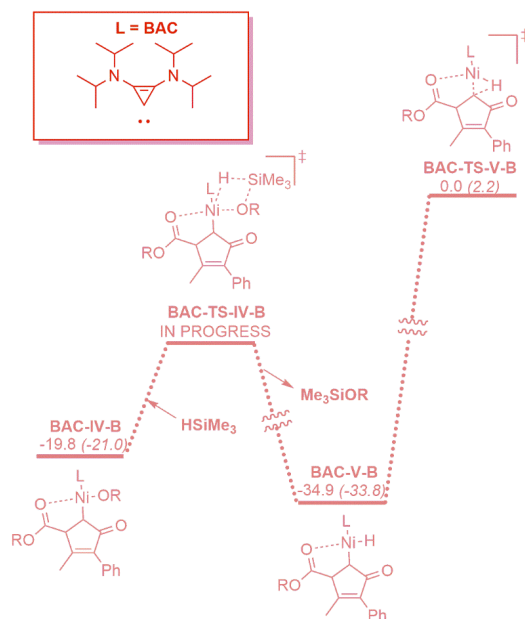
*Figure 4-6: Potential energy surfaces for complex **4-19** in the ketene first pathway[8]*

4.6 Conclusion and Future Directions

As discussed in this chapter, many various Ni(0) complexes were synthesized. The NHC–Ni(0) complexes with fumarate ligands that provided reactivity were found to go through the aldol first pathway to lead to Ni(0) catalyst activation. Additionally, the synthesis of novel BAC–Ni(0) complexes with fumarate ligands were the first of this class to be synthesized. Although these novel BAC–Ni(0) complexes showed to be inactive in the reductive coupling of aldehydes and alkynes compared to the IMes–Ni(0) complexes, it was shown computationally that the BAC–Ni(0) complexes prefer to undergo the ketene first pathway for catalyst activation. However, this pathway leads to a nickel hydride species that is too endergonic and not capable of forming an active catalyst. Future work will need to consist of synthesizing various BAC–Ni(0) complexes with other π–acidic additives. Additional computations could potentially help determine what kind

of π–acidic additives can allow for BAC–Ni(0) complexes to be stable, yet active in the reductive coupling of aldehydes and alkynes.

Furthermore, it would be advantageous to expand the synthesis of Ni(0) complexes to include chiral ligands. A few chiral NHC-Ni(0) complexes have been synthesized (Scheme 4-9). Initial results with these complexes showed trace reactivity in the reductive coupling of aldehydes and alkynes, however, more exploratory work with these complexes need to be done.
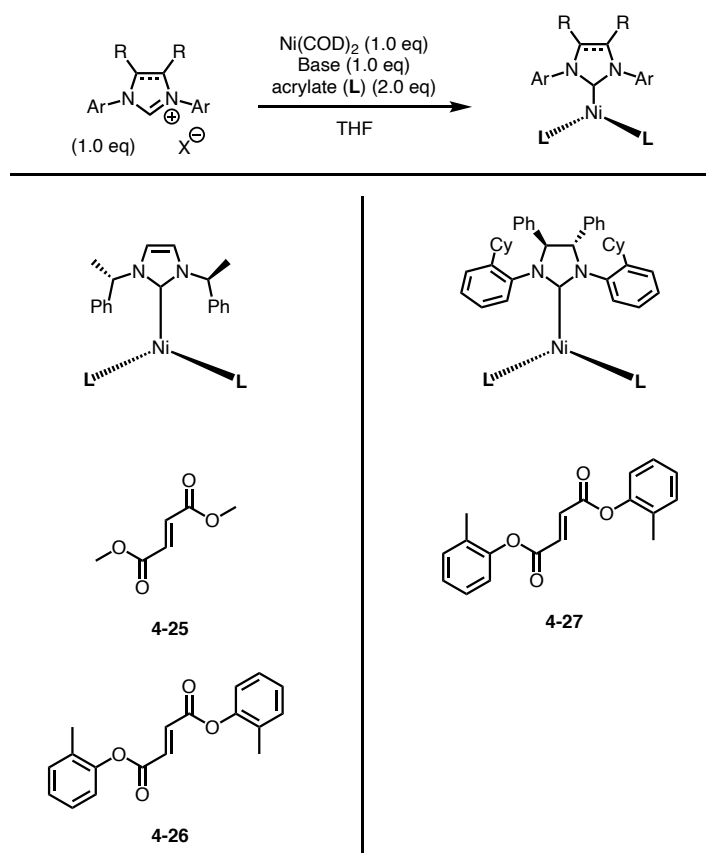
Scheme 4-9: Synthesis of chiral Ni(NHC)(fumarate)$_2$ complexes **4-25** through **4-27**

4.7 Acknowledgements

a former Montgomery lab member, isolated the fumarate decomposition products to provide evidence for the computational studies. Michael Robo, a former Montgomery lab member, provided all of the computational studies.

4.8 References

1. Nett, A. J.; Cañellas, S.; Higuchi, Y.; Robo, M. T.; Kochkodan, J. M.; Haynes, M. T.; Kampf, J. W.; Montgomery, J. *ACS Catal.* **2018**, *8*, 6606–6611.

2. Nett, A. J.; Zhau, W.; Zimmerman, P. M.; Montgomery, J. *J. Am. Chem. Soc.* **2015**, *137*, 7636–7639.

3. Nett, A. J.; Montgomery, J.; Zimmerman, P. M. *ACS Catal.* **2017**, *7*, 7352–7362.

4. Todd, D. P.; Thompson, B. B.; Nett, A. J.; Montgomery, J. *J. Am. Chem. Soc.* **2015**, *137*, 12788–12791.

5. Nett, A. J. Development and Mechanistic Implications of Nickel Pre–Catalysts for Organic Synthesis. Ph.D. Dissertation, University of Michigan, Ann Arbor, MI, 2018.

6. Kuchenbeiser, G.; Donnadieu, B.; Bertrand, G. *J. Organomet. Chem.* **2008**, *693*, 899–904.

7. Jenkins, A. D.; Robo, M. T.; Zimmerman, P. M.; Montgomery, J. *J. Org. Chem.* **2020**, *85*, 2956–2965.

8. Robo, M. T.; Computational Investigation of Chemical Reactions: Exploring the Reactivity of Nickel Enoate and Fumarate Complexes and Radical Assistance in the Force–Enabled Bond Scission of Poly(Acrylic Acid). Ph.D. Dissertation, University of Michigan, Ann Arbor, MI, 2020.

Chapter 5 Introduction to Nickel–Catalyzed Reductive Cross–Electrophile Couplings

5.1 Cyclization of Ynals, Alkynyl Enones and Alkynyl Enals

In addition to developing a reductive coupling of aldehydes and alkynes, the Montgomery lab also extended this reactivity to intramolecular reductive coupling of ynals.[1-9] As discussed in chapter 2, the combination of an ynal and a silane reductant afforded silyl–protected allylic alcohol products **5-2** and **5-4** (Scheme 5-1). Additionally, the Montgomery lab has used other reductants in reductive couplings to generate allylic alcohol products **5-1** and **5-3** (Scheme 5-1). These alternative reductants consisted of alkyl metal reagents such as dialkylzinc and trialkylaluminum. Using these types of reductants, an alkyl group can be appended selectively to the distal position of the alkyne. This reactivity was applied to both internal and terminal ynal substrates affording tetrasubstituted and trisubstituted olefins, respectively. The Jamison lab developed a complementary method in the reductive couplings using trialkylboranes.[10,11] Like the other methods that used an alkyl metal reagent in the reductive couplings, an alkyl group was appended to the distal position of the alkyne.
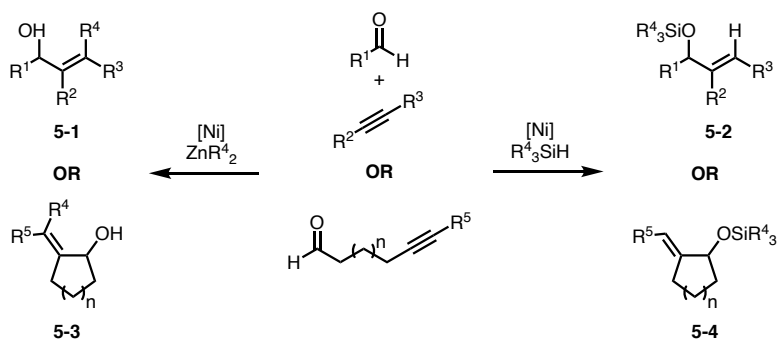
Scheme 5-1: Reductive coupling outcomes when utilizing different reductants

The mechanism of the these ynal cyclizations is very similar to the reductive coupling of aldehydes and alkynes as discussed previously in chapters 1 and 2 (Scheme 5-2).[1-11] The ynal in the presence of a Ni(0) catalyst will form complex **5-5**. Complex **5-5** undergoes an oxidative cyclization to form the five-membered metallacycle **5-6**. The alkyl metal reductant enters the catalytic cycle and performs a σ–bond metathesis with the Ni–O bond of the five-membered metallacycle **5-6** to form the vinylnickel(II) complex **5-7**. Finally, complex **5-7** undergoes reductive elimination to afford the desired allylic alcohol product **5-8**.
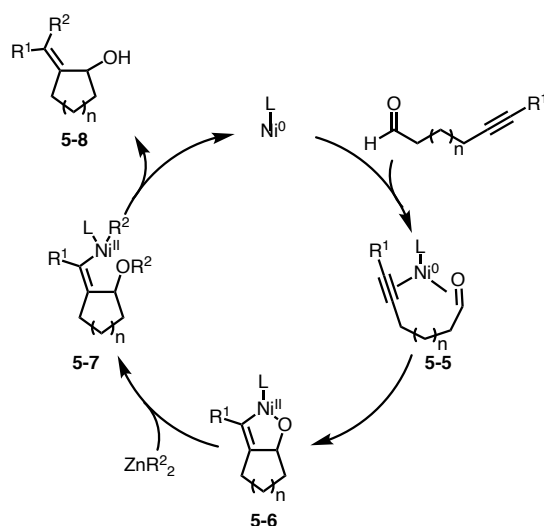
Scheme 5-2: Proposed mechanism for ynal cyclizations

Despite the success of these methodologies, using alkyl metal reagents presents significant limitations to generate tetrasubstituted and trisubstituted olefins.[12] These alkyl metal reagents are highly reactive and generally need to be synthesized prior to use, therefore limiting its scope and functional group tolerance. New methodology would need to be studied to improve the synthesis of tetrasubstituted and trisubstituted olefins making it more applicable for general purposes. To achieve this, the Montgomery lab proposed the idea of intercepting the Ni(II) metallacycle intermediate **5-6** with other methodology (Scheme 5-3). This would improve the synthesis of

tetrasubstituted and trisubstituted olefins by making it more applicable for general purposes and would not require the need to pre-generate stoichiometric amounts of alkyl metal reagents.
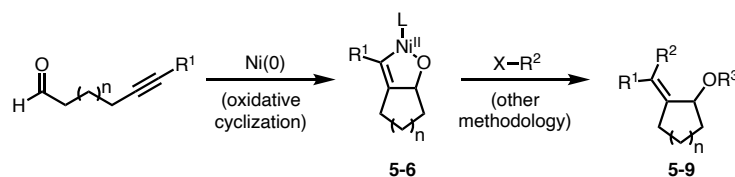
Scheme 5-3: Merging of Ni–catalyzed methodologies

5.2 Cross–Electrophile Couplings

Cross–electrophile couplings have become an extensively studied reaction class to construct C–C bonds.[13] This type of reductive coupling involves the joining of two electrophilic substrates without the use of pre–generated stoichiometric amounts of reactive organometallic coupling partners. Generally speaking, two electrophilic coupling partners in the presence of a catalyst, commonly Ni, and a stoichiometric reductant allow for the formation of C–C bonds.[13-22] For example, an aryl halide and an alkyl halide can provide alkyl substituted aryl species **5-11** (Scheme 5-4).
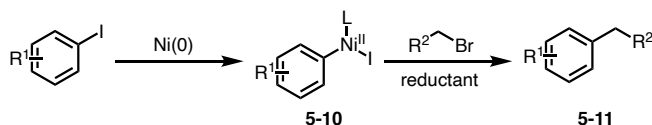
Scheme 5-4: Cross–electrophile couplings

During the formation of these alkyl substituted aryl species, a carbon–centered radical is formed from the alkyl halide species.[13-22] This radical species can then add to the Ni(II) intermediate **5-10** from the aryl halide to form the desired product **5-11**. Generally speaking, it has been found that ligands used in nickel–catalyzed cross–electrophile couplings need to be able to accept electrons to stabilize anionic nickel complexes formed during the reaction.[14] Therefore, previous examples have utilized bipyridine, phenanthroline, bioxazoline (BiOX), bis(oxazoline)

(BOX) and pyridine–bis(oxazoline) (PyBOX) ligands to allow for valence tautomerism (Figure 5-1).[13-22]
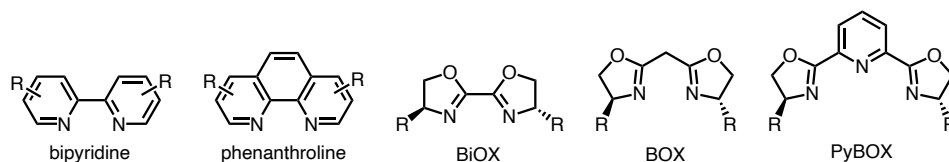
Figure 5-1: Various N–donor ligands

As discussed previously, if the Ni(II) intermediate **5-10** was replaced with the Ni(II) intermediate **5-6** from the ynal cyclization, an alkyl radical species could add in forming tetrasubstituted and trisubstituted olefin products **5-12** (Scheme 5-5).[12] If successful, this would allow for rapid generation of tetrasubstituted alkynes without the need to to pre–generate stoichiometric amounts of reactive organometallic coupling partners.
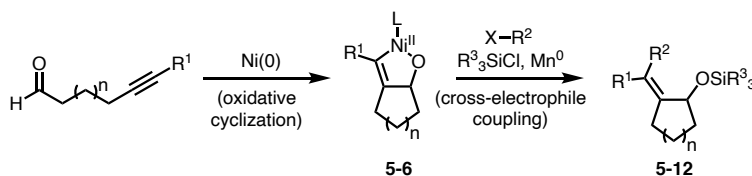
Scheme 5-5: Merging of ynal oxidative cyclization and cross–electrophile couplings

5.3 Merging of Ynal Oxidative Cyclization and Cross–Electrophile Couplings

Studies from the Montgomery lab of these ynal oxidative cyclizations merged with cross–electrophile couplings were successful (Scheme 5-6).[12] Triethylchlorosilane (TESCl) was added as additive to produce the Ni(II) halide species needed for the alkyl radical species to add in generating the desired tetrasubstituted product. Of the various bipyridyl ligands screened, 2,2'-bipyridine was found to be the optimal ligand. To avoid generating the active catalyst *in situ*, (2,2'-bipyridyl)nickel(II) iodide ((bipy)NiI$_2$) was synthesized as an air–tolerant catalyst. Between Mn^0 and Zn^0, Mn^0 proved to be a better reductant. For the reaction solvent, *N, N*–dimethylformamide (DMF) was found to result in higher product yields over *N, N*–dimethylpropyleneurea (DMPU). Lastly, sodium iodide (NaI) was added to the reaction mixture as an additive to allow for an *in situ*

Finkelstein reaction to occur with the alkyl bromides to slow down and prevent dimerization of the alkyl radicals.[23] Esters, acetals, amides, thiophenes, and uracils were tolerated in the nickel–catalyzed reductive cross–electrophile couplings providing moderate to high yields (**5-13** through **5-18**).
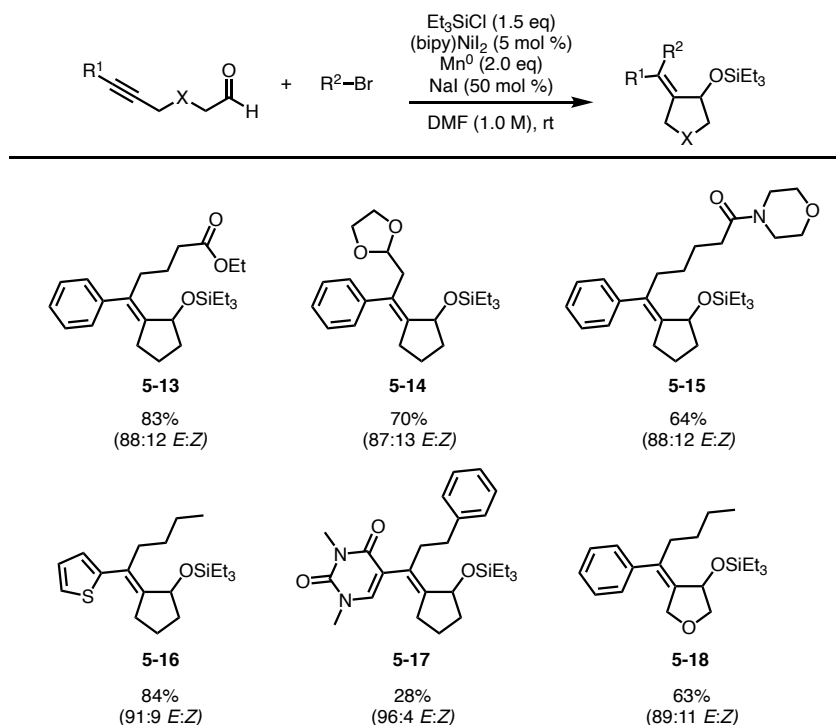
Scheme 5-6: Ni–catalyzed reductive cross–electrophile coupling scope

Furthermore, the desired product was formed as a mixture of *E* and *Z* isomers.[12] This mixture of isomers was thought to be the result of isomerization of the vinylnickel intermediate based on previous literature studies.[20,24-] The concentration of the reaction mixture was found to drastically impact the olefin geometry (Table 5-1).[12] As the concentration of the reaction mixture increased, the *E* to *Z* selectivity became excellent favoring the *E* isomer over the *Z* isomer.

Et$_3$SiCl (1.5 eq)
(bipy)NiI$_2$ (5 mol %)
Mn^0 (2.0 eq)
NaI (50 mol %)

DMF (**X** M), rt

+ *n*Pr—Br

*n*Pr

OSiEt$_3$

5-19
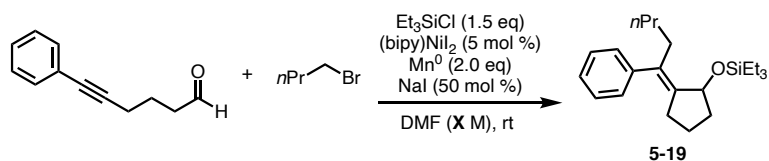
Entry	**X** (M)	Yield (%)	*E:Z* ratio
1	0.05	88	53:47
2	0.1	90	74:26
3	0.2	82	82:18
4	0.5	83	87:13
5	1.0	87	89:11

Table 5-1: Concentration impact on E to Z selectivity

This observation was proposed to be the result of a decreased rate of isomerization of the *E* vinylnickel intermediate to the *Z* vinylnickel intermediate at higher concentrations relative to the addition of the alkyl halide, favoring the *E* isomer over the *Z* isomer (Scheme 5-7).[12]

5-20
E Intermediate

5-22
E Product

5-21
Z Intermediate

5-23
Z Product
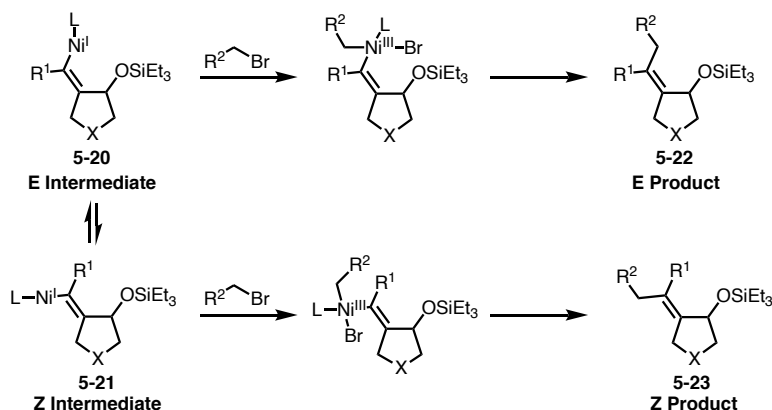
Scheme 5-7: Mechanism for E to Z isomerization

5.4 Proposed Mechanism of Alkylative Cyclizations

In order to better understand the developed reaction, mechanistic studies were undertaken. The general mechanism begins with the reduction of the Ni(II) catalyst to Ni(0) by Mn^0 (Scheme 5-8).[12] Coordination of the ynal can then coordinate to the Ni(0) species allows for oxidative cyclization to yield the five–membered metallacycle **5-24**. The five–membered metallacycle **5-24** formed from the oxidative cyclization then undergoes σ–bond metathesis with the chlorosilane to

form the vinylnickel(II) complex **5-25**. From the vinylnickel(II) complex **5-25**, there are two potential pathways to product formation. Initially, it was proposed that an alkyl radical could add to the vinylnickel(II) complex **5-25** to form the Ni(III) complex **5-27** shown as path A. Instead, it was also proposed that Mn^0 could reduce the vinylnickel(II) complex **5-25** to the vinylnickel(I) complex **5-26**. Addition of the alkyl halide via a single electron transfer (SET) to the vinylnickel(I) complex **5-26** forms the Ni(III) complex **5-27** shown as path B. Both pathways lead to the formation of the Ni(III) complex **5-27**. From there, reductive elimination can occur to provide product formation **5-28**. The Ni(I) complex in then reduced by Mn^0 to Ni(0) in order to reenter that catalytic cycle.
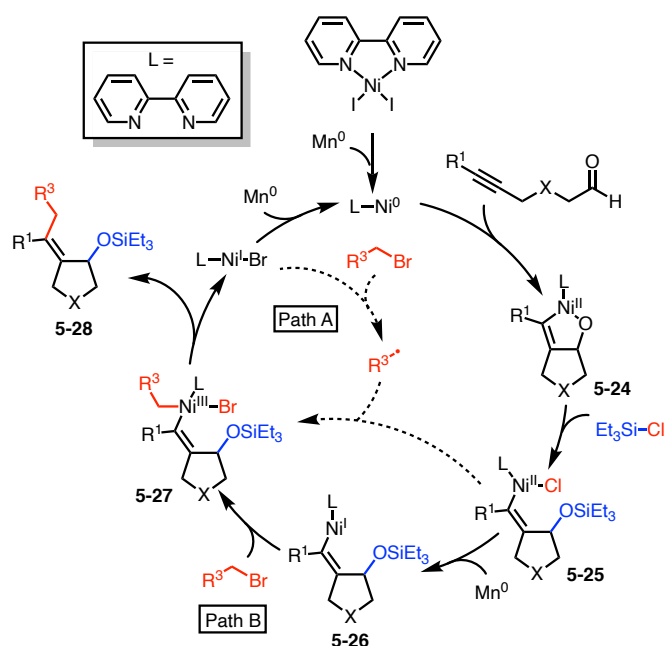
Scheme 5-8: Proposed mechanism for Ni–catalyzed reductive cross–electrophile couplings

Mechanistic studies were conducted where a stoichiometric amount of the Ni(0) catalyst was used in the reaction mixture to omit the use of a reductant.[12] From these studies, there was no product formation suggesting that the formation of the Ni(I) complex **5-26** in pathway B is predominant.

5.5 Conclusion

As discussed in this chapter, the Montgomery lab was able to develop a method to synthesize tetrasubstituted olefins via an oxidative cyclization / reductive cross–electrophile coupling.[12] This provided moderate to high yields along with excellent *E* to *Z* selectivity. Future work would need to be explored to expand the substrate capability of this new methodology (Scheme 5-9).
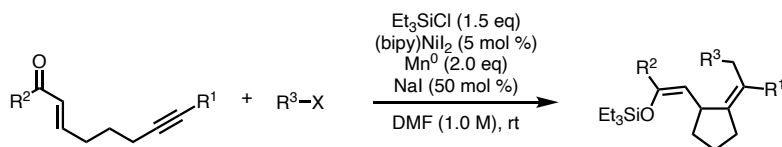
Scheme 5-9: Future substrate exploration for Ni–catalyzed reductive cross–electrophile couplings

5.6 References

1. Montgomery, J.; Amarasinghe, K. K. D.; Chowdhury, S. K.; Oblinger, E.; Seo, J.; Savchenko, A. V. *Pure Appl. Chem.* **2002**, *74*, 129–133.

2. Amarasinghe, K. K. D.; Chowdhury, S. K.; Heeg, M. J.; Montgomery, J. *Organometallics* **2001**, *20*, 370–372.

3. Chowdhury, S. K.; Amarasinghe, K. K. D.; Heeg, M. J.; Montgomery, J.; *J. Am. Chem. Soc.* **2000**, *122*, 6775–6776.

4. Montgomery, J. *Acc. Chem. Res.* **2000**, *33*, 467–473.

5. Chevliakov, M. V.; Montgomery, J. *Angew. Chem. Int. Ed.* **1998**, *37*, 3144–3146.

6. Oblinger, E.; Montgomery, J. *J. Am. Chem. Soc.* **1997**, *119*, 9065–9066.

7. Montgomery, J.; Oblinger, E.; Savchenko, A. V. *J. Am. Chem. Soc.* **1997**, *119*, 4911–4920.

8. Montgomery, J.; Seo, J.; Chui, H. M. P. *Tetrahedron Lett.* **1996**, *37*, 6839–6842.

9. Montgomery, J.; Savchenko, A. V. *J. Am. Chem. Soc.* **1996**, *118*, 2099–2100.

10. Huang, W.; Chan, J.; Jamison, T. F. *Org. Lett.* **2000**, *2*, 4221–4223.

11. Patel, S. J.; Jamison, T. F. *Angew. Chem. Int. Ed.* **2003**, *42*, 1364–1367.

12. Shimkin, K. W.; Montgomery, J. *J. Am. Chem. Soc.* **2018**, *140*, 7074–7078.

13. Knappke, C. E. I.; Grupe, S.; Gärtner, D.; Corpet, M.; Gosmini, C.; Jacobi von Wangelin, A. *Chem. Eur. J.* **2014**, *20*, 6828–6842.

14. Everson, D. A.; Weix, D. J. *J. Org. Chem.* **2014**, *79*, 4793–4798.

15. Peng, L.; Li, Y.; Wang, W.; Pang, H.; Yin, G. *ACS Catal.* **2018**, *8*, 310–313.

16. Moragas, T.; Correa, A.; Martin, R. *Chem. Eur. J.* **2014**, *20*, 8242–8258.

17. Cherney, A. H.; Kadunce, N. T.; Reisman, S. E. *J. Am. Chem. Soc.* **2013**, *135*, 7442–7445.

18. León, T.; Corres, A.; Martin, R. *J. Am. Chem. Soc.* **2013**, *135*, 1221–1224.

19. Liu, Y.; Cornella, J.; Martin, R. *J. Am. Chem. Soc.* **2014**, *136*, 11212–11215.

20. Wang, X.; Liu, Y.; Martin, R. *J. Am. Chem. Soc.* **2015**, *137*, 6476–6479.

21. Börjesson, M.; Moragas, T.; Martin, R. *J. Am. Chem. Soc.* **2016**, *138*, 7504–7507.

22. Serrano, E.; Martin, R. *Angew. Chem. Int. Ed.* **2016**, *55*, 11207–11211.

23. Fujihara, T.; Nogi, K.l Xu, T.; Terao, J.; Tsuji, Y. *J. Am. Chem. Soc.* **2012**, *134*, 9106–9109.

24. Johnson, K. A.; Biswas, S.; Weix, D. J. *Chem. Eur. J.* **2016**, *22*, 7399–7402.

25. Huggins, J. M.; Bergman, R. G. *J. Am. Chem. Soc.* **1979**, *101*, 4410–4412.

26. Huggins, J. M.; Bergman, R. G. *J. Am. Chem. Soc.* **1981**, *103*, 3002–3011.

27. Yamamoto, A.; Suginome, M. *J. Am. Chem. Soc.* **2005**, *127*, 15706–15707.

28. Clarke, C; Incerti–Pradillos, C. A.; Lam, H. W. *J. Am. Chem. Soc.* **2016**, *138*, 8068–8071.

# Chapter 6 Investigation of Nickel–Catalyzed Reductive Cross–Electrophile Couplings

6.1 Optimization Screens with Alkynyl Enals

Given the success of the previous chemistry, the Montgomery lab became interested in extending this methodology to other aldehyde / alkyne coupling partners demonstrated in the traditional Ni–catalyzed reductive couplings. Initial studies began with α–β unsaturated aldehydes tethered to an alkyne called alkynyl enals.[1] Previous studies in the Montgomery lab have shown that alkynyl enals are capable of undergoing a nickel–catalyzed reductive couplings using dialkylzinc as the reductant to provide tetrasubstituted and trisubstituted olefin products **6-2** (Scheme 6-1).[2-10] It is important to note that the oxidative cyclization of these alkynyl enals forms a seven–membered metallacycle instead of a five–membered metallacycle.
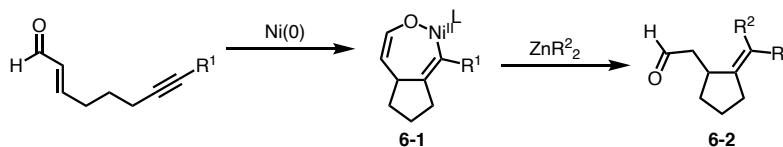
Scheme 6-1: Reductive couplings with alkynyl enals

Using similar methodology as discussed in the previous chapter, an alkyl radical species could add into the Ni(II) complex **6-1** forming tetrasubstituted and trisubstituted olefin products **6-3** (Scheme 6-2).[1] Not only would this class of substrates expand nickel–catalyzed reductive cross–electrophile couplings, but it would also allow manipulation of the silyl enol ethers for further functionalization.
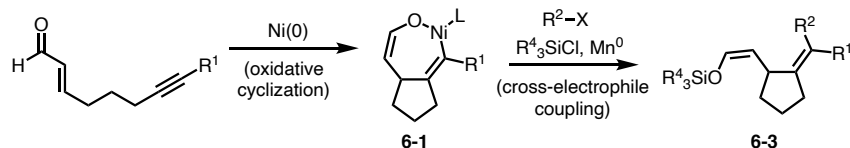
Scheme 6-2: Ni–catalyzed reductive cross–electrophile couplings with alkynyl enals

Initial studies with an alkynyl enal provided only trace amount of product **6-4** (Scheme 6-3). To confirm product **6-4** formation, characterization data was obtained (Figure 6-1). In addition to ^{1}H NMR and ^{13}C NMR, 2D COSY NMR confirmed product formation. Proton H_a was irradiated using 1D NOESY NMR and confirmed that H_a and the *n*-butyl group were *cis* to each other. The protons on the alkene were evaluated by coupling constants. Previous studies from the formation of enone–alkyne reductive couplings in the Montgomery lab provided a coupling constant of J = 6 for the protons on the alkene when they were *cis*.[11] Since the coupling constant obtained from the formation alkynyl enal Ni–catalyzed reductive cross–electrophile coupling is much larger, it is believed that the protons on the alkene are trans to each other.
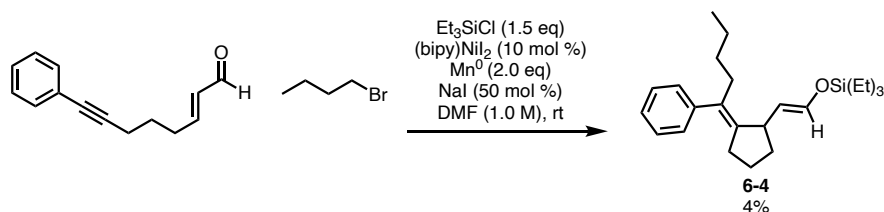
*Scheme 6-3: Alkylative cyclization to provide product **6-4***
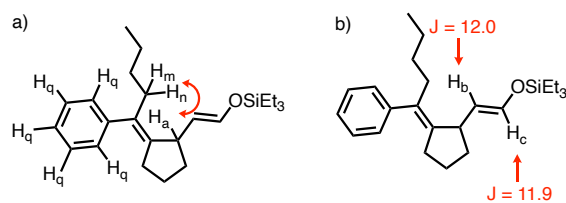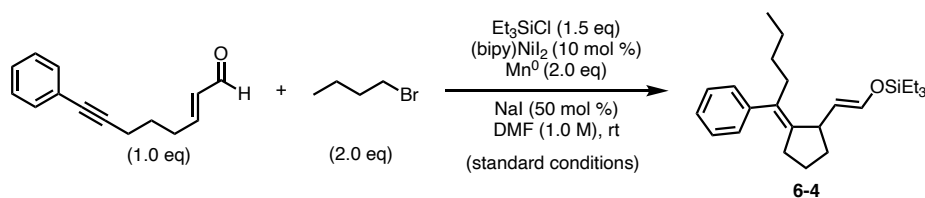

*Figure 6-1: NMR studies for product **6-4** identification*

Optimization screens were conducted by looking at various ligand scaffolds, reductants, additives and solvents, however, trace amounts of product **6-4** was only observed (Table 6-1). It

was thought that the silyl enol ether in the product was unstable leading to decomposition of the desired product **6-4**.

Entry	Deviations	Yield (%)
1	no deviation	4
2	NiBr$_2$•dme; **6-5** instead of (bipy)NiI$_2$	—
3	NiBr$_2$•dme; **6-6** instead of (bipy)NiI$_2$	—
4	NiBr$_2$•dme; **6-7** instead of (bipy)NiI$_2$	trace
5	NiBr$_2$•dme; **6-8** instead of (bipy)NiI$_2$	—
6	NiBr$_2$•dme; **6-9** instead of (bipy)NiI$_2$	—
7	NiBr$_2$•dme; no ligand instead of (bipy)NiI$_2$	—
8	nBu$_4$NI instead of NaI	TBD
9	Zn^0 instead of Mn^0	2
10	DMPU instead of DMF	11*

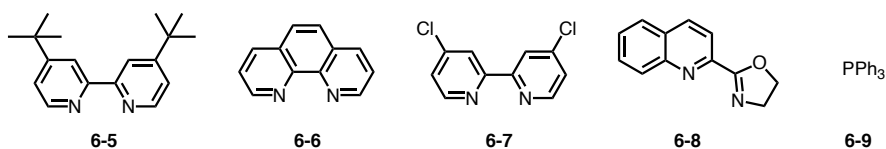* yield includes the presence of an unknown isomer of the product

Table 6-1: Optimization screening with an alkynyl enal

To prevent this from occurring, the silyl enol ether was deprotected by adding a solution of tetrabutylammonium fluoride (TBAF) to the reaction mixture prior to quenching (Scheme 6-4). Once again, only trace amount of product **6-10** was observed with the addition of the TBAF deprotection. Repeating the optimization screens done previously, there was still no improvement to the formation of desired product. However, it is important to note that all of the crude reaction ^{1}H NMRs showed very broad peaks throughout the spectral data. This suggests that oligomerization and / or polymerization may be occurring. The oligomerization and / or polymerization could be potentially happening after the TBAF deprotection of the silyl enol ether. The aldehyde generated from the reduction of the silyl enol ether would become reactive and

undergo further manipulation with unreactive starting material to generate oligomers and / or polymers. Studies with alkynyl enals were halted and further optimization was conducted with alkynyl enamides.
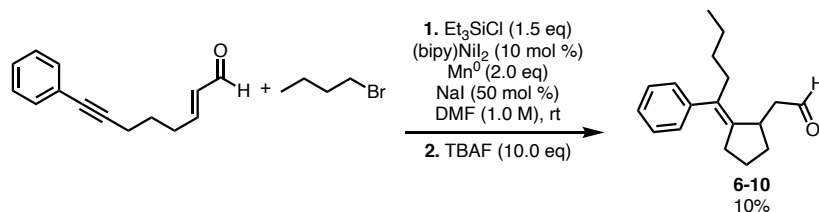
*Scheme 6-4: Alkylative cyclization followed by a TBAF deprotection to provide product **6-10***

## 6.2 Optimization Screens with Alkynyl Enamides

Initial studies with an alkynyl enamide provided a low yield of 22% with moderate *E* to *Z* selectivity (Scheme 6-5). Despite the low reactivity, this was a large improvement compared to the studies conducted with the alkynyl enal. In addition to the desired formation of product **6-11**, there was an additional formation of product **6-12** in much lower yields, presumably via reduction of the corresponding vinylnickel complex.
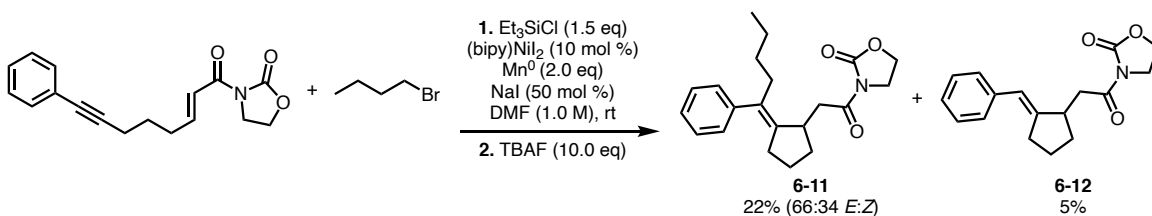
*Scheme 6-5: Alkylative cyclization followed by a TBAF deprotection to provide the desired product **6-11***

Since previous studies discussed in chapter 5 showed that concentration played a key role in the *E* to *Z* selectivity, the concentration of the reaction mixture was screened (Table 6-2).[1] Results from the concentration screen showed relatively no change in the *E* to *Z* selectivity. However, the concentration of the reaction mixture played a large role in the yield of the desired product **6-11**. As the concentration was decreased going from 0.5 M (Entry 2) to 0.1 M (Entry 3),

the yield of the desired product **6-11** increased from 17% to 50%. The yield of the undesired product **6-12** remained low.

Table 6-2: Concentration screening
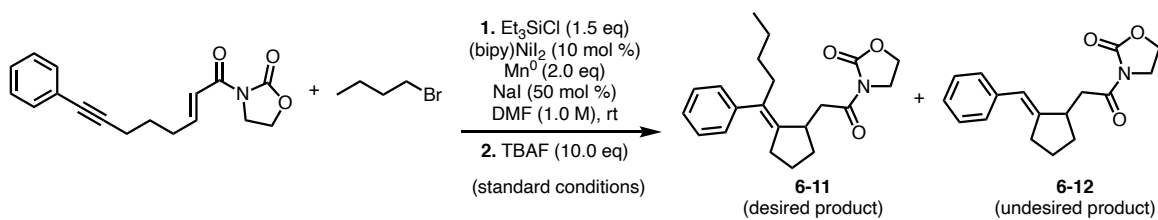
Entry	Deviation	**6-11** (% Yield)	**6-12** (% Yield)	**6-11** (E:Z)
1	no deviation	22	5	66:34
2	DMF (0.5 M)	17	5	64:36
3	DMF (0.2 M)	45	3	71:29
4	DMF (0.1 M)	50	6	73:27
5	DMF (0.07 M)	41	8	74:26

Further studies were conducted using a 0.1 M concentration of the reaction mixture. Looking at other various ligands, they all proved to be less efficient than the 2,2'–bipyridine in terms of the desired formation of product **6-11** (Table 6-3). However, ligands all showed improvement in *E* to *Z* selectivity favoring the *E* product over the *Z* product.
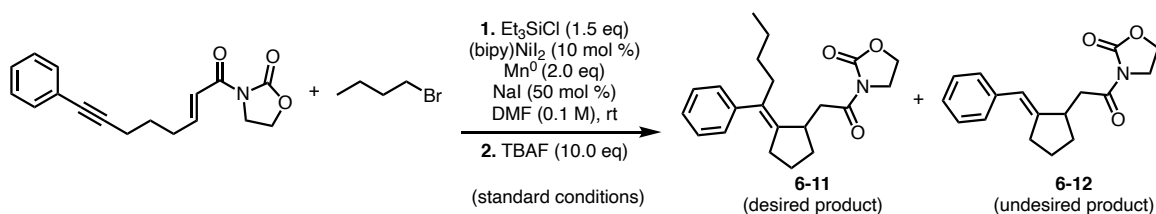
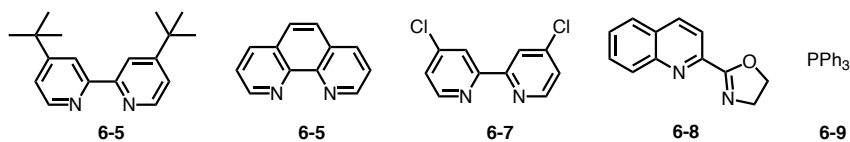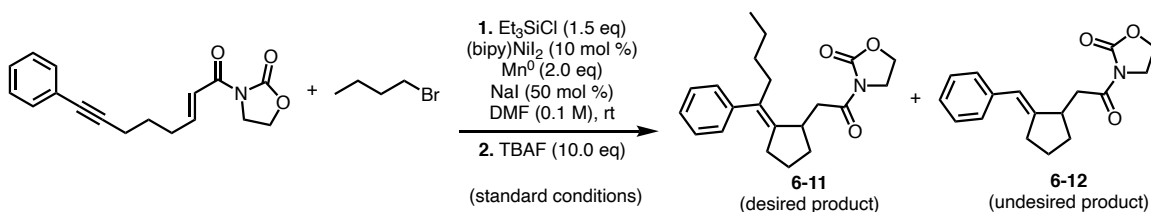| Entry	Deviations	6-11 (% Yield)	6-12 (% Yield)	6-11 (E:Z)
1	no deviation	50	6	73:27
2	NiBr$_2$•dme and 6-5	16	3	75:25
3	NiBr$_2$•dme and 6-6	13	2	87:13
4	NiBr$_2$•dme and 6-7	24	4	80:20
5	NiBr$_2$•dme and 6-8	8	6	87:13
6	NiBr$_2$•dme and 6-9	7	7	96:4

Table 6-3: Ligand screening

Lastly, a few other screening studies were conducted (Table 6-4). Changing the chlorosilane from TESCl to triisopropylsilyl chloride (TIPSCl) (Entry 2, Table 6-4) or *tert*-butyl(chloro)diphenylsilane (TBDPSCl) (Entry 3, Table 6-4) did not result in an improvement in yield of product **6-11**. However, TESCl showed improvement in *E* to *Z* selectivity favoring the *E* product over the *Z* product. Lastly, a secondary alkyl bromide was used instead of a primary alkyl halide and there was no improvement in the yield of product **6-11** (Entry 3, Table 6-4). With many screening studies exhausted, other electron–deficient alkene substrates were looked at using a 0.1 M concentration of the reaction mixture.

1. Et$_3$SiCl (1.5 eq)
(bipy)NiI$_2$ (10 mol %)
Mn^0 (2.0 eq)
NaI (50 mol %)
DMF (0.1 M), rt

2. TBAF (10.0 eq)

(standard conditions)

6-11
(desired product)

6-12
(undesired product)

| Entry	Deviation	6-11 (% Yield)	6-12 (% Yield)	6-11 (E:Z)
1	no deviation	50	6	73:27
2	TIPSCl instead of TESCl	33	16	90:10
3	TBDPSCl instead of TESCl	30	10	63:37
4	cyclohexyl bromide; slow addition	25	10	ND

TIPSCl
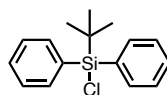
TBDPSCl

Table 6-4: Additional screening

6.3 Substrate Scope with Electron–Deficient Alkenes

Analyzing all of the various electron–deficient alkene substrates subjected to the reaction mixture, the alkynyl enamide **6-13** provided the highest yield in product formation (Scheme 6-6). As discussed previously, the alkynyl enal **6-14** provided a trace amount of product. The substrate with the α–β unsaturated ketone **6-15** only provided decomposition of starting material along with big broad peaks in the crude ^{1}H NMR suggesting that oligomerization and / or polymerization is occurring with this particular substrate as well. The substrate with the α–β unsaturated ester **6-16** provided a low yield of 25% for the desired product.
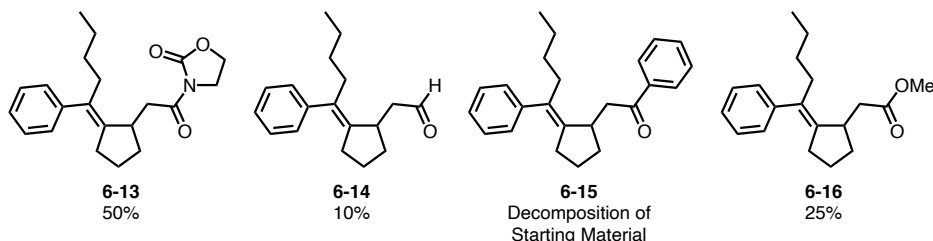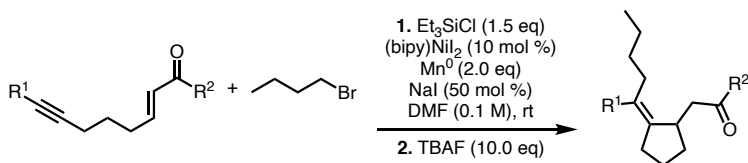
Scheme 6-6: Substrate scope with electron–deficient alkenes

6.4 Conclusion and Future Directions

As discussed in this chapter, the concentration of the reaction mixture played a large role in improving the yield of the desired product from the alkynyl enamide. However, the concentration of the reaction mixture did not seem to change the E to Z selectivity as hypothesized. With a 50% yield of the desired product and moderate E to Z selectivity from the alkynyl enamide, future work would consist of looking at various primary alkyl halides to generate a potential substrate scope.

As for the other electron–deficient substrates, future work would need to consist of preventing oligomerization and / or polymerization from occurring. If the pathway to oligomerization and / or polymerization can be prevented, higher yields of the desired product are thought to be obtained. Other electron–deficient substrates and alkyl halides would also need to be screened as well.

Lastly, there is the potential to synthesize bipyridine–Ni(0) complexes using π–acidic additives, such as fumarates and acrylates (Figure 6-2). This would limit the reduction step needed to reduce the Ni(II) complex to the active Ni(0) complex and potentially increase the yield of product formation.
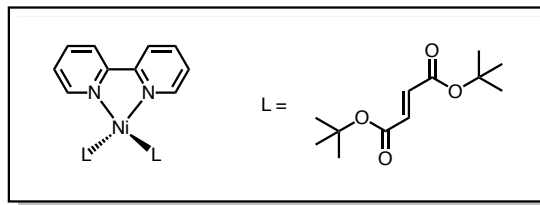
Figure 6-2: Bipyridine–Ni(0) complexes

6.5 References

1. Shimkin, K. W.; Montgomery, J. *J. Am. Chem. Soc.* **2018**, *140*, 7074–7078.

2. Montgomery, J.; Amarasinghe, K. K. D.; Chowdhury, S. K.; Oblinger, E.; Seo, J.; Savchenko, A. V. *Pure Appl. Chem.* **2002**, *74*, 129–133.

3. Amarasinghe, K. K. D.; Chowdhury, S. K.; Heeg, M. J.; Montgomery, J. *Organometallics* **2001**, *20*, 370–372.

4. Chowdhury, S. K.; Amarasinghe, K. K. D.; Heeg, M. J.; Montgomery, J.; *J. Am. Chem. Soc.* **2000**, *122*, 6775–6776.

5. Montgomery, J. *Acc. Chem. Res.* **2000**, *33*, 467–473.

6. Chevliakov, M. V.; Montgomery, J. *Angew. Chem. Int. Ed.* **1998**, *37*, 3144–3146.

7. Oblinger, E.; Montgomery, J. *J. Am. Chem. Soc.* **1997**, *119*, 9065–9066.

8. Montgomery, J.; Oblinger, E.; Savchenko, A. V. *J. Am. Chem. Soc.* **1997**, *119*, 4911–4920.

9. Montgomery, J.; Seo, J.; Chui, H. M. P. *Tetrahedron Lett.* **1996**, *37*, 6839–6842.

10. Montgomery, J.; Savchenko, A. V. *J. Am. Chem. Soc.* **1996**, *118*, 2099–2100.

11. Li, W.; Herath, A.; Montgomery, J. *J. Am. Chem. Soc.* **2009**, *131*, 17024–17029.

Chapter 7 Conclusion and Future Directions

As discussed in chapter 2, obtaining great regioselectivity and high enantioselectivity simultaneously in the small ligand protocol proved to be extremely challenging. An endo product in the ynal cyclizations was serendipitously discovered during the strategy development process, however, it was only observed for one privileged substrate. Additionally, only moderate regioselectivity and low enantioselectivity using small, chiral ligands was obtained. Therefore, future work will need to investigate the synthesis of other novel BAC ligands to simultaneously obtain great regioselectivity and high enantioselectivity. Obtaining mechanistic data by analyzing discrete Ni(0) complexes could gain further insights on how to improve regioselectivity and enantioselectivity in the small ligand protocol.

As discussed in chapter 4, many various novel Ni(0) complexes were synthesized. The NHC–Ni(0) complexes with fumarate ligands that provided reactivity were found to go through the aldol first pathway to lead to Ni(0) catalyst activation. The BAC–Ni(0) complexes with fumarate ligands were unreactive and were found to go through the ketene first pathway to lead to Ni(0) catalyst activation. Future work will need to consist of synthesizing various BAC–Ni(0) complexes with other π–acidic additives. Additional computations could potentially help determine what kind of π–acidic additives can allow for BAC–Ni(0) complexes to be stable, yet active in the reductive coupling of aldehydes and alkynes. Furthermore, it would be advantageous to expand the synthesis of Ni(0) complexes to include chiral ligands.

As discussed in chapter 6, moderate yields were obtained after optimization with an alkynyl enamide. Future work would consist of looking at various primary alkyl halides to generate a potential substrate scope with alkynyl enamides. As for the other electron–deficient substrates, future work would need to consist of preventing oligomerization and / or polymerization from occurring. If the pathway to oligomerization and / or polymerization can be prevented, higher yields of the desired product are thought to be obtained. Additionally, there is the potential to synthesize bipyridine–Ni(0) complexes using π–acidic additives, such as fumarates and acrylates.

Chapter 8 Supporting Information

## 8.1 General Experimental Details

All reactions were conducted in flame-dried or oven-dried (120 ºC) glassware with magnetic stirring under a nitrogen atmosphere in a glovebox or using standard Schlenk techniques, unless otherwise specified. All solvents (except Pentane) were purchased from Fisher Scientific and purified under nitrogen using a solvent purification system (Innovative Technology, Inc. Model # SPS-400-3 and PS-400-3). Solvents used for the synthesis of Ni(0) complexes were additionally freeze pump thawed prior to use. Pentane was purchased anhydrous from Millipore Sigma for the synthesis of Ni(0) complexes and freeze pump thawed prior to use. All deuterated solvents were purchased from Cambridge Isotope Laboratories, Inc. Deuterated benzene-d6 and tetrahydrofuran-d8 were freeze pump thawed prior to use. Ni(COD)$_2$ was purchased from Strem Chemicals, Inc. and stored in the glovebox freezer (-20 ºC). (1,3-dimesitylimidazolin-2-ylidene)bis(dimethyl fumarate)-nickel(0) was prepared according to a previous literature procedure.[1] All amines, aldehydes, alkynes and silanes that were liquids at room temperature were distilled prior to use.

Analytical thin layer chromatography (TLC) was performed on Kieselgel 60 F$_{254}$ (250 μm silica gel) glass plates where compounds were visualized using UV light, potassium permanganate or ceric ammonium molybdate stains. Compounds were purified via flash column chromatography using Kieselgel 60 (230-400 mesh) silica gel. Automated flash column chromatography was performed on a Biotage Isolera™.

1 H–Nuclear Magnetic Resonance (^{1}H NMR) and 13 C–Nuclear Magnetic Resonance (^{13}C

NMR) were recorded on Varian MR400 MHz, Varian Inova 500 MHz, Varian Vnmrs 500 MHz,

and Varian Vnmrs 700 MHz. NMR spectra were recorded in a deuterated solvent from an internal

standard of residual solvent at room temperature unless otherwise stated. High–resolution mass

spectra (HRMS) were recorded on a VG–70–250–s spectrometer manufactured by Micromass

Corp. (Manchester UK) at the University of Michigan Mass Spectrometry Laboratory.

8.2 Chapter 2 Experimental Details

(2R,5S)-5-benzyl-1-(2,3-bis((2S,5S)-5-benzyl-2-(*tert*-butyl)-3-methyl-4-oxoimidazolidin-1-yl)cycloprop-2-en-1-ylidene)-2-(*tert*-butyl)-3-methyl-4-oxoimidazolidin-1-ium tetrafluoroborate (2-9)
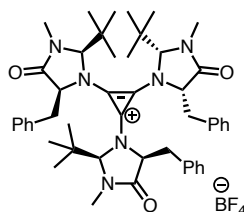
2-9 was prepared in combination of previous literature procedures with slight modifications.[3,4,5]

An oven-dried (120 ℃) round-bottom flask equipped with a stir bar was charged with DCM (1.2

mL, 0.15 M) and tetrachlorocyclopropene (0.042 mL, 1 equiv, 0.3409 mmol). The solution was

cooled to 0 ℃ and imidazolidinone **2-7** (0.4199 g, 5 equiv, 1.7045 mmol) in a solution of DCM

(1.0 mL, 0.15 M) was added dropwise. The solution was warmed to room temperature and stirred

for 6 hours. NaBF$_4$ (0.0374 g, 1 equiv, 0.3409 mmol) was added and the solution stirred vigorously

for 16 hours. Triphenylphospine (0.0894 g, 1 equiv, 0.3409 mmol) was added, followed

immediately by deionized water (2.3 mL, 0.15 M), and the suspension stirred for 10 hours with a

vent to open air. The aqueous layer was decanted, and the resulting suspension was washed 3 times

with deionized water to afford a yellow solution. The yellow solution was dried over MgSO$_4$ and

the volatiles were removed under vacuum to afford a yellow solid. The product was recrystallized from THF/pentanes to afford 0.0926 g of **2-9** (0.1079 mmol, 31.6% yield).

^{1}H NMR (500 MHz, CDCl$_3$): δ 7.43 – 7.32 (m, 12H), 7.24 (d, J = 7.3 Hz, 3H), 5.23 (dd, J = 10.5, 3.3 Hz, 3H), 4.55 (s, 3H), 3.46 – 3.37 (m, 6H), 2.57 (s, 9H), 0.96 (s, 27H).

^{13}C NMR (126 MHz, CDCl$_3$): δ 169.69, 134.78, 129.21, 128.44, 127.39, 126.08, 87.58, 61.26, 40.40, 37.60, 31.09, 25.97.

HRMS (ESI+) (m/z): [M-BF$_4$]$^+$ predicted for C$_{48}$H$_{63}$N$_6$O$_3$, 771.4956; found, 771.4957.

Triethyl((2-methylcyclopent-2-en-1-yl)oxy)silane (2-19)
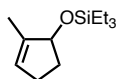
An oven-dried (120 ºC) round-bottom Schlenk flask equipped with a stir bar was charged with Ni(COD)$_2$ (0.0138 g, 0.1 equiv, 0.05 mmol), ligand **2-20** (0.0357 g, 0.1 equiv, 0.05 mmol) and KO-t-Bu (0.0056 g, 0.01 equiv, 0.05 mmol). THF (4.0 mL, 0.5 M) was added to the reaction mixture. The flask was then placed in an ice bath at 0 ºC and left to stir for approximately 50 minutes. The ice bath was removed, and the flask was charged with Et$_3$SiH (0.0878 g, 1.1 equiv, 0.55 mmol). The flask was then transferred to an oil bath set at 45 ºC for 5 minutes and was charged with the ynal (0.0481 g, 1.0 equiv, 0.5 mmol) in a solution of THF (1.0 mL, 0.5 M). The reaction was left to stir overnight. The material was left to cool to room temperature and quenched with saturated NaHCO$_3$. The aqueous layer was extracted with 3 times with Et$_2$O. The combined organic layers were washed with brine, dried with MgSO$_4$, filtered and concentrated. The crude material was purified via flash chromatography using Biotage with a hexanes:ethyl acetate gradient and concentrated/high–vaced to afford 0.0445 g of **2-19** (0.2095 mmol, 42% yield).
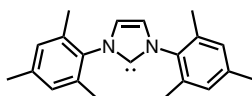
^{1}H NMR (500 MHz, CDCl₃): δ 5.47 (s, 1H), 4.63 (t, J = 6.3 Hz, 1H), 2.45 – 2.31 (m, 1H), 2.29 – 2.20 (m, 1H), 2.20 – 2.09 (m, 1H), 1.72 (d, J = 2.2 Hz, 3H), 1.70 – 1.65 (m, 1H), 0.98 (t, J = 7.9 Hz, 9H), 0.63 (q, J = 7.9 Hz, 6H).

^{13}C NMR (126 MHz, CDCl₃): δ 142.12, 127.19, 79.91, 34.52, 29.91, 13.90, 6.99, 5.03.
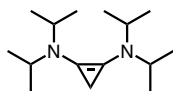
8.3 Chapter 4 Experimental Details

8.3.1 Synthesis of Carbenes

1,3-bis-(2,4,6-trimethylphenyl)imidazole-2-ylidene (IMes)

IMes was prepared according to a previous literature procedure.[2] All spectral data was in agreement with previously reported data.[2]

Bis(diisopropylamino)cyclopropenylidene (*i*-Pr-BAC)

***i*-Pr-BAC** was prepared according to a previous literature procedure with slight modifications.[3] An oven-dried (120 ºC) Schlenk flask equipped with a stir bar was charged brought into the glovebox and charged with ***i*-Pr-BAC•HBF₄** (1.0g, 1 equiv, 3.0844 mmol) and potassium bis(trimethylsilyl)amide (0.6153 g, 1 equiv, 3.0844 mmol). The Schlenk flask was brought out of the glovebox and stored under nitrogen. The Schlenk flask was cooled to -78 ºC and Et₂O (23 mL, 0.13 M) was slowly added. The suspension stirred for 10 minutes and then warmed to room temperature. The volatiles were removed under vacuum and the Schlenk was brought back into the glovebox. Pentane (approximately 23 mL) was added and the suspension stirred for 10 minutes. The suspension was filtered and the yellow-orange filtrate was stored in the glovebox freezer (-20

ºC) overnight. The mother liquor was decanted away from the yellow crystals. The yellow crystals were washed with cold pentanes to afford 0.2907 g of **i-Pr-BAC** (1.2296 mmol, 40% yield). All spectral data was in agreement with previously reported data.[3]

Bis(diisopropylamino)cyclopropenium tetrafluoroborate (*i*-Pr-BAC•HBF₄)
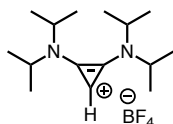
i-Pr-BAC•HBF₄ was prepared in combination of previous literature procedures with slight modifications.[3,4,5] An oven-dried (120 ºC) round-bottom flask equipped with a stir bar was charged with DCM (60 mL, 0.15 M) and tetrachlorocyclopropene (1.1 mL, 1 equiv, 8.9687 mmol). The solution was cooled to 0 ºC and diisopropylamine (6.3 mL, 5 equiv, 4.4843 mmol) was added dropwise. The solution was warmed to room temperature and stirred for 6 hours. NaBF₄ (0.9847 g, 1 equiv, 8.9687 mmol) was added and the solution stirred vigorously for 16 hours. Triphenylphospine (2.3524 g, 1 equiv, 8.9687 mmol) was added, followed immediately by deionized water (60 mL, 0.15 M), and the suspension stirred for 10 hours with a vent to open air. The aqueous layer was decanted, and the resulting suspension was washed 3 times with deionized water to afford a yellow solution. The yellow solution was dried over MgSO₄ and the volatiles were removed under vacuum to afford a yellow solid. The product was recrystallized from THF/pentanes to afford 1.5507g of **i-Pr-BAC•HBF₄** (4.7830 mmol, 53% yield). All spectral data was in agreement with previously reported data.[5]

8.3.2 Synthesis of Fumarates
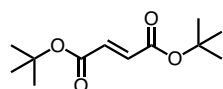
General Procedure A

An oven-dried (120 ºC) round-bottom flask equipped with a stir bar was charged with alcohol (2.0 equiv), triethylamine (2.0 equiv) and THF (0.15 M). The solution was cooled to 0 ºC and fumaryl

chloride (1.0 equiv) was slowly added. A precipitate formed immediately. The solution was allowed to warm to room temperature and stirred overnight. The reaction was quenched with the addition of a small amount of triethylamine. The crude reaction solution was absorbed onto silica gel and then added on top of a small silica gel plug. The silica gel plug was rinsed with dichloromethane and subsequently concentrated. In most cases, the product crystallized out upon the addition of pentane. In other cases, the product was purified via an alternative recrystallization method. In cases where the product was an oil, it was purified by flash column chromatography using ethyl acetate/hexanes.

General Procedure B

An oven-dried (120 ºC) round-bottom flask equipped with a stir bar was charged with alcohol (2.0 equiv) and THF (0.15 M). The solution was cooled to 0 ºC where fumaryl chloride (1.0 equiv) and triethylamine (2.4 equiv) were added dropwise. The solution was refluxed overnight. The reaction was cooled to room temperature and the solvent was evaporated. The product was purified by flash column chromatography using 100% DCM.

Di-*tert*-butyl fumarate

Di-tert-butyl fumarate was prepared according to a previous literature procedure.[6] All spectral data was in agreement with previously reported data.[7]

Di-*o*-tolyl fumarate
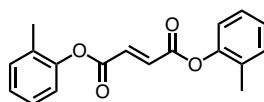
Following general procedure A: o-cresol (1.081 g, 10.0 mmol), triethylamine (1.4 mL, 10.0 mmol) and fumaryl chloride (0.54 mL, 5.0 mmol) produced 0.966 g of **di-*o*-tolyl fumarate** (3.3 mmol, 65% yield). The product was washed with pentane to afford an off-white solid.
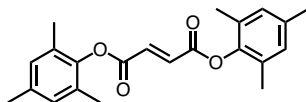
^{1}H NMR (700 MHz, CDCl$_3$): δ 7.26 – 7.23 (m, 4H + chloroform-d), 7.17 (t, J = 7.4 Hz, 2H), 7.07 (d, J = 7.9 Hz, 2H), 2.20 (s, 6H).

^{13}C NMR (176 MHz, CDCl$_3$): δ 163.06, 149.03, 134.39, 131.47, 130.06, 127.23, 126.67, 121.68, 16.33.

HRMS (ESI+) (m/z): [M+H]$^+$ predicted for C$_{18}$H$_{17}$O$_4$, 297.1121; found, 297.1123.

*Synthesized and characterized by Alex Nett.[8]

Dimesityl fumarate

Following general procedure A: 2,4,6-trimethylphenol (11.2512 g, 82.6 mmol), triethylamine (11.5 mL, 82.6 mmol) and fumaryl chloride (4.5 mL, 41.3 mmol) produced 1.968 g of **dimesityl fumarate** (5.6 mmol, 14% yield). The product was recrystallized by dissolving the product in hot EtOH and adding a small amount of H$_2$O. The material was stored at 0 ºC and then filtered to afford micro-crystallized product.

*Please note that the reaction only ran for 2 hours instead of overnight. Additionally, the crude fumarate was absorbed onto silica gel and then added on top of a small silica gel plug. The silica gel plug was rinsed with Et$_2$O instead of DCM as described in the general procedure and then subsequently concentrated.
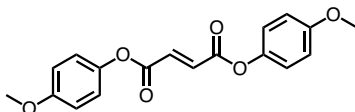
^{1}H NMR (700 MHz, CDCl$_3$): δ 7.31 (s, 2H), 6.93 – 6.90 (m, 4H), 2.29 (s, 6H), 2.15 (s, 12H).

^{13}C NMR (176 MHz, CDCl$_3$): δ 162.94, 145.67, 136.04, 134.15, 129.64, 129.54, 20.94, 16.42.

HRMS (ESI+) (m/z): [M+H]$^+$ predicted for C$_{22}$H$_{25}$O$_4$, 353.1753; found, 353.1747.

*Synthesized by Alex Nett and characterized by Amie Frank.

Bis(4-methoxyphenyl) fumarate

Following general procedure A: 4-methoxyphenol (1.241 g, 10.0 mmol), triethylamine (1.4 mL, 10.0 mmol) and fumaryl chloride (0.54 mL, 5.0 mmol) produced 3.071 g of **bis(4-methoxyphenyl) fumarate** (4.7 mmol, 94% yield). The product was recrystallized from DCM/pentane.
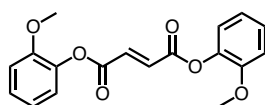
^{1}H NMR (700 MHz, CDCl$_3$): δ 7.21 (s, 2H), 7.11 – 7.07 (m, 4H), 6.95 – 6.90 (m, 4H), 3.82 (s, 6H).

^{13}C NMR (176 MHz, CDCl$_3$): δ 163.70, 157.74, 143.91, 134.50, 122.17, 114.72, 55.77.

HRMS (ESI+) (m/z): [M+H]$^+$ predicted for C$_{18}$H$_{17}$O$_6$, 329.1020; found, 329.1022.

*Synthesized and characterized by Alex Nett.[8]

Bis(2-methoxyphenyl) fumarate

Following general procedure B: 2-methoxyphenol (1.14 g, 8.4 mmol), triethylamine (1.4 mL, 10.0 mmol) and fumaryl chloride (0.4 mL, 4.2 mmol) produced 0.9374 g of **bis(2-methoxyphenyl) fumarate** (2.8 mmol, 66% yield). The product was purified via flash column chromatography using 100% DCM to afford a white crystalline solid.

^{1}H NMR (700 MHz, CDCl$_3$): δ 7.27 (s, 2H), 7.26 – 7.24 (m, 2H + chloroform-d), 7.11 (dd, J = 7.9, 1.6 Hz, 2H), 7.01 (dd, J = 8.2, 1.4 Hz, 2H), 6.98 (td, J = 7.7, 1.4 Hz, 2H), 3.85 (s, 6H).
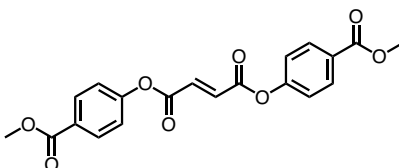
^{13}C NMR (176 MHz, CDCl$_3$): δ 162.94, 151.12, 139.43, 134.25, 127.49, 122.71, 120.97, 112.69, 56.03.

HRMS (ESI+) (m/z): [M+H]$^+$ predicted for $C_{18}H_{17}O_6$, 329.1025; found, 329.1020.

*Synthesized by Santiago Cañellas and characterized by Amie Frank.

Bis(4-(methoxycarbonyl)phenyl) fumarate

Following general procedure A: 4-hydroxybenzoate (919 mg, 6.0 mmol), trimethylamine (0.84 mL, 6.0 mmol), and fumaryl chloride (0.33 mL, 3.0 mmol) produced 2.374 g of **bis(4-(methoxycarbonyl)phenyl) fumarate** (4.3 mmol, 71% yield). The product was recrystallized from DCM/pentane.

^{1}H NMR (700 MHz, CDCl$_3$): δ 8.12 (d, J = 8.2 Hz, 4H), 7.27 – 7.25 (m, 6H + chloroform-d), 3.93 (s, 6H).

^{13}C NMR (176 MHz, CDCl$_3$): δ 166.28, 162.58, 153.85, 134.64, 131.49, 128.47, 121.44, 52.45.

HRMS (ESI+) (m/z): [M+H]$^+$ predicted for $C_{20}H_{17}O_8$, 385.0918; found, 385.0928.

*Synthesized and characterized by Alex Nett.[8]

Dibenzhydryl fumarate
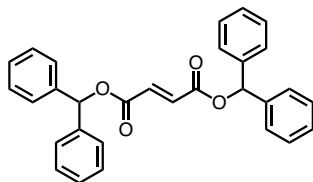
Following general procedure A: diphenylmethanol (1.8323 g, 10.0 mmol), triethylamine (1.4 mL, 10.0 mmol) and fumaryl chloride (0.54 mL, 5.0 mmol) produced 0.822 g of **dibenzhydryl fumarate** (1.8 mmol, 37% yield). The product was washed with pentane to afford a white solid.

^{1}H NMR (700 MHz, CDCl$_3$): δ 7.37 – 7.33 (m, 16H), 7.30 (tdd, J = 5.1, 4.2, 2.9 Hz, 4H), 7.03 (s, 2H), 6.98 (s, 2H).

¹³C NMR (176 MHz, CDCl₃): δ 164.02, 139.62, 134.15, 128.76, 128.34, 127.28, 78.15.

HRMS (ESI+) (m/z): [M-$C_{17}H_{13}O_4{}^{\bullet}$] predicted for $C_{13}H_{11}{}^{\bullet}$, 167.0861; found, 167.0854.

*Synthesized by Alex Nett and characterized by Amie Frank.

8.3.3 Synthesis of Complexes

General Procedure C

An oven-dried (120 ºC) vial equipped with a stir bar was charged with Ni(COD)₂ (1.0 equiv). A solution of fumarate (2.2 equiv) in THF was added dropwise directly to the vial containing Ni(COD)₂ and the resulting bright red solution stirred for 15 minutes. A solution of IMes (1.0 equiv) in THF was added and the reaction mixture stirred overnight. Volatiles were removed *en vacuo*. The desired product was either extracted with pentane and isolated by crystallization at -20 ºC or precipitated out with the addition of pentane followed by isolation via filtration.

General Procedure D

An oven-dried (120 ºC) vial equipped with a stir bar was charged with Ni(COD)₂ (1.0 equiv). A solution of IMes (1.0 equiv) in THF was added dropwise directly to the vial containing Ni(COD)₂ and the resulting dark blue-purple solution stirred for 10 minutes. A solution of fumarate (2.0 equiv) in THF was added dropwise and the reaction mixture stirred for approximately 2.5 hours. Volatiles were removed *en vacuo*. The desired product was stirred in a solution of THF/pentane and then isolated via filtration.

General Procedure E

An oven-dried (120 ºC) vial equipped with a stir bar was charged with Ni(COD)₂ (1.0 equiv) and IMes/*i*-Pr-BAC (1.0 equiv). THF was added and the resulting solution stirred for approximately 10 minutes. A solution of fumarate (2.0 equiv) in THF was added and the red reaction mixture

stirred overnight. Volatiles were removed *en vacuo*. The desired product was crystallized and then collected by decantation, washed with pentanes and then dried.

Ni(IMes)(di-*tert*-butyl fumarate)$_2$ (4-6)
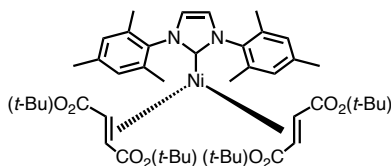
Ni(IMes)(di-*tert*-butyl fumarate)$_2$ was prepared according to a previous literature procedure.[6] All spectral data was in agreement with previously reported data.[7]

Ni(IMes)(di-*o*-tolyl fumarate)$_2$ (4-12)
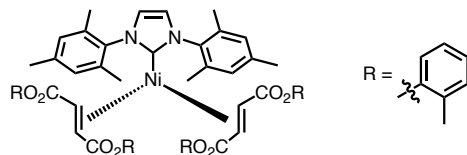
Following general procedure C: Ni(COD)$_2$ (200 mg, 0.73 mmol), IMes (222 mg, 0.73 mmol), and di-*o*-tolyl fumarate (432 mg, 1.46 mmol) provided a crude reaction mixture. Product was precipitated out as a dark red crystalline solid from the crude reaction mixture with the addition of pentane. Product was isolated by filtration and dried. (1.45 mg, 0.51 mmol, 70% yield)

^{1}H NMR (500 MHz, C$_6$D$_6$): δ 7.33 (dd, *J* = 8.0, 1.4 Hz, 2H), 7.15 (d, *J* = 1.2 Hz, 2H + benzene-d$_6$), 7.04 (td, *J* = 7.5, 2.0 Hz, 2H), 6.94 (dtd, *J* = 14.7, 7.6, 1.7 Hz, 4H), 6.87 – 6.80 (m, 4H), 6.73 (dtd, *J* = 27.2, 7.6, 1.6 Hz, 4H), 6.46 (d, *J* = 2.0 Hz, 2H), 6.40 (s, 2H), 5.24 (d, *J* = 11.1 Hz, 2H), 4.45 (d, *J* = 11.1 Hz, 2H), 2.43 (s, 6H), 2.20 (s, 6H), 2.07 (s, 6H), 1.97 (s, 7H), 1.93 (s, 6H).

^{13}C NMR (126 MHz, C$_6$D$_6$): δ 184.39, 169.54, 167.32, 150.49, 150.38, 138.83, 136.58, 135.82, 134.72, 131.50, 131.24, 130.68, 130.54, 130.21, 129.46, 126.78, 126.54, 125.70, 125.39, 125.16, 123.44, 122.44, 64.80, 57.05, 20.92, 19.93, 19.57, 16.85, 16.29.

Elemental Analysis for C$_{57}$H$_{56}$N$_2$NiO$_8$: predicted, C (71.63%), N (2.93%), H (5.91%); found, C (71.97%), N (2.83%), H (6.39%).

*Synthesized and characterized by Alex Nett.[8]

Ni(IMes)(dimesityl fumarate)$_2$ (4-11)
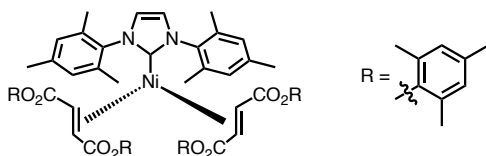
Following general procedure D: Ni(COD)$_2$ (27.5 mg, 0.10 mmol), IMes (30.4 mg, 0.10 mmol), and dimesityl fumarate (70.5 mg, 0.20 mmol) provided a crude reaction mixture. Product was precipitated out as an orange-brown solid from the crude reaction mixture. Product was stirred in a solution of THF/pentane, isolated via filtration and then dried to provide an orange solid. (70.7 mg, 0.07 mmol, 66% yield)

^{1}H NMR (700 MHz, C$_6$D$_6$): Too many impurities for accurate data. NMR is attached for reference.

^{13}C NMR (176 MHz, C$_6$D$_6$): Too many impurities for accurate data. NMR is attached for reference.

Elemental Analysis for C$_{65}$H$_{72}$N$_2$NiO$_8$: predicted, C (73.10%), H (6.80%), N (2.62%); found, C (70.73%), N (6.98%), H (2.46%). Would need to acquire better elemental analysis data due to impurities.

*Synthesized by Alex Nett and characterized by Amie Frank.

Ni(IMes)(di-*p*-anisole fumarate)$_2$ (4-9)
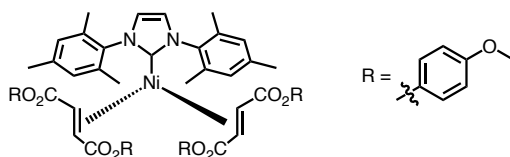
Following general procedure C: Ni(COD)$_2$ (28 mg, 0.1 mmol), IMes (30 mg, 0.1 mmol) and bis(4-methoxyphenyl) fumarate (66 mg, 0.2 mmol) provided a crude reaction mixture. Product was precipitated from the crude reaction mixture with the addition of pentane and collected by filtration. Product was recrystallized from THF/pentane at room temperature as a dark red crystalline solid. (71 mg, 0.07 mmol, 71% yield)

^{1}H NMR (500 MHz, C$_6$D$_6$): δ 7.10 – 7.06 (m, 4H), 7.04 – 6.99 (m, 4H), 6.93 (d, J = 2.0 Hz, 2H), 6.71 – 6.67 (m, 4H), 6.67 – 6.63 (m, 2H), 6.53 – 6.48 (m, 4H), 6.43 (s, 2H), 5.24 (d, J = 11.0 Hz, 2H), 4.38 (d, J = 11.1 Hz, 2H), 3.25 (s, 6H), 3.14 (s, 6H), 2.49 (s, 6H), 2.14 (s, 6H), 2.04 (s, 6H).

^{13}C NMR (126 MHz, C$_6$D$_6$): δ 170.17, 167.89, 157.35, 157.32, 145.38, 145.22, 138.82, 136.53, 135.86, 134.68, 130.75, 129.58, 125.07, 123.66, 123.00, 114.37, 114.30, 64.59, 57.23, 55.04, 54.90, 21.09, 19.59, 19.53.

Elemental Analysis for C$_{57}$H$_{56}$N$_2$NiO$_{12}$: predicted, C (67.14%), H (5.54%), N (2.75%); found, C (67.33%), N (5.49%), H (3.05%).

*Synthesized and characterized by Alex Nett.[8]

Ni(IMes)(di-o-anisole fumarate)$_2$ (4-8)
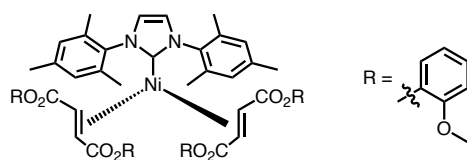
Following general procedure E: Ni(COD)$_2$ (28 mg, 0.10 mmol), IMes (30 mg, 0.10 mmol), and diphenyl fumarate (54 mg, 0.20 mmol) provided a crude reaction mixture. Product was precipitated out as a red-orange solid/oil from the crude reaction mixture. Product was precipitated from the crude reaction mixture with the addition of a minimal amount of THF followed by the addition of pentane until formation of crystals appeared. Product was isolated by decantation, washed with pentanes and then dried to provide a dark red crystalline solid. (76.9 mg, 0.075 mmol, 75% yield)

^{1}H NMR (700 MHz, C$_6$D$_6$): δ 7.33 (dd, J = 7.9, 1.6 Hz, 2H), 7.04 (dd, J = 7.8, 1.6 Hz, 2H), 6.93 (td, J = 7.8, 1.6 Hz, 2H), 6.85 (d, J = 2.1 Hz, 2H), 6.78 (td, J = 7.7, 1.4 Hz, 2H), 6.75 – 6.70 (m, 4H), 6.53 (dd, J = 8.2, 1.4 Hz, 2H), 6.46 (td, J = 7.7, 1.4 Hz, 2H), 6.42 (s, 2H), 6.35 (dd, J = 8.1, 1.4 Hz, 2H), 5.54 (d, J = 11.1 Hz, 2H), 4.53 (d, J = 11.1 Hz, 2H), 3.19 (s, 7H), 3.14 (s, 7H), 2.49 (s, 6H), 2.18 (s, 6H), 1.99 (s, 6H).

^{13}C NMR (176 MHz, C$_6$D$_6$): δ 185.96, 169.19, 167.46, 152.09, 152.03, 141.25, 141.10, 138.56, 136.67, 136.17, 134.74, 130.60, 129.56, 126.07, 125.84, 124.93, 124.85, 123.72, 120.49, 120.31, 112.44, 112.18, 63.80, 57.42, 55.21, 55.17, 21.00, 19.81, 19.52.

Elemental Analysis for C$_{57}$H$_{56}$N$_2$NiO$_{12}$: predicted, C (67.14%), H (5.54%), N (2.75%); found, C (67.73%), N (5.44%), H (3.07%).

*Synthesized by Alex Nett and characterized by Amie Frank.

Ni(IMes)(dimethylbenzoate fumarate)$_2$ (4-7)
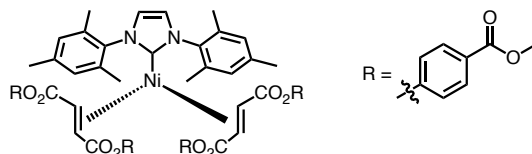
Following general procedure C: Ni(COD)$_2$ (28 mg, 0.1 mmol), IMes (30 mg, 0.1 mmol) and bis(4-(methoxycarbonyl)phenyl) fumarate (77 mg, 0.2 mmol) provided a crude reaction mixture. Product was precipitated out as a dark red crystalline solid from the crude reaction mixture with the addition of pentane. Product was isolated by filtration and dried. (101 mg, 0.09 mmol, 90% yield)

^{1}H NMR (400 MHz, C$_6$D$_6$): δ 8.05 (d, J = 8.7 Hz, 3H), 7.87 (d, J = 8.7 Hz, 3H), 7.04 (d, J = 8.7 Hz, 3H), 6.99 (d, J = 8.7 Hz, 3H), 6.87 (d, J = 2.0 Hz, 2H), 6.50 – 6.43 (m, 2H), 6.29 (s, 2H), 5.06 (d, J = 10.9 Hz, 2H), 4.29 (d, J = 10.9 Hz, 2H), 3.47 (s, 5H), 3.40 (s, 5H), 2.38 (s, 5H), 1.98 (s, 6H), 1.88 (s, 6H).

¹³C NMR (126 MHz, C₆D₆): δ 183.23, 168.54, 166.01, 165.55, 165.53, 154.64, 154.50, 138.80, 135.79, 135.12, 134.22, 130.71, 130.54, 130.10, 129.19, 124.94, 122.25, 121.32, 121.11, 65.50, 63.48, 56.51, 51.24, 51.07, 22.31, 20.64, 18.82, 18.48, 15.18.

Elemental Analysis for C₆₁H₅₆N₂NiO₁₆: predicted, C (64.73%), H (4.99%), N (2.48%); found, C (63.80%), N (5.21%), H (2.27%).

*Synthesized and characterized by Alex Nett.[8]

Ni(*i*-Pr-BAC)(dimethyl fumarate)₂ (4-18)
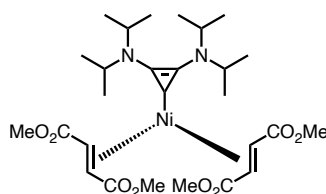
Following general procedure E: Ni(COD)₂ (27.5 mg, 0.10 mmol), *i*-Pr-BAC (23.6 mg, 0.10 mmol), and dimethyl fumarate (28.8 mg, 0.20 mmol) provided a crude reaction mixture. Et₂O/pentane mixture was added to the crude reaction mixture. A brown sludge formed and was filtered away. The filtrate was concentrated. Product was precipitated by adding a minimal amount of Et₂O followed by the addition of pentane until formation of crystals appear. The crystals were left to form at room temperature for 10 to 30 minutes followed by enhanced crystal formation by moving the vial of crystals into the freezer (-20 ºC) for 30 minutes to a 1 hour. Product was isolated by decantation, washed with cold pentanes and then dried. (19.5 mg, 0.033 mmol, 33% yield)

*Please note that the reaction ran for 48 hours instead of overnight.

¹H NMR (700 MHz, C₆D₆): δ 4.56 (d, *J* = 10.1 Hz, 4H), 3.68 (s, 4H), 3.59 (s, 6H), 3.29 (s, 6H), 1.08 (s, 24H).

¹³C NMR (176 MHz, C₆D₆): δ 171.95, 153.25, 152.30, 60.54, 59.99, 51.08, 50.52, 49.77, 21.69, 21.57.

Elemental Analysis for C$_{27}$H$_{44}$N$_2$NiO$_8$: predicted, C (55.59%), H (7.60%), N (4.80%); found, C (55.17%), N (7.58%), H (5.11%).

Ni(*i*-Pr-BAC)(di-*o*-tolyl fumarate)$_2$ (4-19)
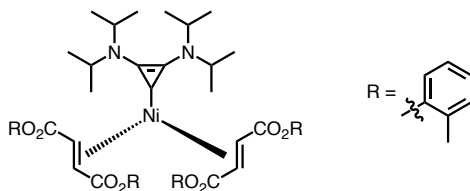
Following general procedure E: Ni(COD)$_2$ (27.5 mg, 0.10 mmol), *i*-Pr-BAC (23.6 mg, 0.10 mmol), and di-*o*-tolyl fumarate (59.3 mg, 0.20 mmol) provided a crude reaction mixture. Product was precipitated by adding a minimal amount of THF followed by the addition of pentane until formation of crystals appear. The crystals were left to form at room temperature overnight. Product was isolated by decantation and then dried. A second recrystallization was performed using THF/pentane and stored in the freezer (-20 ºC) overnight. Product was isolated by decantation and then dried. (61.9 mg, 0.070 mmol, 70% yield)

**^{1}H NMR (700 MHz, C$_6$D$_6$):** δ 7.58 (d, *J* = 8.0 Hz, 2H), 7.21 (d, *J* = 7.9 Hz, 2H), 6.94 (d, *J* = 8.0 Hz, 6H), 6.90 (p, *J* = 7.6 Hz, 4H), 6.84 (t, *J* = 7.5 Hz, 2H), 5.31 (dd, *J* = 11.0, 2.4 Hz, 2H), 5.10 (dd, *J* = 10.9, 2.4 Hz, 2H), 3.71 (s, 4H), 2.31 (d, *J* = 2.3 Hz, 6H), 2.11 (d, *J* = 2.3 Hz, 6H), 1.09 (d, *J* = 77.7 Hz, 24H).

^{13}C NMR (176 MHz, C$_6$D$_6$): δ 169.32, 168.90, 152.97, 150.98, 150.62, 149.30, 131.13, 131.03, 130.89, 130.77, 127.10, 126.44, 125.59, 125.39, 123.32, 122.36, 61.46, 59.95, 50.12, 21.72, 16.99, 16.82.

Elemental Analysis for C$_{27}$H$_{44}$N$_2$NiO$_8$: predicted, C (69.00%), H (6.81%), N (3.16%); found, C (69.36%), N (6.72%), H (3.49%).

Ni(*i*-Pr-BAC)(dibenzhydryl fumarate)$_2$ (4-20)
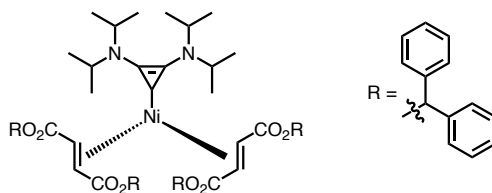
Following general procedure E: Ni(COD)$_2$ (27.5 mg, 0.10 mmol), *i*-Pr-BAC (23.6 mg, 0.10 mmol), and dibenzhydryl fumarate (59.3 mg, 0.20 mmol) provided a crude reaction mixture. Et$_2$O/pentane mixture was added to the crude reaction mixture. A brown sludge formed and was filtered away. The filtrate was concentrated. Product was precipitated by adding a minimal amount of Et$_2$O followed by the addition of pentane until formation of crystals appear. The crystals were left to form in the freezer (-20 °C) overnight. Product was isolated by decantation and then dried. (93.9 mg, 0.079 mmol, 79% yield)

^{1}H NMR (700 MHz, C$_2$D$_3$N): δ 7.52 – 7.49 (m, 4H), 7.35 (t, *J* = 7.6 Hz, 4H), 7.30 (dd, *J* = 15.0, 7.5 Hz, 10H), 7.27 – 7.20 (m, 20H), 7.18 (p, *J* = 4.2 Hz, 2H), 6.87 (s, 2H), 6.48 (s, 2H), 4.21 (d, *J* = 10.9 Hz, 2H), 4.01 (d, *J* = 10.9 Hz, 2H), 3.73 (s, 4H), 0.99 (s, 24H).

^{13}C NMR (176 MHz, C$_2$D$_3$N): δ 170.97, 170.94, 153.10, 142.96, 142.35, 142.03, 141.85, 129.61, 129.51, 129.47, 129.40, 129.38, 129.03, 128.66, 128.62, 128.51, 128.41, 128.20, 127.76, 127.63, 127.20, 127.17, 77.37, 60.90, 58.88, 21.83.

Elemental Analysis for C$_{27}$H$_{44}$N$_2$NiO$_8$: predicted, C (75.56%), H (6.43%), N (2.35%); found, C (74.42%), N (6.37%), H (2.37%).

8.3.4 Synthesis of Byproducts

***o*-tolyl 5-((4-fluorophenyl)((triethylsilyl)oxy)methyl)-2-methyl-4-oxo-3-phenylcyclopent-2-ene-1-carboxylate (4-23)**
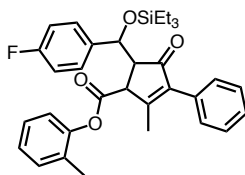
In the glovebox Ni(IMes)(di-o-tolylfumarate)$_2$ (71.7mg, 0.075mmol) and THF (3mL) were added to a large vial equipped with a stir bar. In another vial the following were added: 4-fluorobenzaldehyde (156.1μL, 0.15 mmol), 1-phenyl-1-propyne (18.8μL, 0.15mmol), triethylsilane (47.9 μL, 0.30 mmol), and THF (1mL). This solution was then added to the catalyst solution, capped, and stirred at room temperature for 12 hours, after which dichloromethane (3 mL) was added, and all solvent was removed by rotary evaporation. The crude mixture was then dissolved in dichloromethane, pushed through a plug of silica, and the solvent was removed. The crude material was loaded on a column (1 inch diameter, 3-4 inches of silica) and pure hexanes was used as the eluent to collect the following compounds: aryl silyl ether (Rf= ~0.5 in pure hexanes), silyl-protected allylic alcohol (Rf= ~0.4 in pure hexanes), and hydrosilyated aldehyde (Rf= ~0.3 in pure hexanes). After the third compound eluted, the column was flushed with EtOAc to collect all baseline compounds. The solvent was removed and the mixture of baseline compounds was loaded on a second column (1/2 inch diameter, 3 inches of silica) and 1% EtOAc/hexanes was used as the eluent to collect the following compounds: di-o-tolyl fumarate (Rf= ~0.3 in 5% EtOAc/hex), cyclopentenone byproduct (EB-I-168-6, 10.7 mg, 14% yield) (Rf= ~0.25 in 5% EtOAc/hex), and another byproduct (EB-I-200-E, possibly the minor regioisomer of cyclopentenone)(Rf= ~0.1 in 5% EtOAc/hex).

¹H NMR (500 MHz, CDCl₃): δ 7.40 – 7.29 (m, 5H), 7.29 – 7.14 (m, 3H + chloroform-d), 7.05 (d, J = 7.1 Hz, 2H), 7.02 – 6.96 (m, 3H), 5.50 (d, J = 4.6 Hz, 1H), 3.87 (s, 1H), 3.61 (dd, J = 4.6, 2.6 Hz, 1H), 2.23 (s, 3H), 2.07 (s, 3H), 0.92 (t, J = 7.9 Hz, 9H), 0.66 – 0.57 (m, 6H).

¹³C NMR (126 MHz, CDCl₃): δ 204.42, 170.33, 166.60, 163.38, 161.43, 149.35, 142.33, 136.26, 136.23, 131.48, 130.72, 130.01, 129.09, 128.45, 128.32, 128.12, 128.06, 127.20, 126.53, 121.60, 115.14, 114.97, 72.71, 58.54, 50.55, 16.80, 16.51, 6.93, 4.84.

HRMS (ESI+) (m/z): [M+H]⁺ predicted for C₃₃H₃₈FO₄Si, 545.2518; found, 545.2518.

*Synthesized and characterized by Ellen Butler. HRMS data obtained by Amie Frank.

8.4 Chapter 6 Experimental Details

General Procedure F

An oven-dried (120 °C) vial equipped with a stir bar was charged with (bipy)NiI₂ (0.1 equiv), Mn⁰ (2.0 equiv) and NaI (0.5 equiv). A solution of ynal (1.0 equiv) in DMF was added dropwise directly to the vial containing (bipy)NiI₂. Et₃SiCl (1.5 equiv) and alkyl bromide (2.0 equiv) were added sequentially. The reaction mixture stirred overnight. The reaction mixture was diluted with Et₂O and quenched with brine. The organic layer was pipetted away and passed through a small silica plug. The aqueous layer was washed with Et₂O two more times and the organic layers were passed through the small silica plug. The organic layers were combined, and the volatiles were removed *en vacuo*. The crude material was purified via flash chromatography using Biotage with a hexanes:ethyl acetate gradient and concentrated/high–vaced to afford the desired product.

### Triethyl(((E)-2-((E)-2-(1-phenylpentylidene)cyclopentyl)vinyl)oxy)silane (6-4)
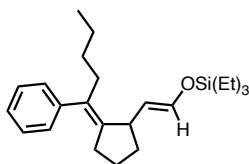
Following general procedure F: (bipy)NiI₂ (23.4 mg, 0.05 mmol), Mn⁰ (54.9 mg, 1.0 mmol), NaI (37.5 mg, 0.25 mmol), (E)-8-phenyloct-2-en-7-ynal (99.1 mg, 0.5 mmol), Et₃SiH (0.1259 mL, 0.75 mmol), 1-bromobutane (0.1074 mL, 1.0 mmol) and DMF (0.5 mL, 1.0 M) provided a crude

reaction mixture. The reaction was quenched by adding water and Et$_2$O. The organic layer was washed twice with brine, dried over MgSO$_4$, filtered and the volatiles were removed *en vacuo*. The crude material was purified via flash chromatography using Biotage with a hexanes:ethyl acetate gradient and concentrated/high–vaced to afford the desired product. (7.0 mg, 0.019 mmol, 4% yield)

^{1}H NMR (500 MHz, CDCl$_3$): δ 7.30 (t, *J* = 7.5 Hz, 2H), 7.19 (t, *J* = 7.4 Hz, 1H), 7.11 (d, *J* = 6.6 Hz, 2H), 6.29 (d, *J* = 10.8 Hz, 1H), 5.05 (dd, *J* = 12.0, 7.4 Hz, 1H), 3.34 – 3.26 (m, 1H), 2.45 – 2.36 (m, 1H), 2.36 – 2.26 (m, 1H), 2.07 (ddt, *J* = 24.4, 16.4, 9.0 Hz, 2H), 1.85 – 1.77 (m, 1H), 1.64 – 1.46 (m, 3H), 1.30 – 1.17 (m, 4H), 1.00 (t, *J* = 7.9 Hz, 9H), 0.82 (q, *J* = 7.8, 7.1 Hz, 3H), 0.68 (q, *J* = 7.9 Hz, 6H).

^{13}C NMR (126 MHz, CDCl$_3$): δ 144.17, 140.97, 140.12, 134.46, 128.46, 128.06, 125.92, 115.12, 40.58, 34.99, 34.46, 31.71, 30.69, 24.10, 23.00, 14.16, 6.71, 4.64.

HRMS (ESI+) (m/z): [M+H]$^+$ predicted for C$_{24}$H$_{39}$OSi, 371.2770; found, 371.2765.

3-((Z)-2-((E)-2-(1-phenylpentylidene)cyclopentyl)-1-((triethylsilyl)oxy)vinyl)oxazolidin-2-one
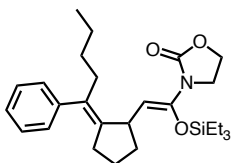
Following general procedure F: (bipy)NiI$_2$ (9.4 mg, 0.02 mmol), Mn^0 (22.0 mg, 0.4 mmol), NaI (15.0 mg, 0.1 mmol), (*E*)-3-(8-phenyloct-2-en-7-ynoyl)oxazolidin-2-one (56.7 mg, 0.2 mmol), Et$_3$SiH (0.0504 mL, 0.3 mmol), 1-bromobutane (0.0430 mL, 0.4 mmol) and DMF (0.2 mL, 1.0 M) provided a crude reaction mixture. The crude material was purified via flash chromatography using Biotage with a hexanes:ethyl acetate gradient and concentrated/high–vaced to afford the desired product. (2.3 mg, 0.005 mmol, 2.5% yield)

¹H NMR (500 MHz, CDCl₃): Too many impurities for accurate data. NMR is attached for reference.

HRMS (ESI+) (m/z): [M+Na]⁺ predicted for $C_{27}H_{41}NNaO_3Si$, 478.2753; found, 478.2746.

(*E*)-3-(2-(2-(1-phenylpentylidene)cyclopentyl)acetyl)oxazolidin-2-one (6-11)
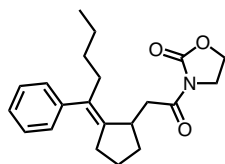
Following general procedure F: (bipy)NiI₂ (9.4 mg, 0.02 mmol), Mn⁰ (22.0 mg, 0.4 mmol), NaI (15.0 mg, 0.1 mmol), (*E*)-3-(8-phenyloct-2-en-7-ynoyl)oxazolidin-2-one (56.7 mg, 0.2 mmol), Et₃SiH (0.0504 mL, 0.3 mmol), 1-bromobutane (0.0430 mL, 0.4 mmol) and DMF (0.2 mL, 1.0 M) provided a crude reaction mixture. The reaction was left to stir for approximately 1 hour. The vial was placed in an ice bath at 0 ºC TBAF (2.0 mL, 10 equiv, 2 mmol) was added dropwise. The reaction was quenched with NaHCO₃ and transferred to a sepratory funnel and 3 extractions with Et₂O were conducted. The aqueous layer was washed twice with brine, dried over MgSO₄, filtered and the volatiles were removed *en vacuo*. The crude material was purified via flash chromatography using Biotage with a hexanes:ethyl acetate gradient and concentrated/high–vaced to afford the desired product. (4.7 mg, 0.014 mmol, 7% yield)

¹H NMR (500 MHz, CDCl₃): δ 7.30 (t, *J* = 7.4 Hz, 2H), 7.19 (t, *J* = 7.4 Hz, 1H), 7.12 (d, *J* = 7.5 Hz, 2H), 4.43 (t, *J* = 8.1 Hz, 2H), 4.06 (t, *J* = 8.1 Hz, 2H), 3.37 (q, *J* = 7.4 Hz, 1H), 3.14 – 2.99 (m, 2H), 2.37 (t, *J* = 7.7 Hz, 2H), 2.17 (dt, *J* = 14.8, 6.5 Hz, 1H), 2.05 (dt, *J* = 16.1, 7.6 Hz, 1H), 1.87 (dq, *J* = 13.9, 7.5, 7.0 Hz, 1H), 1.65 (dt, *J* = 16.7, 8.0 Hz, 1H), 1.54 (h, *J* = 6.0, 5.4 Hz, 2H), 1.23 (dq, *J* = 28.6, 7.4 Hz, 4H), 0.81 (t, *J* = 7.1 Hz, 3H).

¹³C NMR (126 MHz, CDCl₃): δ 172.76, 153.69, 143.70, 141.64, 134.32, 128.50, 128.07, 126.07, 62.15, 42.77, 40.02, 37.57, 34.50, 32.53, 31.40, 30.88, 29.86, 24.03, 22.89, 14.17.

8.5 References

1. Clement, N. D.; Cavell, K. J.; Ooi, L. L. Zerovalent N-Heterocyclic Carbene Complexes of Palladium and Nickel Dimethyl Fumarate: Synthesis, Structure, and Dynamic Behavior. *Organometallics* **2006**, *25*, 4155-4165.

2. Bantreil, X.; Nolan, S. P. Synthesis of *N*-heterocyclic carbene ligands and derived ruthenium olefin metathesis catalysts. *Nat. Protoc.* **2011**, *6*, 69-77.

3. Lavallo, V.; Canac, Y.; Donnadieu, B.; Schoeller, W. W.; Bertrand, G. Cyclopropenylidenes: From Interstellar Space to an Isolated Derivative in the Laboratory. *Science* **2006**, *312*, 722-724.

4. Kuchenbeiser, G.; Soleilhavoup, M.; Donnadieu, B.; Bertrand, G. Reactivity of Cyclic (Alkyl)(amino)carbenes (CAACs) and Bis(amino)cyclopropenylidenes (BACs) with Heteroallenes: Comparisons with their N-heterocyclic Carbene (NHCs) Counterparts. *Chem. Asian J.* **2009**, *4*, 1745-1750.

5. Malik, H. A.; Sormunen, G. J.; Montgomery, J. A General Strategy for Regiocontrol in Nickel-Catalyzed Reductive Couplings of Aldehydes and Alkynes. *J. Am. Chem. Soc.* **2010**, *132*, 6304-6305.

6. Nett, A. J.; Canellas, S.; Higuchi, Y.; Robo, M. T.; Kochkodan, J. M.; Haynes, M. T.; Kampf, J. W.; Montgomery, J. Stable, Wee-Defined Nickel(0) Catalysts for Catalytic C-C and C-N Bond Formation. *ACS Catal.* **2018**, *8*, 6606-6611.

7. Geny, A.; Agenet, N.; Iannazzo, L.; Malacria, M.; Aubert, C.; Gandon, V. Air-Stable {(C$_5$H$_5$)Co} Catalysts for [2+2+2] Cycloadditions. *Angew. Chem. Int. Ed.* **2009**, *48*, 1810-1813.

8. Nett, A. J.; Development and Mechanistic Implications of Nickel Pre-Catalysts for Organic Synthesis. Ph.D. Dissertation, University of Michigan, Ann Arbor, MI, 2017.

8.6 NMR Spectra

8.6.1 Chapter 2 NMR Spectra

(2*R*,5*S*)-5-benzyl-1-(2,3-bis((2*S*,5*S*)-5-benzyl-2-(*tert*-butyl)-3-methyl-4-oxoimidazolidin-1-yl)cycloprop-2-en-1-ylidene)-2-(*tert*-butyl)-3-methyl-4-oxoimidazolidin-1-ium tetrafluoroborate (2-9)
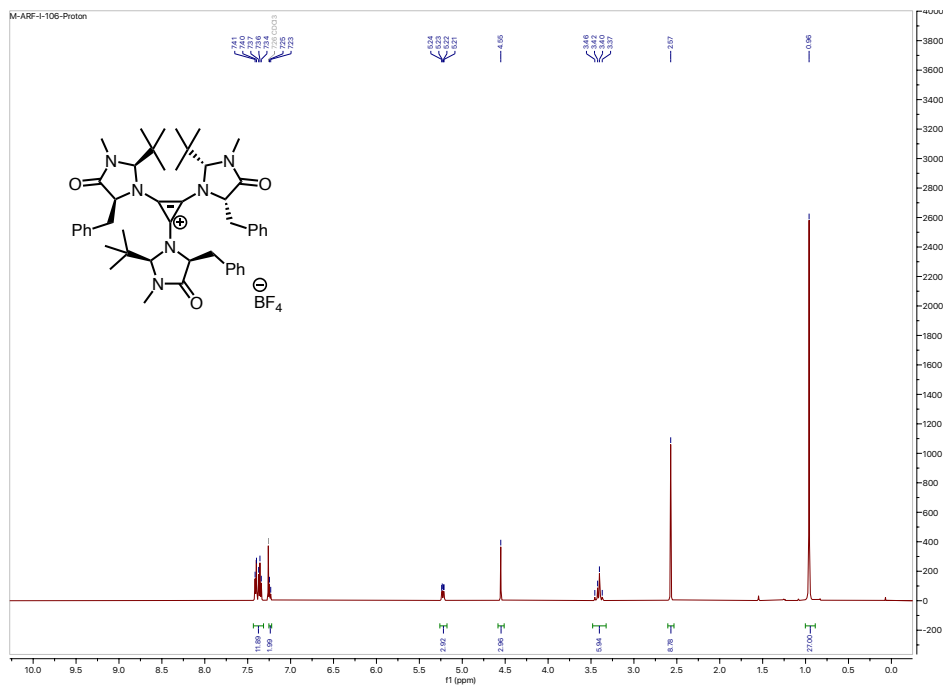
Figure 8-1: Proton spectra of 2-9
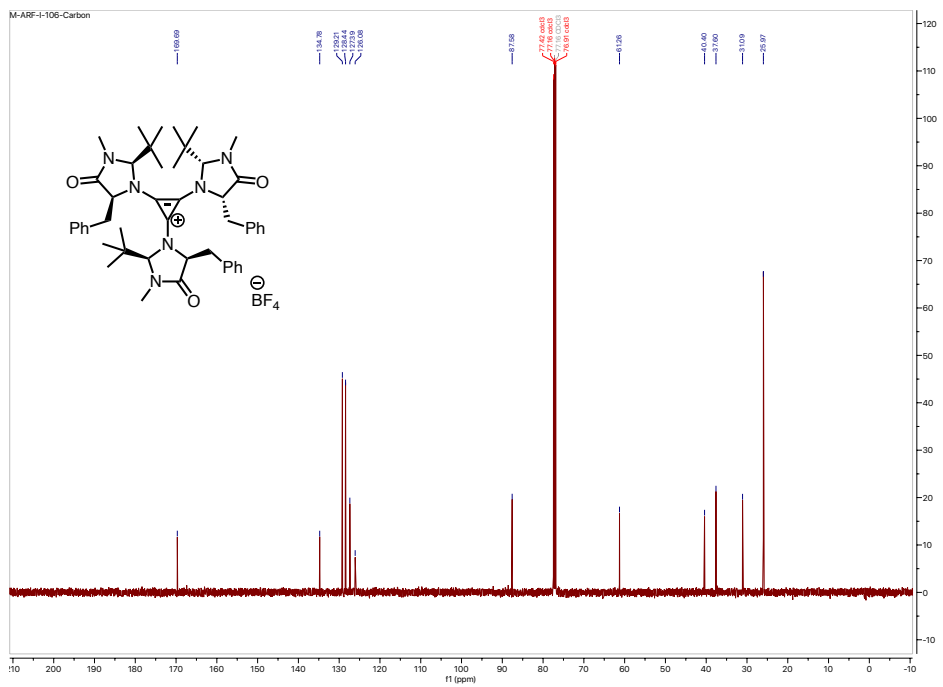
Figure 8-2: Carbon spectra of 2-9

Triethyl((2-methylcyclopent-2-en-1-yl)oxy)silane (2-19)
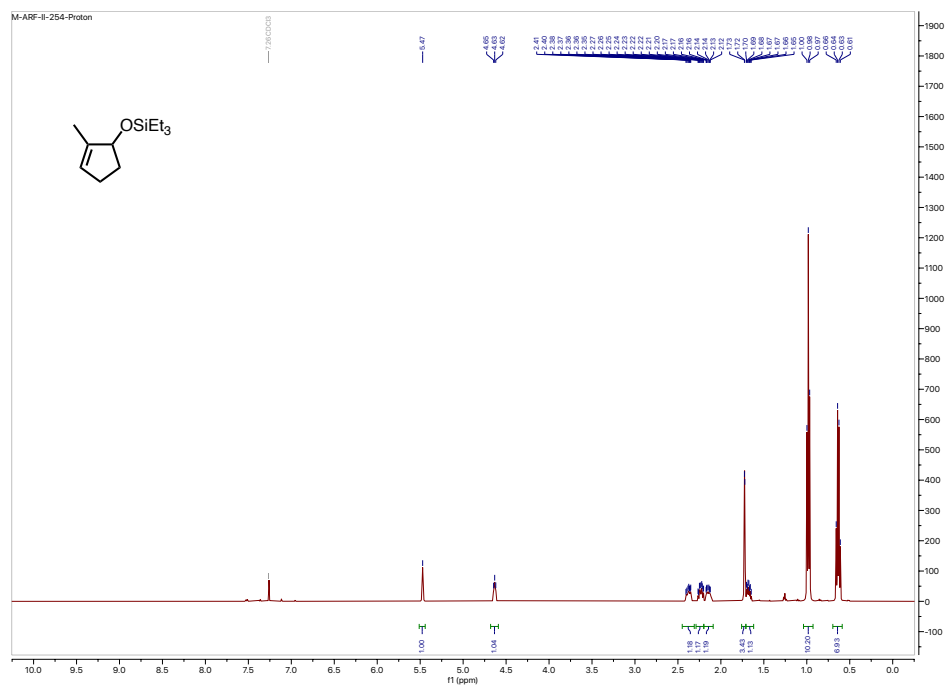
*Figure 8-3: Proton spectra of **2-19***
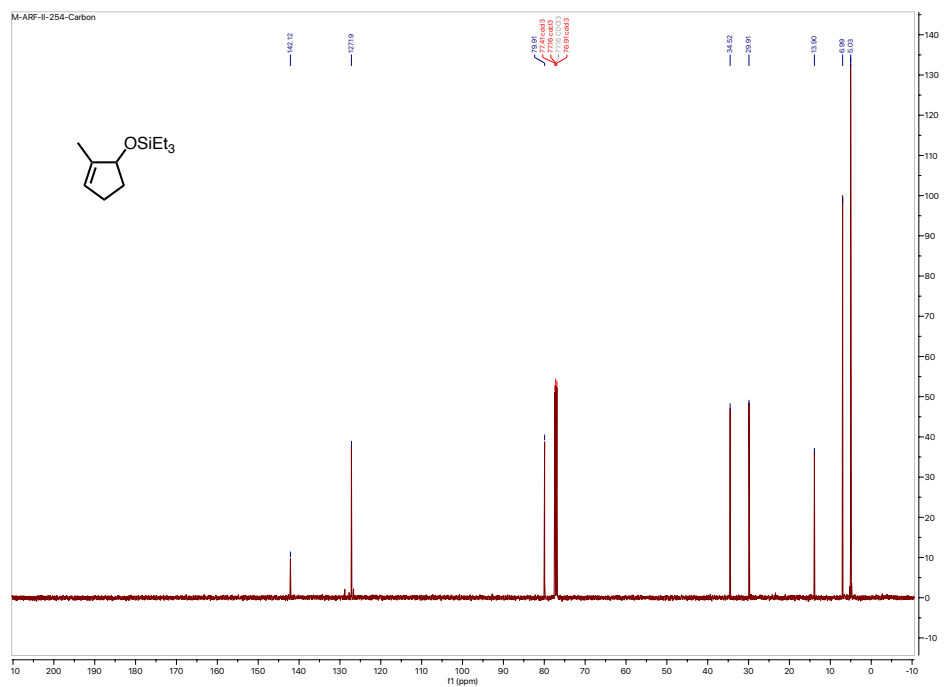
*Figure 8-4: Carbon spectra of **2-19***

8.6.2 Chapter 4 NMR Spectra

Di-*o*-tolyl fumarate
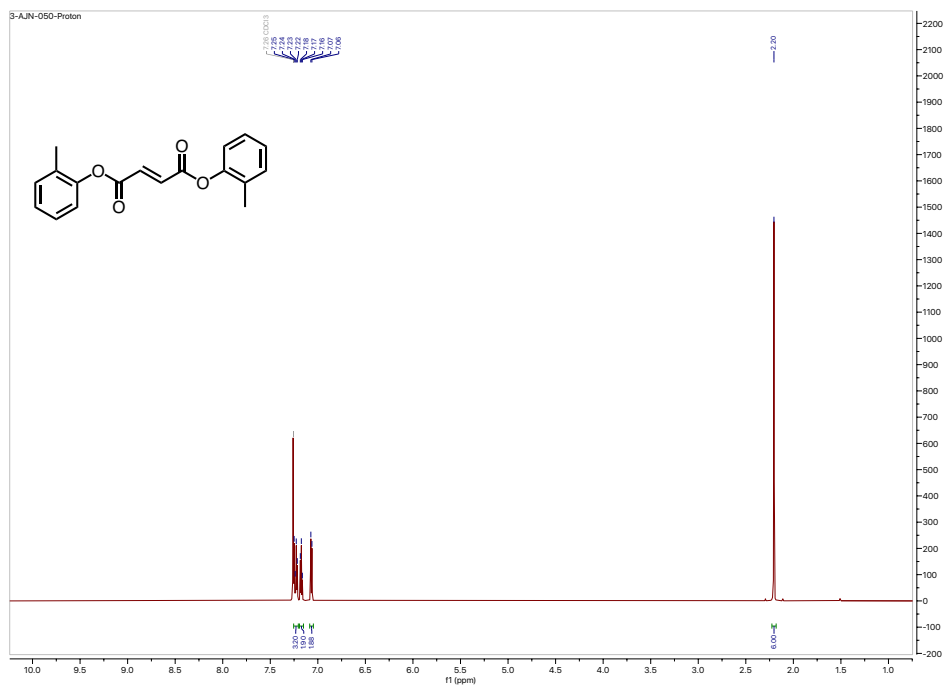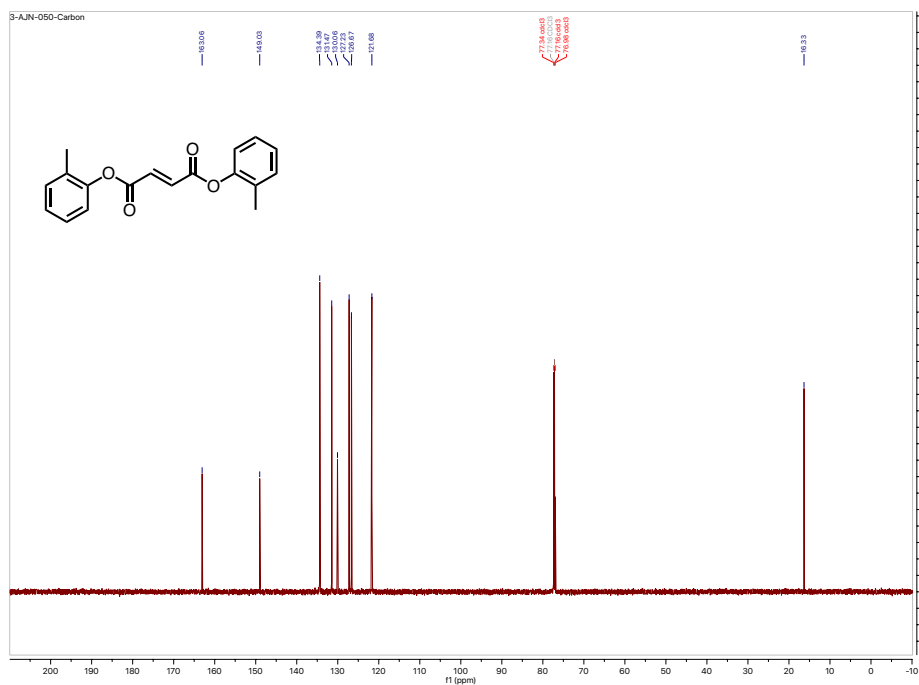

Figure 8-5: Proton spectra for di-o-tolyl fumarate

Figure 8-6: Carbon spectra for di-o-tolyl fumarate
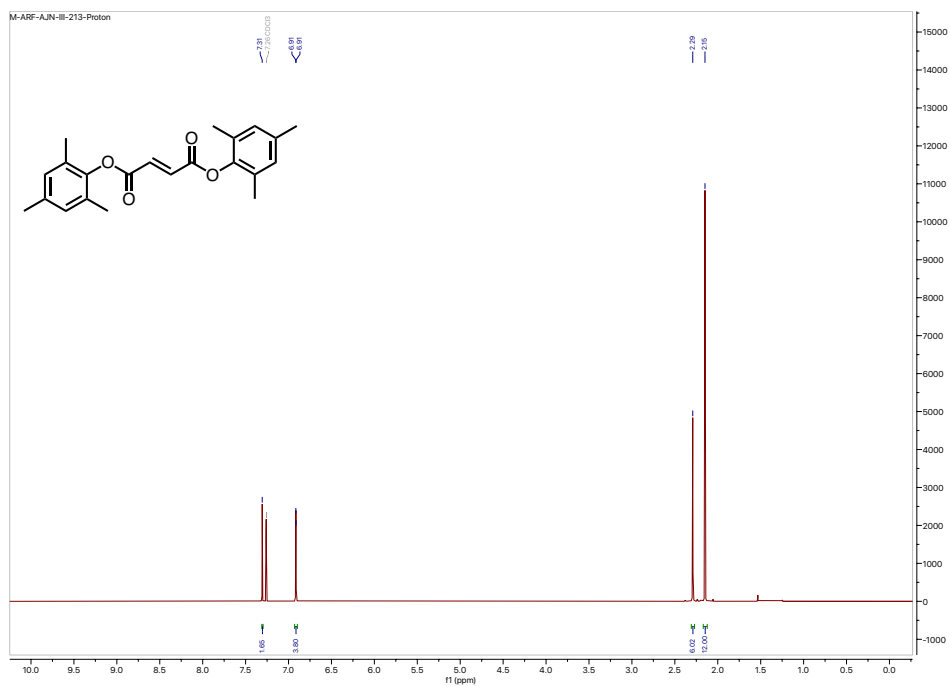
Dimesityl fumarate
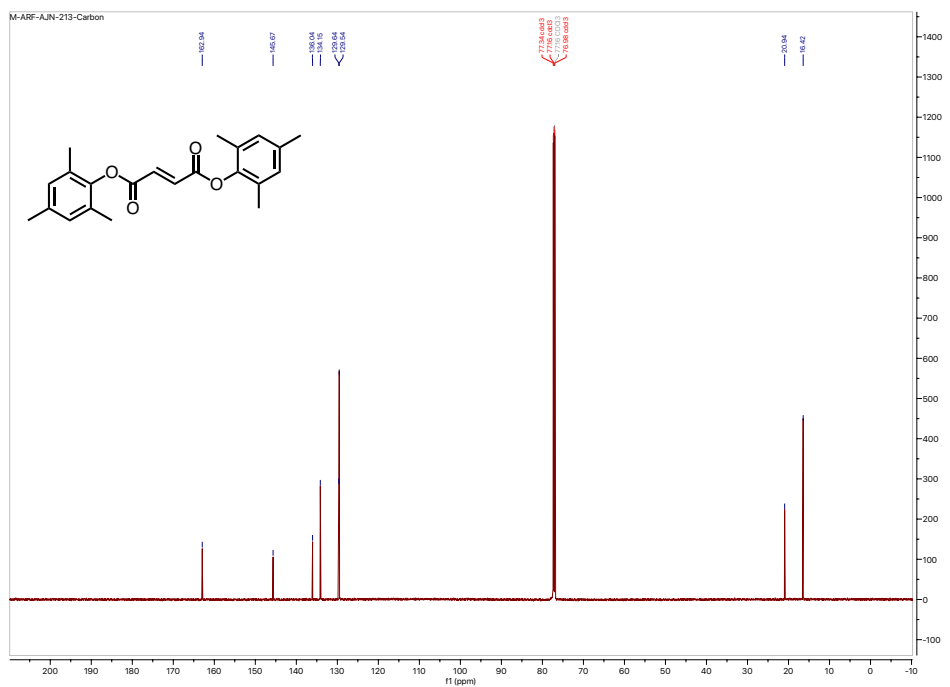

Figure 8-7: Proton spectra for dimesityl fumarate

Figure 8-8: Carbon spectra for dimesityl fumarate

Bis(4-methoxyphenyl) fumarate
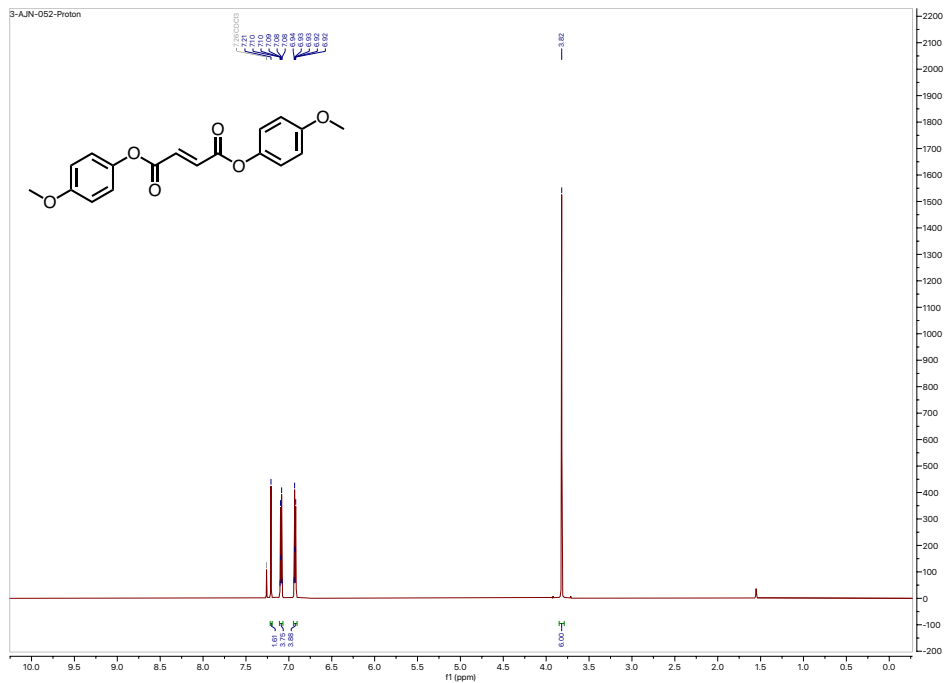
Figure 8-9: Proton spectra for bis(4-methoxyphenyl) fumarate
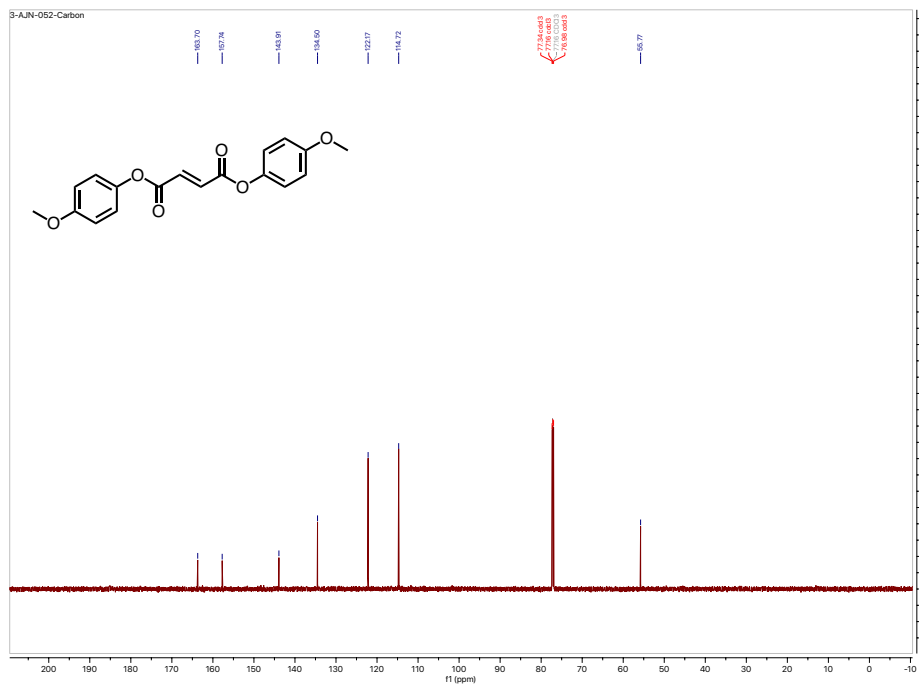
Figure 8-10: Carbon spectra for Proton spectra for bis(4-methoxyphenyl) fumarate

Bis(2-methoxyphenyl) fumarate

Figure 8-11: Proton spectra for bis(2-methoxyphenyl) fumarate

Figure 8-12: Carbon spectra for bis(2-methoxyphenyl) fumarate

Bis(4-(methoxycarbonyl)phenyl) fumarate
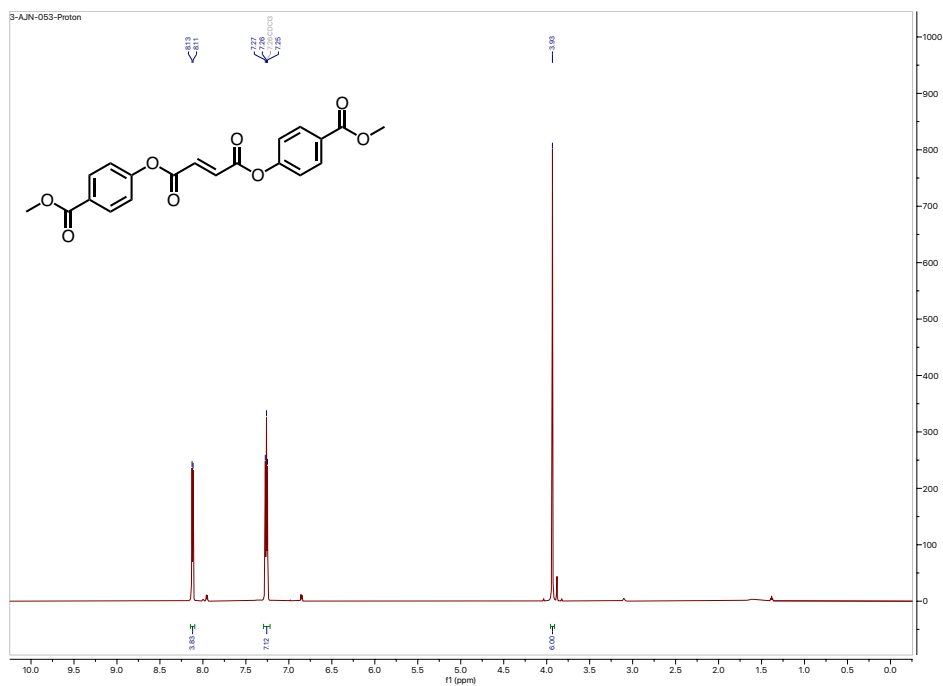
Figure 8-13: Proton spectra for bis(4-(methoxycarbonyl)phenyl) fumarate
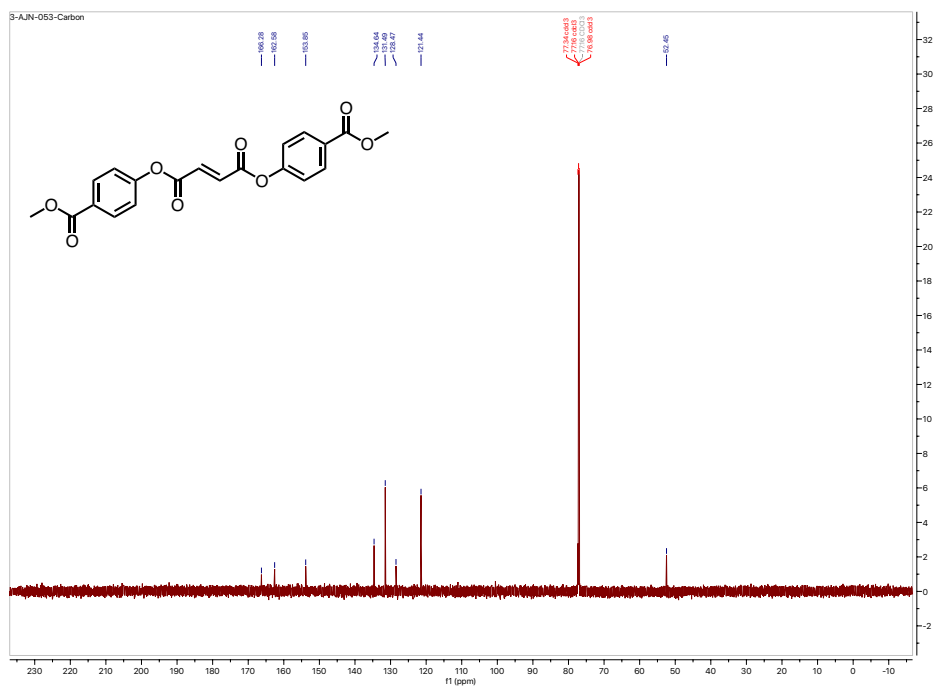
Figure 8-14: Proton spectra for bis(4-(methoxycarbonyl)phenyl) fumarate

Dibenzhydryl fumarate
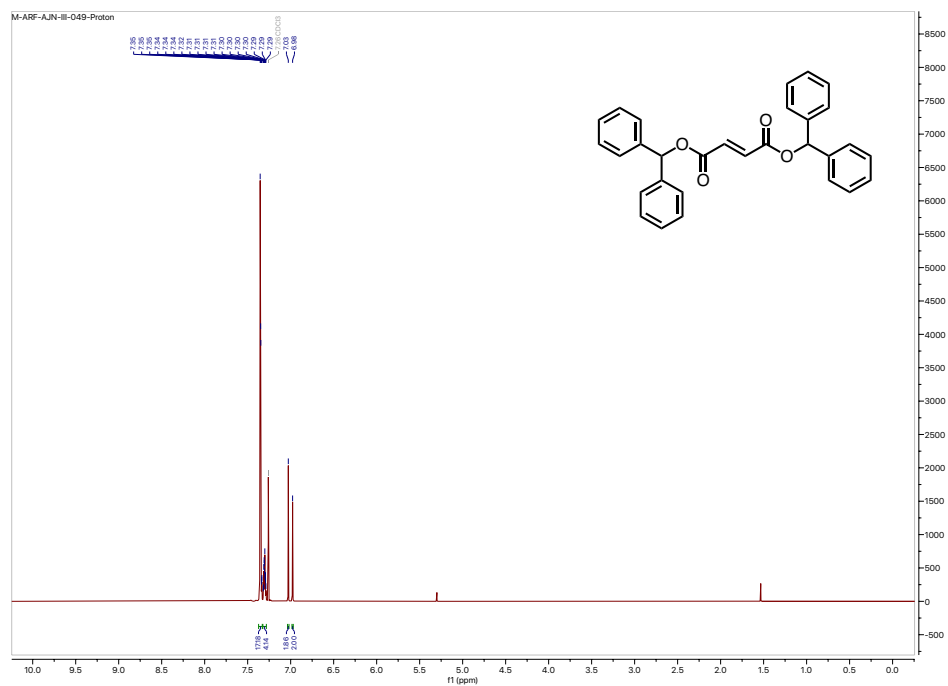
Figure 8-15: Proton spectra for dibenzhydryl fumarate
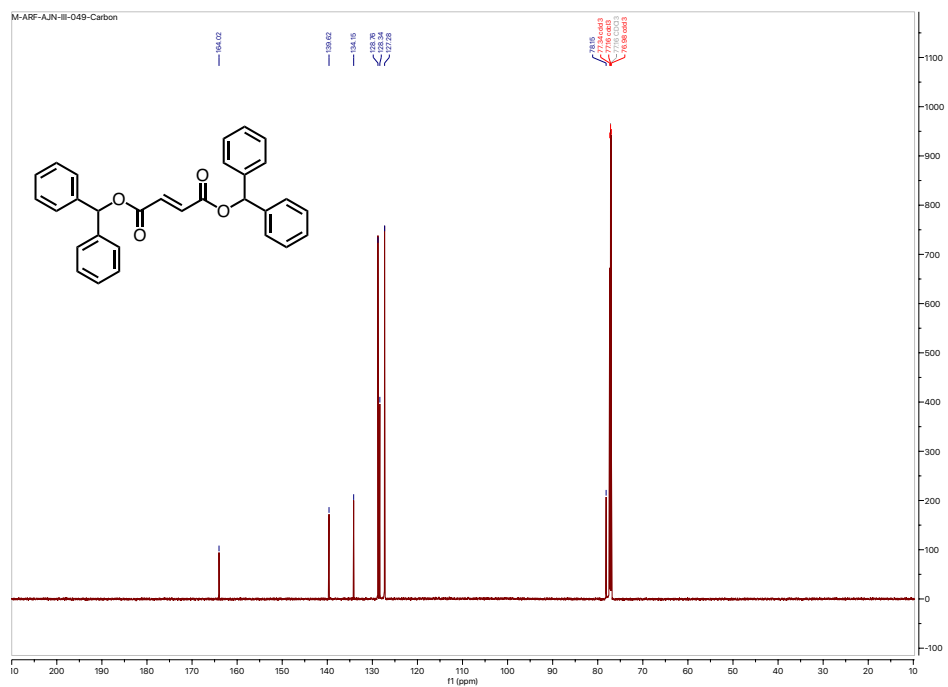
Figure 8-16: Carbon spectra for dibenzhydryl fumarate

Ni(IMes)(di-*o*-tolyl fumarate)₂ (4-12)
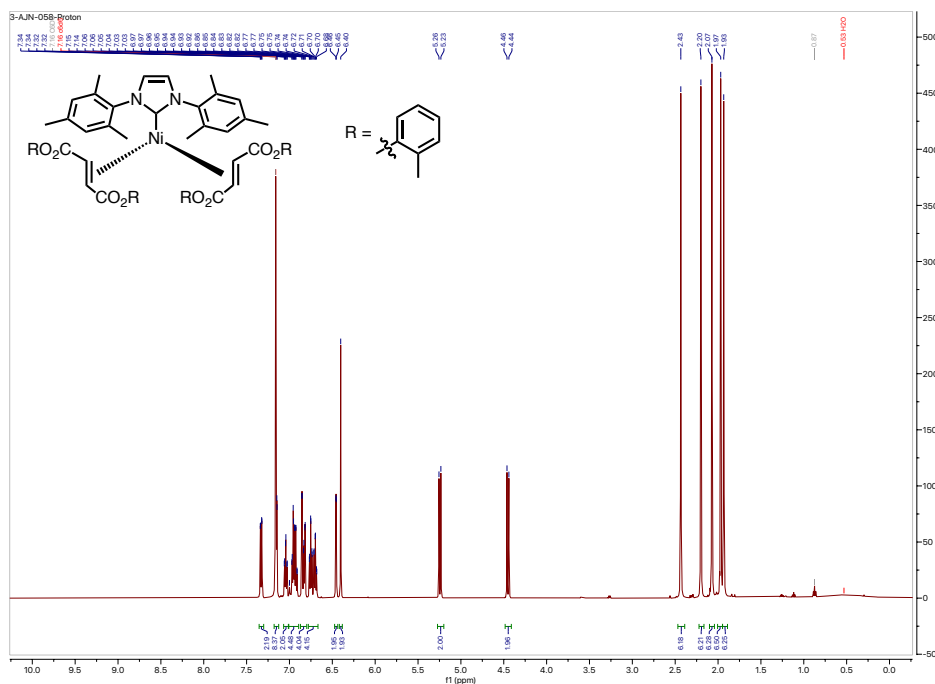
*Figure 8-17: Proton spectra for **4-12***

Figure 8-18: Carbon spectra for **4-12**

103
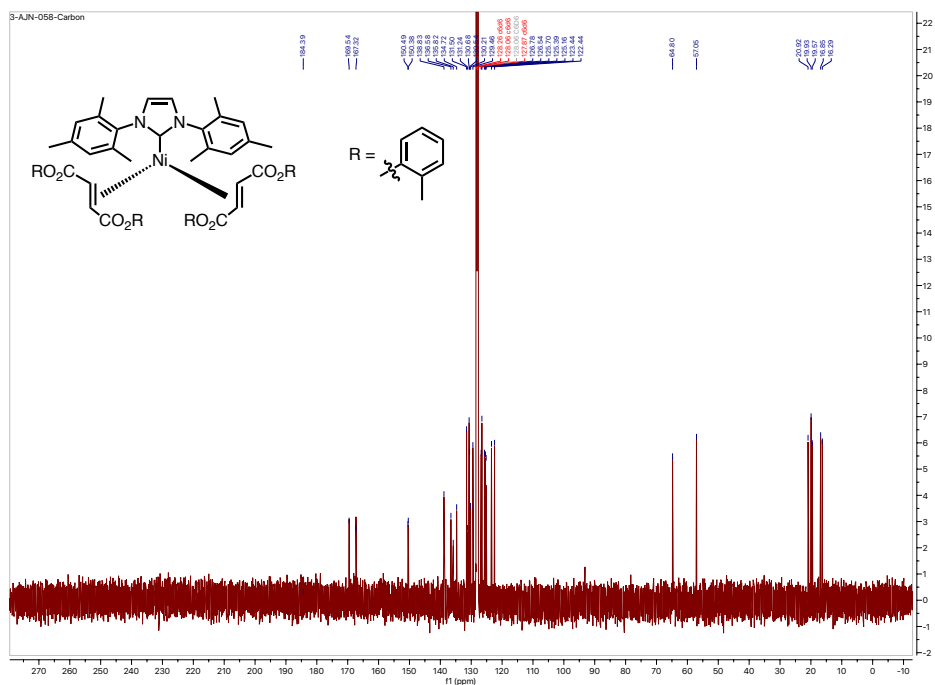
Ni(IMes)(dimesityl fumarate)₂ (4-11)
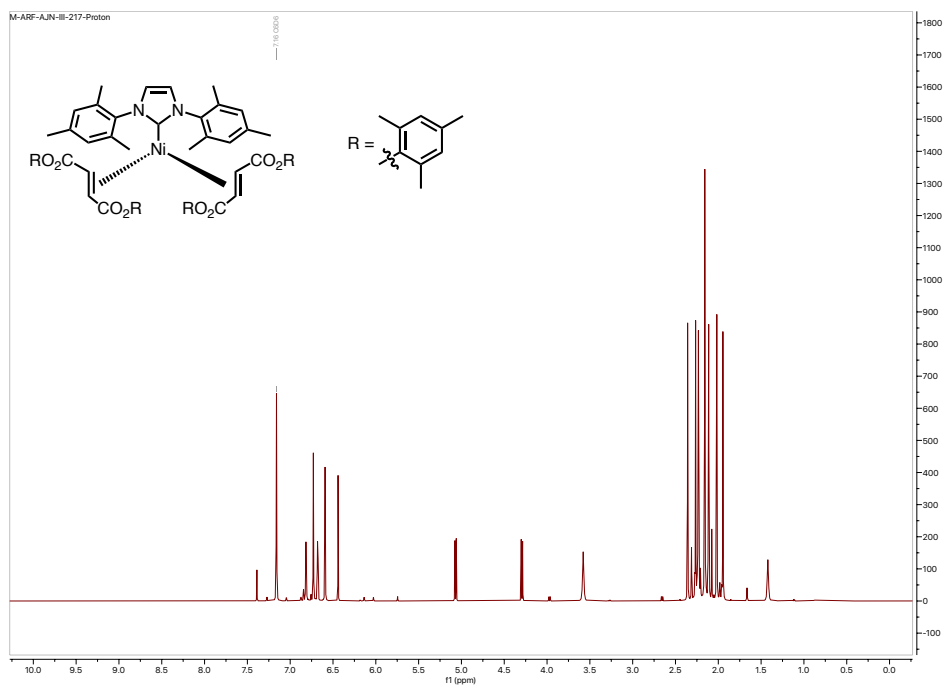
*Figure 8-19: Proton spectra for **4-11***
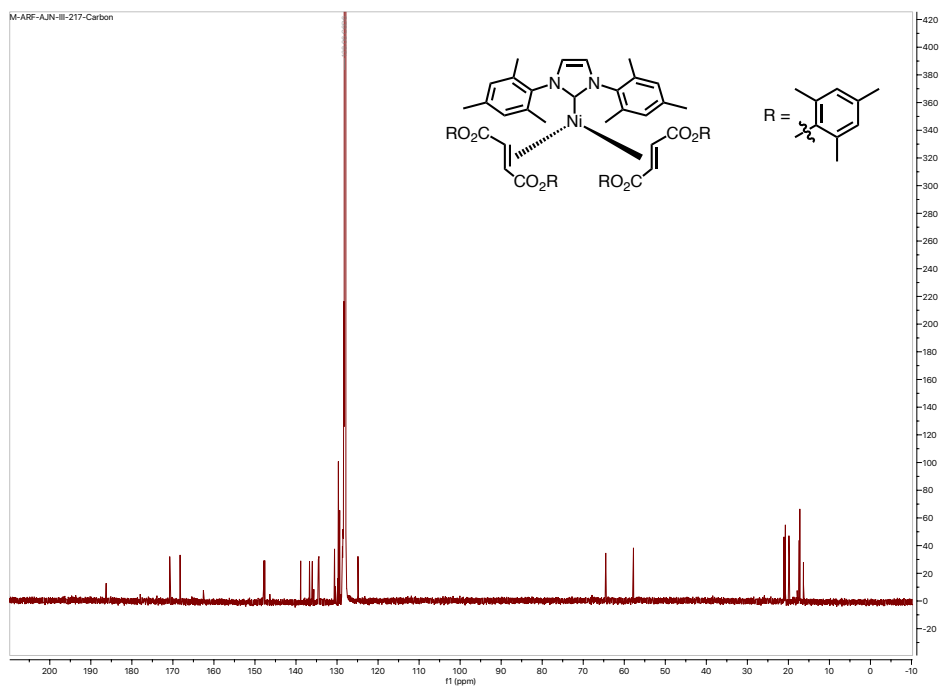
*Figure 8-20: Carbon spectra for **4-11***

Ni(IMes)(di-*p*-anisole fumarate)₂ (4-9)

*Figure 8-21: Proton spectra for **4-9***

Figure 8-22: Carbon spectra for **4-9**

105

Ni(IMes)(di-*o*-anisole fumarate)₂ (4-8)

Figure 8-23: Proton spectra for 4-8

Figure 8-24: Carbon spectra for 4-8
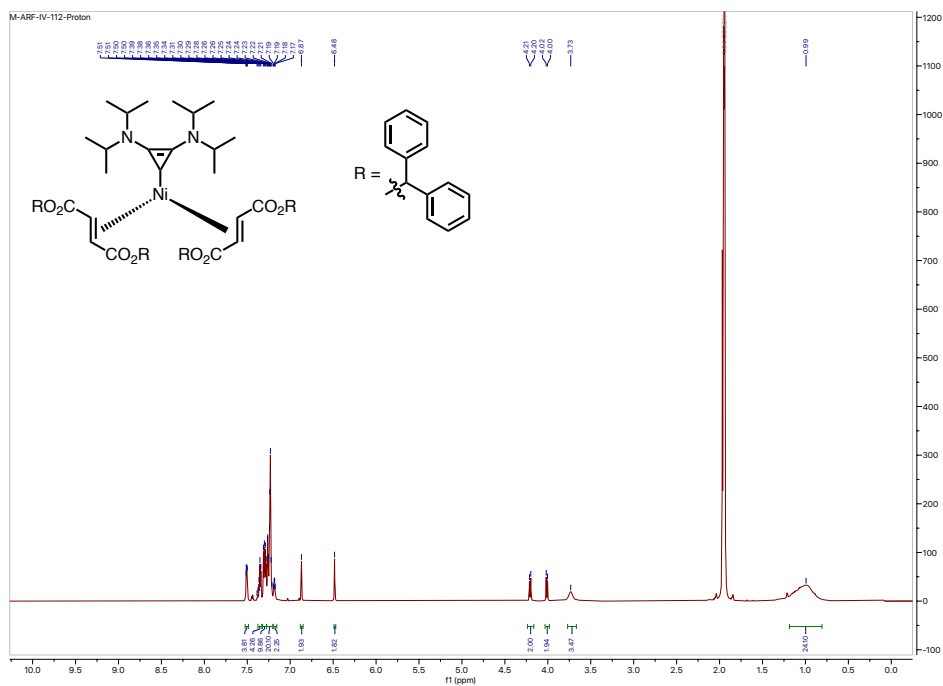
Ni(*i*-Pr-BAC)(dimethyl fumarate)₂ (4-18)
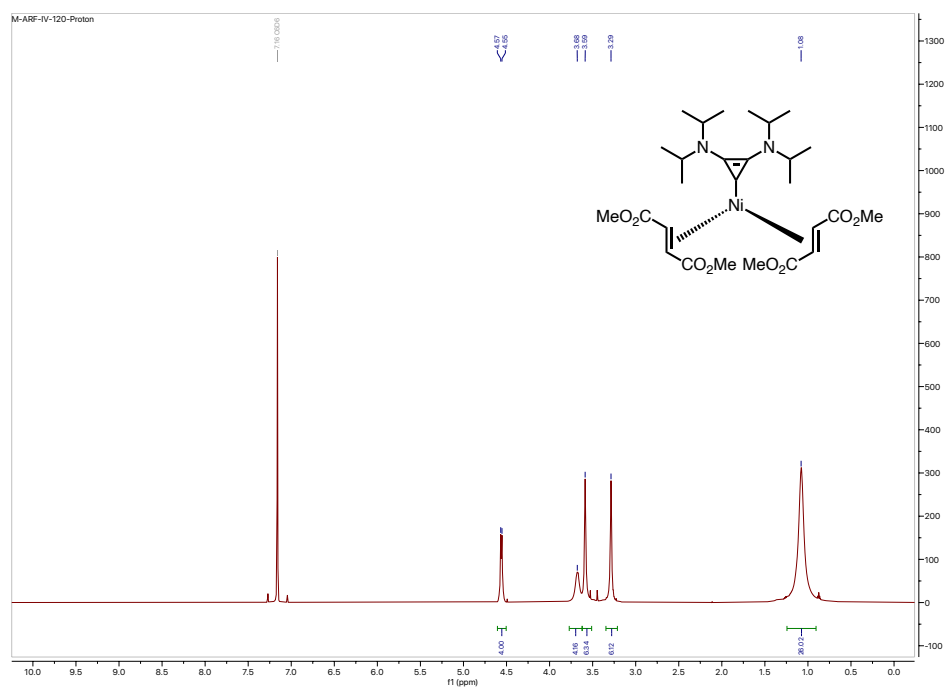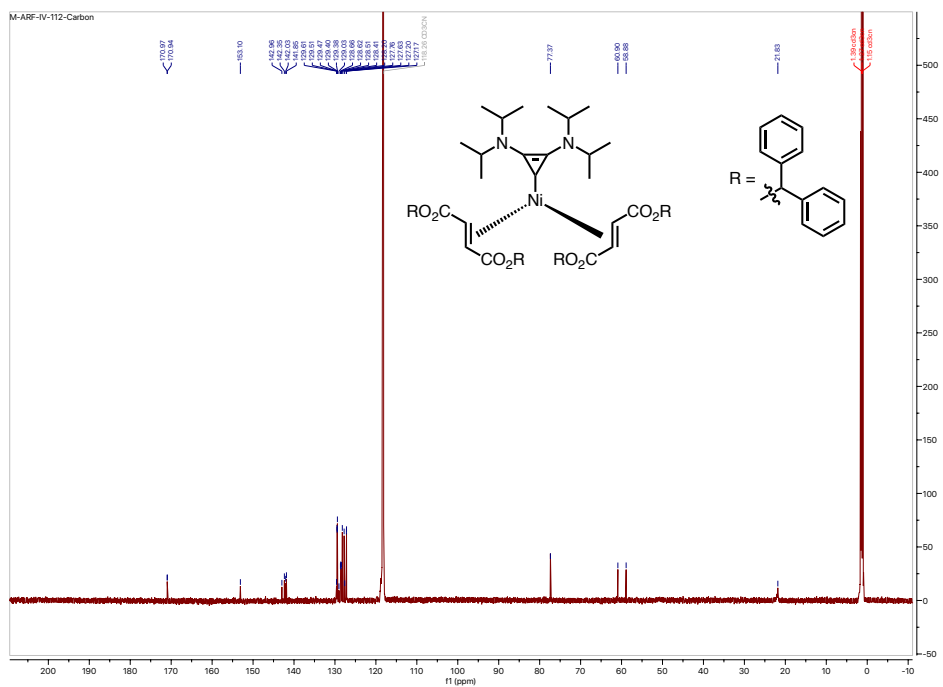

Figure 8-25: Proton spectra for 4-18
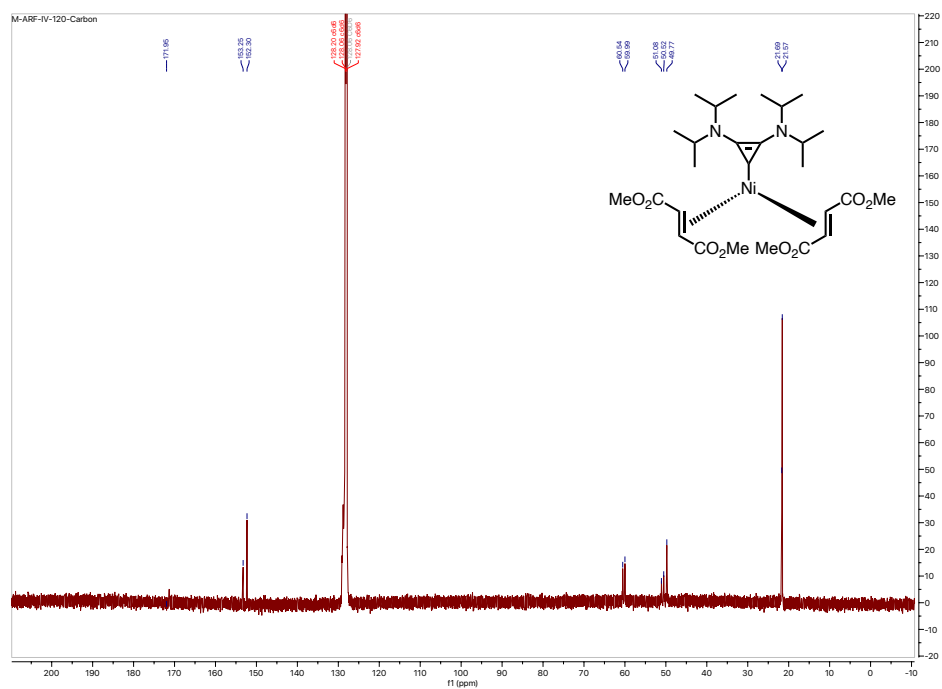
Figure 8-26: Carbon spectra for 4-18

Ni(*i*-Pr-BAC)(di-*o*-tolyl fumarate)₂ (4-19)
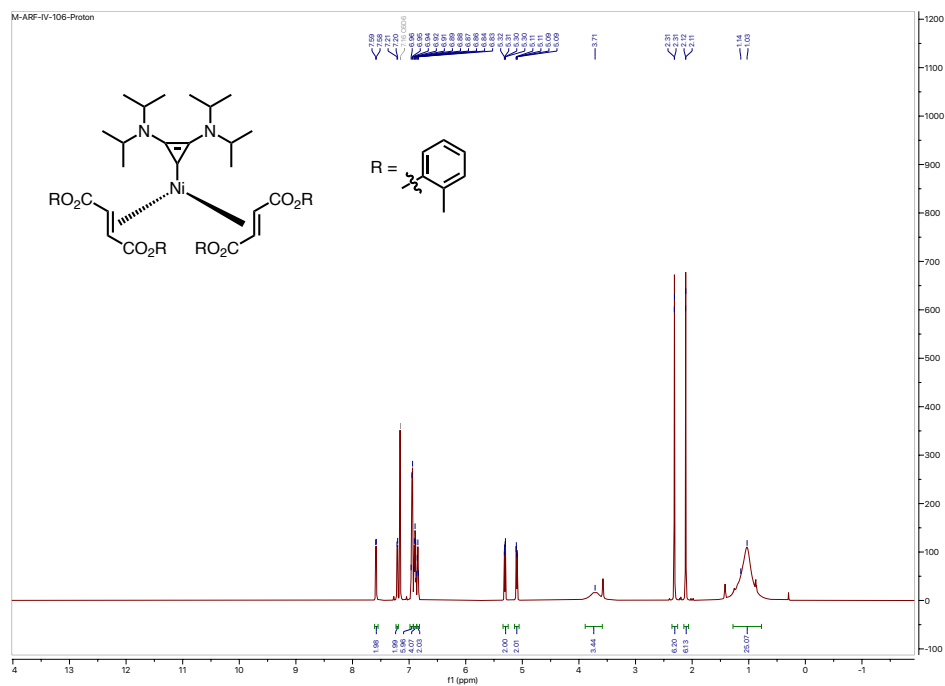
*Figure 8-27: Proton spectra for **4-19***
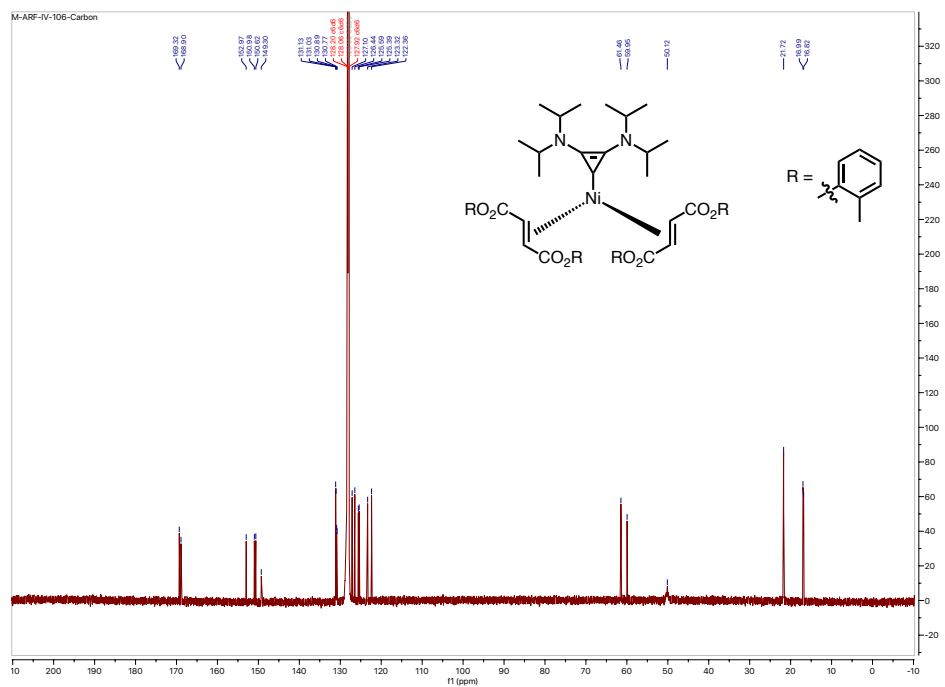
*Figure 8-28: Carbon spectra for **4-19***

Ni(*i*-Pr-BAC)(dibenzhydryl fumarate)₂ (4-20)

*Figure 8-29: Proton spectra for **4-20***

*Figure 8-30: Carbon spectra for **4-20***

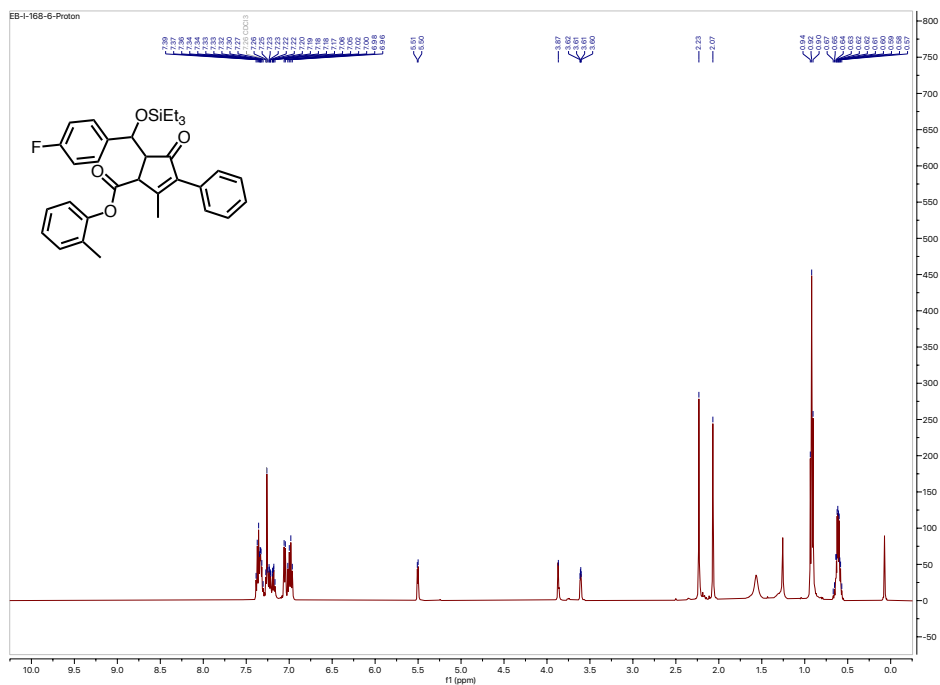***o*-tolyl 5-((4-fluorophenyl)((triethylsilyl)oxy)methyl)-2-methyl-4-oxo-3-phenylcyclopent-2-ene-1-carboxylate (4-23)**

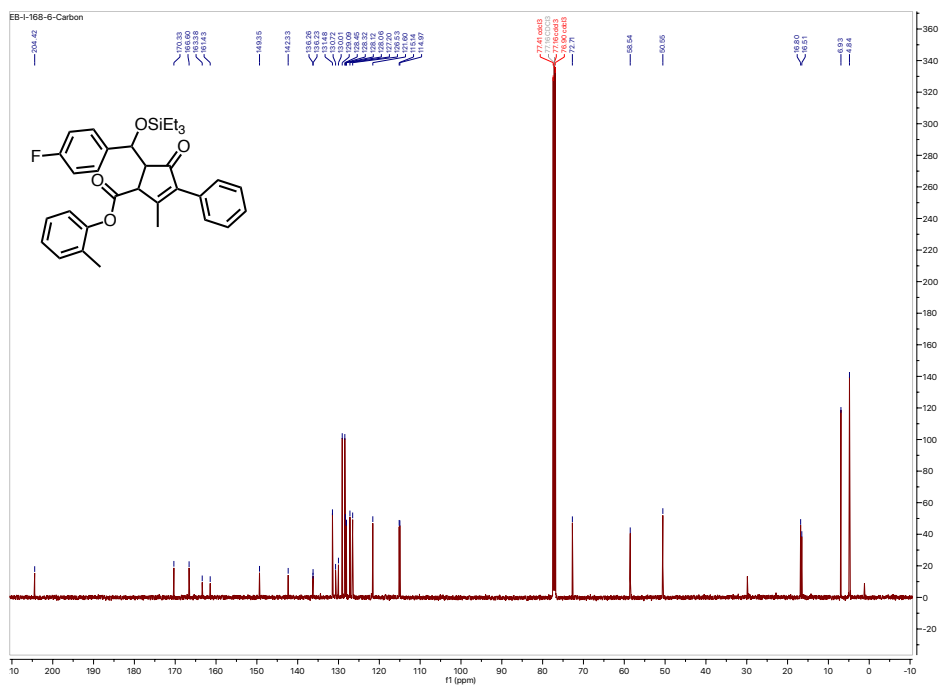*Figure 8-31: Proton spectra for 4-23*

Figure 8-32: Carbon spectra for 4-20

110

Triethyl(((*E*)-2-((*E*)-2-(1-phenylpentylidene)cyclopentyl)vinyl)oxy)silane (6-4)
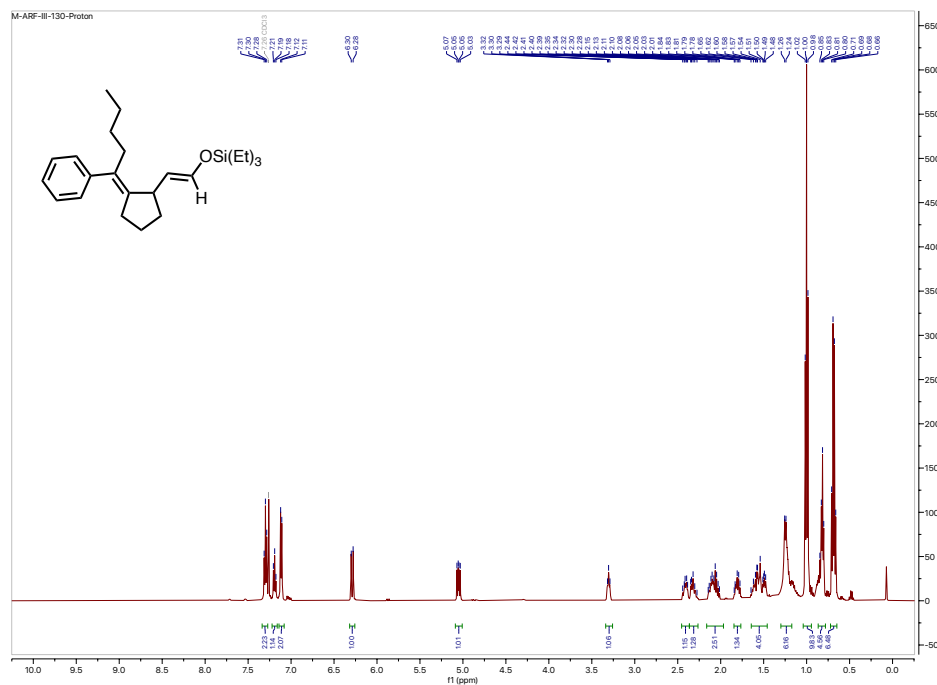
Figure 8-33: Proton spectra for 6-4
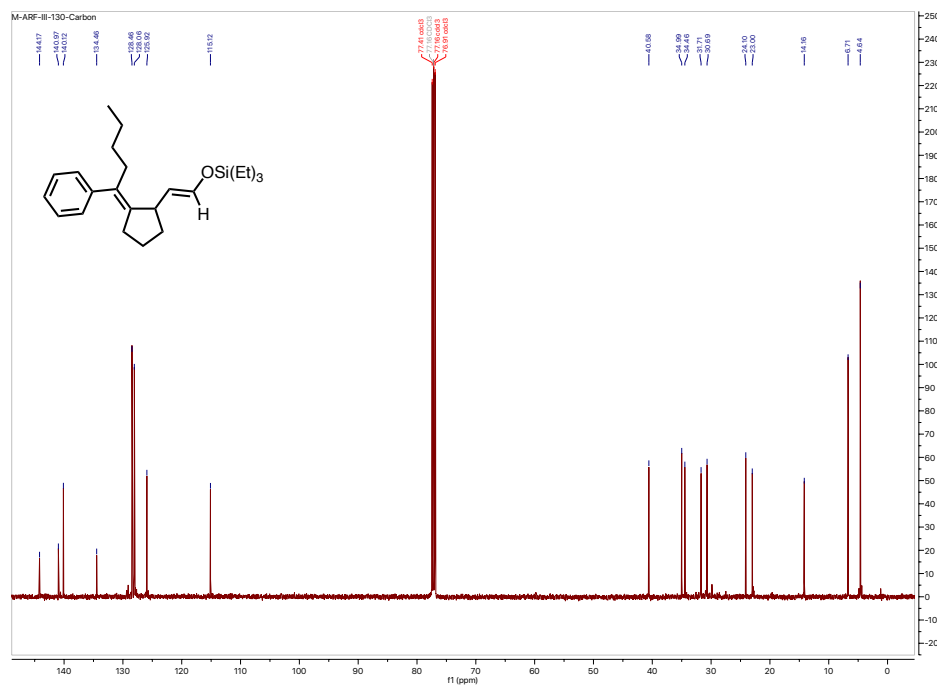
Figure 8-34: Carbon spectra for 6-4

111

3-((*Z*)-2-((*E*)-2-(1-phenylpentylidene)cyclopentyl)-1-((triethylsilyl)oxy)vinyl)oxazolidin-2-one

Figure 8-35: Proton spectra for 3-((Z)-2-((E)-2-(1-phenylpentylidene)cyclopentyl)-1-((triethylsilyl)oxy)vinyl)oxazolidin-2-one

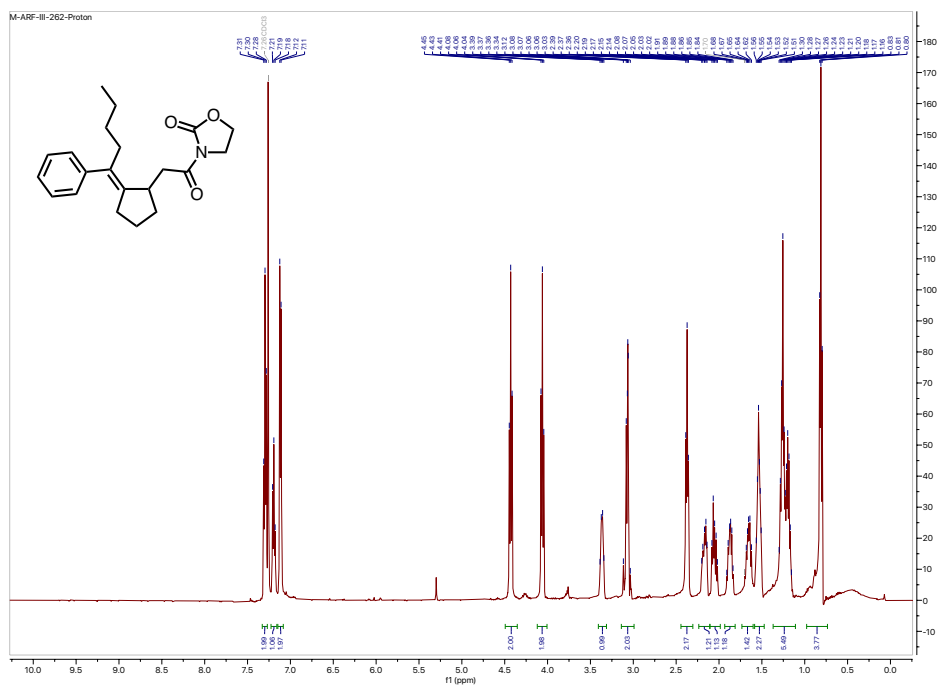# (*E*)-3-(2-(2-(1-phenylpentylidene)cyclopentyl)acetyl)oxazolidin-2-one (6-11)
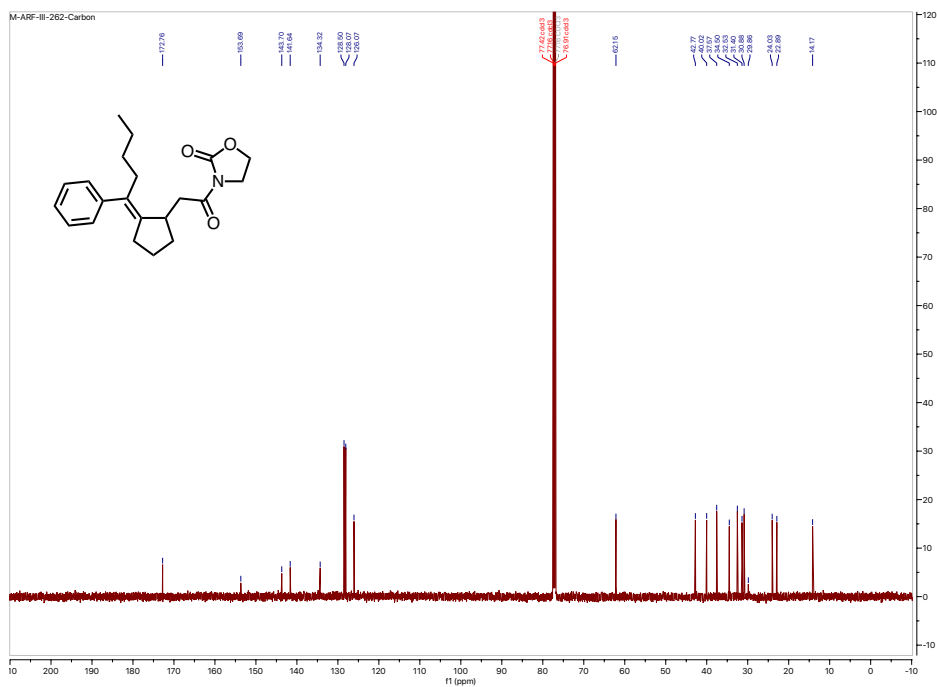

*Figure 8-36: Proton spectra for **6-11***

*Figure 8-37: Carbon spectra for **6-11***